Observations of Gamma-Ray Burst Afterglows with the AEOS Burst Camera

by

Heather Anne Flewelling

A dissertation submitted in partial fulfillment
of the requirements for the degree of
Doctor of Philosophy
(Physics)
in The University of Michigan
2009

Doctoral Committee:

Professor Carl W. Akerlof, Chair
Professor Joel N. Bregman
Professor Katherine Freese
Professor Timothy A. McKay
Associate Professor James T. Liu

To my grandmother, Helen Williams

ACKNOWLEDGEMENTS

with chess. And of course, all of my friends, who made graduate school fun, and were always there for me.

TABLE OF CONTENTS

LIST OF FIGURES

LIST OF TABLES

CHAPTER I

Introduction

1.1 Introduction

Gamma-ray Bursts (GRBs) are bright explosions of gamma rays, lasting on average 2-3 seconds. They were first discovered serendipitously about 40 years ago (Klebesadel et al., 1973), (Strong et al., 1974), by satellites designed to detect violations of the nuclear test ban treaty. It was determined that these blasts of gamma rays originated not on the Earth, but from space (Strong et al., 1974).

GRBs are elusive and mysterious. Like most other astrophysical phenomena, it has taken decades to discover their properties. This is in part because the gamma-ray emission only lasts a short amount of time and because the initial coordinates of the GRB are not accurate, making it difficult to follow up in other wavebands. The first detected GRB occurred on July 2, 1967, but the first GRB with a detected optical afterglow happened on February 28, 1997, and the first GRB with a measured redshift came on May 8th, 1997, both nearly 30 years after the discovery of GRBs.

$Swift$ is one of the current satellites dedicated to detecting GRBs, with an onboard X-ray telescope and UV and optical telescope for observing the afterglow. With $Swift$, GRBs are detected within seconds, and very accurately (3' error circles). The coordinates are disseminated to observers via the GRB Coordinates Network

(GCN), within ~ 20 seconds permitting follow-up observations in other wavebands. About a hundred GRBs per year are detected by $Swift$.

GRB afterglows are detected in many other wavelengths: X-ray, optical, IR, UV, and radio. Not all GRBs have detectable afterglows, despite reasonable efforts to search for them. Approximately 90% of $Swift$ bursts have X-ray afterglows, and these can last for weeks. Only about 50% of bursts both before $Swift$ and during the $Swift$ era have optical afterglows; this is discussed in detail in Chapter VI. Of the 50% that are observed, these can last for up to a week or so, and it is the optical afterglows that enable the redshift of the host galaxy to be measured. There are now redshifts, or limits on the redshift, for over 150 GRBs (http://www.mpe.mpg.de/$\sim$jcg/grbgen.html).

The organization of the thesis is as follows: This chapter introduces the subject of GRBs by describing their characteristics, some of the satellites that have detected them in the past and that currently detect them, some of the current optical telescopes that observe GRB afterglows, and the motivations for why we built the AEOS Burst Camera (ABC). Chapter II is a description of the AEOS Burst Camera (ABC), its mechanical and optical design, and the software which controls the ABC. The observation scheme for the ABC, and the data analysis (and pipeline) is described in Chapter III. Details about all GRB notifications to the AEOS control room are included in Chapter IV, with sections on all the optically detected GRBs, and the interesting non-detections. Whenever possible, data from ROTSE and data from the GCN is included. Chapter V discusses the ABC, ROTSE, XRT and other data in the context of current GRB afterglow theory. Chapter VI discusses the dark burst problem, the relationship to any of the GRBs observed by the ABC, followed by an estimation of the GRB afterglow apparent optical luminosity distribution function,

calculated in (Akerlof & Swan, 2007). Finally, Chapter VII the conclusion chapter of the thesis, sums up what has been learned by the ABC.

1.2   Gamma Ray Bursts

The first GRB was detected in 1967, by the Vela satellites, but it wasn't reported until 1973 (Klebesadel et al., 1973). These satellites were designed to detect violations of the nuclear test ban treaty, by detecting flashes of gamma-ray radiation. When it was determined that these flashes were cosmic in origin, researchers tried to identify GRBs with other astronomical objects in other wavelengths, but this required more accurate positions. To do this, the Inter-Planetary Network (IPN) was created, which consisted of the Vela satellites and other satellites with gamma-ray detectors attached to them. Positions were derived by triangulation: the positions of the satellites were known, as well as the timing of when the GRB was detected by each satellite. Typical error boxes/circles ranged from 0.7 - 7 arcminutes (Cline et al., 1984), (Barat et al., 1984), and the first afterglow searches involved old archival plates and late (months after the burst) observations. No optical counterparts were found in these early efforts.

BATSE was the most successful satellite to detect GRBs, detecting a total of 2704 GRBs between 1991 and 2000. BATSE could detect GRBs quickly ($< 10s$), but not accurately ($8°$ error circle). With the large sample of GRBs that BATSE detected, many unexpected characteristics of GRBs were discovered, one of them is that the distribution of GRBs is isotropic on the sky.

GRBs last from milliseconds to hundreds of seconds. During the BATSE era, people defined the duration of a burst (called T_{90}) to be the time needed to accumulate between 5%-95% of the total number of counts in the 50keV-300keV band. Plotting

the hardness ratio of a burst versus the T_{90} duration reveals 2 types of bursts, short hard bursts, with $T_{90} < 2s$ and long soft bursts, with $T_{90} > 2s$. Prior to $Swift$, no afterglows or host galaxies were ever detected for short GRBs.

Each GRB looks unique. Many GRBs have a fast rise exponential decay (FRED), but many do not, and many GRBs have variability within the gamma ray emission. There can be one pulse of gamma ray emission, or several.

The spectra of the emission is non-thermal, and is fit by the Band function, which is 2 smoothly connected power laws:

$$
(1.1) \qquad N(\nu) = \begin{cases} N_0(h\nu)^\alpha exp(-\frac{h\nu}{E_0}) & \text{for } h\nu < H \\ \\ N_0[(\alpha - \beta)E_0]^{(\alpha-\beta)}(h\nu)^\beta exp(\beta - \alpha) & \text{for } h\nu > H \end{cases}
$$

where $H \equiv (\alpha - \beta)E_0$, and α and β are the decay indexes. No theory predicts this purely phenomenological fit. The lower energy spectral index (α) is usually between $1/3$ and $-1/2$ which agrees reasonably well with a synchrotron emission model.

Redshift measurements, from optical observations, indicate that for isotropic emission the total energy is $10^{51} - 10^{54} ergs$. The energy of the afterglow is $10^{50} - 10^{52} ergs$. There is evidence that the emission is beamed (visible as a break in the light curve at late times, known as a jet break), so the actual total emission is lower, at about $10^{52} ergs$.

Extrapolating from the BATSE GRB detection rate, GRBs occur about twice per day. However, due to sky coverage of BATSE, $Swift$ and other satellite missions, GRBs are not detected this frequently. $Swift$ currently detects about 2 GRBs per week.

1.2.1 X-ray afterglow

Prior to $Swift$, most X-ray observations started hours after the GRB detection, with sparsely spaced ToO observations. This was enough to determine that there was an X-ray afterglow, and that it was fading, but not much else. $Swift$'s onboard X-Ray Telescope (XRT) starts observing the GRB field typically 1-2 minutes after the burst is detected, and performs continuous follow up observations for about $10^5 s - 10^6 s$. With the large number of bursts that $Swift$ has detected, this has provided a much larger sample of X-ray afterglows than in the pre-$Swift$ era, with each burst being better sampled, and covering large ranges of time.

Roughly 90% of the bursts have X-ray afterglows, and most have similar features. These are the features that are seen in the $Swift$ data (from Zhang et al. (2006)):

1. A steep temporal decay of ~ -3 is seen at times $< 10^2 - 10^3 s$; at later times it breaks to a shallower decay of -0.5. In some cases, the steep decay has a different spectral index β than the rest of the X-ray afterglow, implying that it is not related to the conventional afterglow component. This steep decay is shown as segment I in Figure 1.1, with the shallower part as segment II.

2. Large fractions of the GRBs have a transition from the shallow to normal decay, occurring at $10^3 - 10^4 s$. The spectral index is not changed, the early temporal decay is usually about -0.5, and the decay after is usually about -1.2. This corresponds to segments II and III in Figure 1.1.

3. In some cases, there is further steepening after the normal decay. This is consistent with a jet break, and occur at around $10^4 - 10^5 s$. The jet break is segment IV in Figure 1.1.

4. X-ray flares have been seen in about half of the bursts, they typically happen at hundreds of seconds, usually during the flatter decay (segment II) of Figure 1.1.

A cartoon of a 'typical' burst from Zhang et al. (2006) is given in Figure 1.1. Prior to $Swift$, only segments III and IV were seen, because most X-ray observations started at much later times than $Swift$ XRT. Segment III is well explained by the fireball model, and about half of the bursts detected by the ABC are consistent with this picture. Segment II can be explained by adding energy injection to the fireball. The fireball model, with energy injection and without, and how the ABC data fits this model is explained in Chapter V.
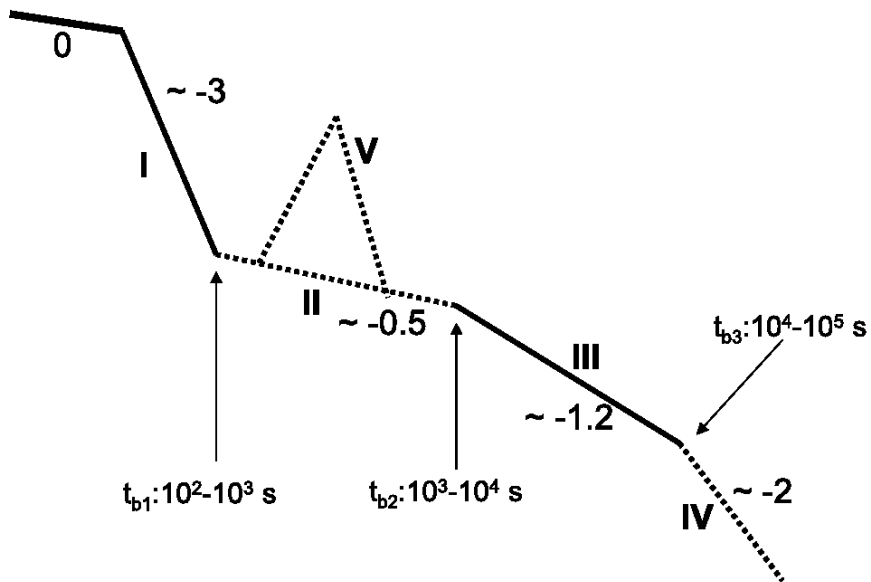
Figure 1.1 Cartoon lightcurve for a 'typical' X-ray lightcurve, from Zhang et al. (2006)

1.2.2   Optical detection of GRBs

The gamma-ray emission of a GRB lasts on average 2-3 seconds. To learn more about GRBs, they are observed in other wavelengths, where the afterglow lasts much longer. There are many advantages of using optical wavelengths, some of them include: the ability to measure the redshift of the host galaxy, the large number of optical telescopes available for use for studying a GRB over a large span of time, the

wide variety of optical instruments which enable both the early, bright afterglow to be detected and the late, faint afterglow to be detected.

Optical afterglows, if found, typically fade like $t^{-\alpha}$, with $\alpha \sim 1$. At early times, this will generally not be true, but wait a while, and the afterglow will fade like that. There can be breaks in the lightcurve, but each segment can be fit with different power law exponents. Almost always, if there is a break, it is flatter at early times, and steeper at later times.

Only half of all GRBs have optical afterglows in the $Swift$ era. Before $Swift$, when there were not prompt localizations for GRBs, only half of all GRBs had optical afterglows. This might have been because the afterglow was not observed early enough, when the afterglow was brighter, and easier to detect. In the $Swift$ era, the locations of the GRBs are found in mere seconds and optical observations start within a minute or less, yet half of all GRBs still have no optical counterpart. This is a mystery which is discussed further in Chapter VI. Reasons for why GRBs are dark include obscuration of the optical afterglow by dust, the GRB is at a high $(z > 6)$ redshift, or the GRB is just intrinsically fainter.

$Swift$'s fast detection of GRBs and GCN's fast dissemination of coordinates allows for simultaneous observations in gamma-rays and optical for some GRBs. This first occurred in 1999 with GRB 990123, a GRB detected by BATSE and seen in the optical by ROTSE-I (Akerlof et al., 1999), but it was extraordinarily bright. In the $Swift$ era, robotic telescopes observe optical afterglows contemporaneously with gamma-ray emission much more frequently. Some GRBs seem to have correlations with the optical and gamma-ray emission (Vestrand et al., 2005), some do not (Rykoff et al., 2005a).

Optical afterglow detections allow later observers to do spectroscopy, which can

measure a redshift. This is not the actual redshift of the GRB, but either a redshift of the host, or of the intervening gas. There are redshift detections for about 2/3rds of GRBs with optical afterglows, with a mean redshift of about 2.8 for $Swift$ bursts (Jakobsson et al., 2006a).

1.3   Motivations for building the ABC

Prior to the NSF proposal for the ABC, it was known that half of all GRBs had no optical afterglows. There were several possible reasons for this, ranging from intrinsically faint afterglows, locations at high redshift, or the GRB being obscured by dust. One way to probe the dark burst problem, or why half of all GRBs have no optical afterglows, is to use a big, fast optical telescope to perform follow up observations. Some of the GRBs which were labeled as dark because they were observed at late times with a large telescope, might have optical counterparts if they are viewed at early times with a large telescope. The lack of fast, large telescopes searching for GRB optical afterglows and the opportunity to do so is why the ABC was proposed, and later built.

Around the time of the NSF proposal for the ABC, HETE-2 was about to be launched, and INTEGRAL and $Swift$ were planning to be launched. These three satellites were dedicated to detecting GRBs. HETE-2, which launched on October 9, 2002, obtained localizations within a few minutes, but the error boxes were at best 10 arcminutes in size. INTEGRAL was launched October 17, 2002 and located GRBs in under a minute with 2.5 arcminute error circles. $Swift$ didn't launch until November 20, 2004, but promised positions within 6 seconds, 3 arcminute error circles, and about 100 GRBs a year. $Swift$ was the satellite that we were counting on for the bulk of the GRB triggers, as HETE-2 and INTEGRAL detect only a

fraction as many GRBs per year, and with much worse errors in the localizations.

What makes the Advanced Electro-Optical System (AEOS) telescope ideal for GRBs is that it is a large (3.67 m) optical telescope with fast slew. The AEOS is normally used for tracking satellites, which means that it can be re-pointed to GRB coordinates much more quickly than other large telescopes. With the ABC mounted on the AEOS, the fastest response to a GRB is 5 minutes, and this is the time between when the GRB is detected, coordinates are faxed to the operators, current operations are interrupted, the telescope is moved, and the first images are taken. The large size and quick speed of the AEOS makes the ABC ideal for probing the dark GRB problem.

The AEOS Burst Camera (ABC), was designed primarily to observe $Swift$ GRBs, but also works for HETE-2 and INTEGRAL detected GRBs as well. The ABC has a 6'x6' field of view, which is ideal for $Swift$'s 3' error circles and takes a series of 10s exposures since the camera is mounted on a Cassegrain port, so there is no de-rotator. It was expected that the ABC would observe about 6 GRBs per year, based on that 100 GRBs are detected by $Swift$ per year x 1/3 of the time it is dark x 1/3 of the time the GRB is above the horizon in Maui x 3/5ths of the time the weather will be good. The ABC was initially granted 6 ToO observations per year, which was later converted into 45 hours of of ToO per year.

Half of all GRBs have no detected afterglow, and there were three possible explanations for this: high redshift, intervening dust, or the afterglow is just intrinsically fainter. The ABC was well suited to observe these GRBs, because it was mounted on a large telescope, so could observe fainter afterglows, and had a camera that has some sensitivity in the near IR, which is helpful in observing higher redshift GRBs, and GRBs in areas with high galactic extinction. Another goal of the ABC was to

observe GRB afterglows with a low resolution grating at early (within a few minutes) times after the burst. Early simultaneous color information hadn't been collected before, and the models predicted different color changes in the optical, which should be possible to detect with the ABC.

The ABC was installed in late 2002, and responded to bursts from 2004-2008. Fifty GRB alerts were faxed or called in, but due to weather, equipment and other problems, 21 GRB fields were observed by the ABC. Of those fields, 10 had detected afterglows, and 4 had interesting upper limits. These results were compared with the fireball model, which found that about half the time the model works.

CHAPTER II

The AEOS Burst Camera (ABC)

2.1 Introduction

The first chapter described what a GRB is and some of the prior observations of GRB afterglows, including observations in the optical portion of the spectrum that have enhanced our understanding of GRBs. $Swift$, a satellite designed to localize GRBs to within 3', allows large instruments such as the Advanced Electro-Optical System (AEOS) telescope, with small field of views, to observe GRBs very quickly. The AEOS Burst Camera (ABC), mounted on the 3.67 m AEOS telescope, is dedicated to observing optical afterglows detected by $Swift$. This chapter describes the ABC hardware and software, as well as the observation scheme for the ABC.

The ABC was built to provide quick and deep observations of GRBs. The speed and sensitivity of the ABC enables the study of the dark burst problem, the question of why approximately half of all GRBs have no optical afterglow. The AEOS is especially suited to this task because it moves fast compared to other large telescopes, allowing deep images at much earlier times than these telescopes are capable of. Early observations of GRBs are commonplace with small robotic telescopes, like ROTSE, but the AEOS allows for deeper observations, at later, but still early, times.

Though ROTSE and ABC are very different, they complement each other. The

	ABC	ROTSE
Field of View	6'x6'	1.85°x1.85°
Trigger Response Time	5-15 minutes	7 seconds
Primary Mirror Diameter	3.67 m	0.45 m
Typical Sensitivity	23rd mag	19th mag
Observations	Target of Opportunity observations	Fully robotic, automated response

Table 2.1 Comparison of ABC and ROTSE

ABC is a 6′x6′ FoV camera, and ROTSE is a 1.85°x1.85° FoV camera. ROTSE is much faster than the ABC, obtaining GRB images on average only 7 seconds after the GRB trigger, while the first ABC images are taken 5-15 minutes after the trigger. ROTSE is a much smaller telescope, with a primary mirror diameter of 0.45m, compared to 3.67 m on the AEOS telescope (on which the ABC is mounted). This difference in size means the ABC is more sensitive ($\sim$22-23 magnitude) than ROTSE ($\sim$18-19 magnitude). Another difference is that ROTSE is fully robotic, and is able to observe all GRBs, while the AEOS is not robotic, and requires Target of Opportunity (ToO) observations. These differences are useful, for once the afterglow has faded below ROTSE's threshold, the ABC is already on target and taking images. However, due to the geographic locations of ROTSE and ABC, and the weather, GRB observations with both ABC and ROTSE rarely overlap.

This chapter describes the AEOS telescope and GRB response protocol (Section 2.2, ABC Hardware (Section 2.3), followed by a description of the Software (Section 2.4).

2.2 AEOS Telescope

In this section, the AEOS telescope is described in detail, the burst response protocol is explained, as well as procedures on how the AEOS does the pointing and focus for the ABC.

2.2.1 Description of the AEOS

The Advanced Electro-Optical System (AEOS) telescope is a 3.67 m telescope located on Haleakala, Hawaii, at 10,000ft. It is the largest optical Air Force telescope, and it can slew to any position within about 20 seconds, as it was designed to track fast moving satellites. The AEOS is on an alt-az mount, and if the telescope tracks a given RA and DEC, the field will rotate with time. This rotation limits the ABC exposures to about 10 seconds, because longer exposures result in star trails. The AEOS has 4 Cassegrain ports, and 6 Coudé ports. The ABC is mounted on a Cassegrain port, therefore it is attached to the optical tube assembly (OTA).

2.2.2 Burst Response Protocol

Responding to GRBs using the AEOS is quite a bit different than for other telescopes, partly because of the security restrictions. In this section, the steps the operators follow to observe a GRB are explained.

First, if a burst passes the filters described in section 2.3.5, a fax is automatically sent to the fax machine in the control room. There is always an operator in the control room if the AEOS dome is open, and the fax machine has an additional ringer, making it quite loud and unlikely that the operators will miss the fax.

At this point, the operators must determine if they are going to observe the burst. This project had 45 hours of Target of Opportunity (ToO) time per year, and the ABC was given priority over almost all AEOS observations. Provided the weather is

Figure 2.1 Image of the AEOS.

good, there are no higher priority observations, and all of the equipment is working, the operators will get ready to use the ABC. One operator moves the AEOS to the proper coordinates, adjusts the the focus position, and moves the tertiary mirror to the ABC position. Another operator uses the "Priority Data Acquisition Request" window in the ABC to initiate a series of images to be taken by the ABC. Once the first few images are displayed, the operator will check that the focus is good and that the images match what was provided on the finding chart.

There is another GRB camera, Rice University CCD(RUCCD) on the AEOS, with a 45"x45" field of view. Because of the limited field of view, this camera is only used if there is a $Swift$ XRT position or an optical afterglow reported by a GCN. This camera shares a Coudé port which is not always available. When it is, when better coordinates are available, the operators switch between the ABC and RUCCD every 15-30 minutes, frequently resulting in gaps in the ABC data.

The goal is for the operators to take data with the ABC and RUCCD for at least an hour. Observations are terminated if there are higher priority observations, the weather turns bad, or the sun rises. If there are reports on the GCN of deep upper limits, but no detections of an afterglow, the operators were called to tell them to stop taking data. Once the observations are completed, the operators copy the data onto CDs, and transfer the CDs to a computer connected to the Internet. From there, the images are downloaded, but it takes anywhere between a few hours to a few days to get the data from Maui.

2.2.3   Pointing

Initially, the ABC didn't have a working pointing model, and when the operators moved to a given RA and Dec, it would be miss-pointed by an average of 30 arcminutes. This is a problem when your field of view is only 6 arcminutes across!

Before the pointing control software was fixed, the operators came up with an ingenious way around the pointing problem although it slowed them down by a few minutes. First, they would move to a nearby wiki star (a very bright star, 10th magnitude or brighter), and would nudge the position until the wiki star was centered on the ABC image. Then, they would go to the RA and DEC of the requested observations, and adjust the ABC as they did for the wiki star. This would get the ABC onto the RA and DEC to within less than 30 arcseconds of the specified location.

It took several years to fix the pointing, because everyone was looking for a hardware problem, when actually it was a problem in the software. A bug in the pointing code, specific only to the port the ABC was using, was found. Once the bug was removed and the pointing software was recompiled, the pointing was fixed. The pointing is now accurate to within a few arc seconds. When the operators have spare time, they build new pointing models, which keeps the ABC pointing very accurate.

2.2.4 Focus

Although a focus motor is in the ABC package, the operators found it is easier to adjust the position of the secondary mirror to do the focus. This simplifies operations for them as other equipment also uses this method for focus adjustment.

There is no focus model for the ABC. This is unusual, because the focus changes with temperature and elevation, and a model will predict what the focus should be and adjust it. Instead of a model, the operators kept a log of the best focus position (from prior observations), and moved the secondary mirror to the previous focus position while they are moving the telescope. Within the first couple of images, the operators can determine if they need to adjust the focus, and will adjust it while the images are taken. They will record the new focus for future observations.

This method works reasonably well for finding the best focus, and can be done quickly. If the focus is extremely poor, stars will look like donuts. The starting focus is usually close to the best position, therefore the images usually contain larger than optimal dots, and not donuts, for the stars.

2.3   ABC Hardware

The ABC consists of many parts which are packaged in a large box (known as the ABC enclosure) that is mounted on the AEOS telescope. This section describes the ABC optics, the mechanical design, and the CCD camera, which reside in the ABC package as well as the computers, fax machine and other peripherals which allow the ABC to be remotely operated from the control room.

2.3.1   Optics

The ABC optics, designed by Carl Akerlof, consist of a turning flat, a reducing (parabolic) mirror, a grating or filters, and a correcting lens. The light from the tertiary mirror is reflected by the turning flat, to the reducing mirror. The converging beam threads through a hole in the turning flat, through the grating or filter, and then through the simple lens finally reaching a focus on the CCD surface. The optical path can be seen in Figure 2.2. The only moveable parts are the CCD camera head, which is controlled by the focus motor, and the grating/filter, which can be removed to swap out the grating or filters.

Due to space restrictions, the ABC has a filter holder, and not a filter wheel. This means that filters can be changed, but not easily or quickly. Initially, a broadband filter, BK7 glass, was installed. With the broadband filter, the ABC achieves very deep limiting magnitudes up to 23rd mag.

About 2 years into the project, a blazed transmission grating replaced the broad-

AEOS TELESCOPE IMAGE REDUCER DESIGN

REDUCER MIRROR

FOLD MIRROR

CCD CAMERA

1
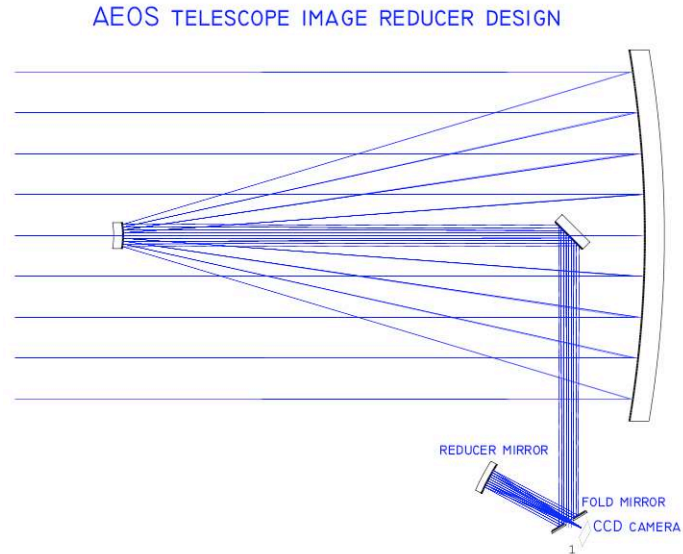
Figure 2.2 Diagram of the optical path of the light through the AEOS and ABC.

band filter. At the time, there was no early spectroscopy of GRB afterglows, which the grating would be able to do. The blazed transmission grating has a blaze angle of 2.2°, and 35 lines per mm. This allows for low resolution (R∼10) spectroscopy, with most of the light falling in the first order, centered at 640nm. Low resolution spectroscopy is useful to observe color changes in early GRB afterglows, a prediction of models but not yet observed. The limiting magnitude with the grating in place was 19th magnitude, but due to the difficulty with observing GRB afterglows, was swapped back with the broadband filter after a year.

2.3.2 Mechanical Design

The mechanical design was performed by Alan Schier, who designed and built the optical tube assemblies and mounts for the ROTSE-III telescopes (Akerlof et al., 2003). There were certain size restrictions to allow the ABC to be mounted on the AEOS. It had to withstand the rapid slewing of the AEOS, and also provide access for swapping out filters and other maintenance. The top half of the package houses the optics and CCD camera, and the bottom half contains the electronics necessary

to control the CCD camera and the coolant to maintain the proper temperature for the ABC and the enclosure. This keeps the ABC enclosure at the same temperature as the AEOS, which is important to reduce background noise for IR observations by the AEOS. There are also several environmental sensors installed throughout the package, which monitor the camera temperature, enclosure temperature, and coolant flow rate. The ABC package is mounted on a trunnion port, which is located just below the large primary mirror on the AEOS telescope. The panels are removable, to provide access to the top half and bottom half of the package, while the ABC is mounted on the AEOS.

2.3.3   CCD Camera

The CCD camera and all of its peripherals are identical to the ROTSE cameras, simplifying many aspects of the ABC since a large fraction of ROTSE data acquisition and analysis code could be reused as well as some of the ROTSE spare parts. The camera head was designed and assembled by Bob Leach of Astronomical Research Cameras, and is thermoelectrically cooled to a temperature of -50F. The CCD chip is an E2V back-illuminated 2048 x 2048 sensor with 13.5 μm pixels. The read noise is 8 e^-, and the gain is 3. The chip is equipped with 2 amplifiers, which can be selected through the software, and the readout time is 6 seconds per image.

2.3.4   Computers

There are 2 computers that are used to run the ABC, located in the control room. They are the Control Computer (abc), and the Camera Computer (camabc) and they are networked together and isolated from the Internet due to security restrictions imposed by the Air Force.

The Control Computer has 3 main functions. First, it provides an interface for

the operators for data acquisition. Second, it runs the Data Acquisition (daq) software which controls the camera and verifies that the camera is functioning properly. Third, it communicates with the Camera Computer, giving the Camera Computer instructions on how to take the data, and transfer it onto the Control Computer. The Control Computer is connected to the focus motor, environmental sensors, Inter-range instrumentation group (IRIG) time feed, and video feed by optical fibers.

The Camera Computer only interacts with the Control Computer and the camera. It waits for instructions from the Control Computer to take data, and then initiates communications with the camera. This demands a lot of computer resources, requiring a dedicated processor.

2.3.5 Fax Machine

The fax machine alerts the operators that there is a GRB that they should observe, which is an atypical protocol for a burst alert. Most robotic GRB telescopes, like ROTSE, get a trigger directly from the GCN, via an Internet connection. However, due to security restrictions, the ABC cannot be connected to the Internet, preventing the ABC from receiving triggers directly. Most GRB observers carry a cell phone or pager that receives a text message or page alerting them of a GRB. Cell phones are not permitted on the site, and the pager did not consistently get a strong enough signal to receive pages. Given these restrictions and problems, using a fax machine to alert the operators was a practical solution.

There is always at least one operator present in the control room when the telescope is in use, so placing the fax machine in the control room ensures that a GRB alert will notify the operators when the telescope is open and able to take data with the ABC. A very loud ringer was attached to the fax machine, to ensure that the fax was recognized. A computer in Michigan determines if a GRB is suitable for Maui

by meeting the following criteria: the GRB must be less than an hour old, above the horizon for at least 15 minutes, and it must be dark in Maui. If a GRB passes these cuts, then a fax with the RA, Dec, and a finding chart customized for the ABC is sent to Maui. Additionally, to verify that the fax is operational, a test fax is sent every day at 11:30 pm EST.

2.4   ABC Software

There are two requirements for the ABC software. First is that it must control the hardware, and second is that it needs to provide an interface for the operators to request images. Controlling the hardware is easier than providing an interface for the operators. In essence, the ABC is a stripped-down ROTSE. ROTSE-III has many things to contend with: the CCD camera, the weather station, the mount, scheduling of observations other than GRBs, scheduling GRB observations, operation of the clamshell, and monitoring of a few other things, like various temperature sensors. ROTSE-III also has to worry about analyzing the data in real time, due to the amount of data that is taken each night. The ABC is simply a camera, same model as the ROTSE-III CCD, mounted right on a Cassegrain port, that is used only during GRB observations. Analysis of ABC data is done later, once the data is transported back to Michigan. Providing an interface for the operators is more difficult. ROTSE-III telescopes were controlled through the Internet, therefore a low bandwidth method was preferred. This method used `ssh` and the ROTSE telescope was controlled by typing in various commands at an ssh terminal. This was not appropriate for an operator in a control room who may have several other instruments that require special commands. A graphical interface which is intuitive and easy to use is a must for the ABC.

The ABC software is the code that controls the hardware and is similar to the ROTSE software with a few changes to give the operators a friendly interface (ABC Control). A more detailed description of the ROTSE software, was described in the PhD thesis by Eli Rykoff (Rykoff, 2005) and also in (Akerlof et al., 2003). The ROTSE/ABC software is organized as a number of daemons, programs that are run in the background and not under direct control of a user. The ROTSE daemons schedule observations, monitor the weather and other sensors, and issue commands to the camera.

The ROTSE daemons that ABC has adapted are `rotsed`, `mountd`, `alertd`, `camerad` and `camserverd`, as well as a new daemon, `envirod`. The `rotsed` daemon is the main daemon. It spawns the other daemons, and which daemons are run are controlled through configuration files. The daemons that the ABC does not require, like `weatherd` (to monitor the weather), and `clamd` (to control the ROTSE clamshell) are therefore not run. The ROTSE version of the `mountd` daemon controls both the mount and the focus motor. Since the ABC does not have control of the AEOS mount, `mountd` has been modified to only control the focus motor present in the ABC package. The `alertd` daemon waits for GRB triggers from the GCN, and parses them. It has been modified so that it accepts all alerts, and a GCN connection has been "faked", so that ABC Control (the operator GUI) can instead send these sorts of alerts. The `camerad` and `camserverd` daemons are mostly unchanged. The `camerad` daemon runs on the control computer, and the `camserverd` daemon runs on the camera computer, waiting for commands to issue to the camera. The new daemon, `envirod`, monitors the environmental sensors, which include the flow rate of the coolant, and the temperatures of the enclosure and camera. If any of these daemons encounters a problem, the system shuts down cleanly. This happens
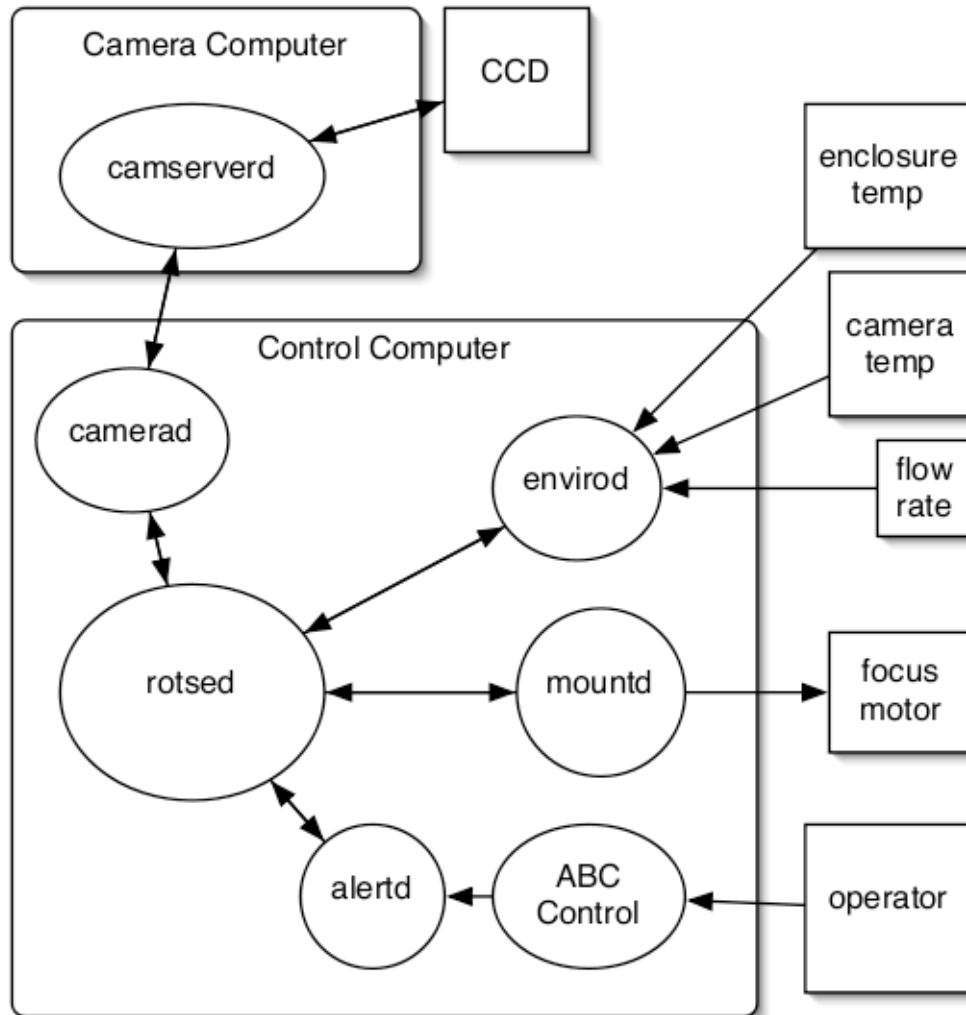
Figure 2.3 Diagram of the ABC software. The squares represent things like hardware (except for the operator) that interacts with the computers. The squares with rounded corners represent the computers, and the ovals represent the software that runs on the computers. All of the software, except for ABC Control, is run as daemons.

if the camera computer is powered off, or if the connections to the camera, focus motor, or environmental sensors are cut off.

2.4.1 ABC Control

ABC Control is the interface that the operators use to control the ABC and to copy data to CDs. It is designed to be easy to use, and has 2 data acquisition windows (one for GRBs, and another for other observations), a window to let the operators monitor the ABC, a function to create CDs, and a stop button to terminate the current observations. Figure 2.4 shows a screen capture of what the interface looks like. This section will explain how ABC Control interacts with the ROTSE daemons, what each window does, and how to use them.

ABC Control interacts with the ROTSE daemons in a very simple way. For the ROTSE telescopes, GRB alerts from the GCN are received by one of the ROTSE daemons, parsed, and scheduled into the queue. The ABC, with no Internet connection, can't do this. Instead, it mimics the GCN connection so when the operators request images, it fakes a GRB alert which is then parsed by the ABC and queues up the requested images.

The "Priority Data Acquisition" window is used when the operators respond to a GRB. All that is required is that the operators enter the RA, DEC and type, and hit "GO". This queues a series of 180 10 second images, with the correct file name with the RA and Dec included in the header, for future reference. The "type" refers to the tiling, or how the images are tiled if the burst error box is larger than the ABC FoV. If the tiling is set to anything other than 11 (no tiling), the software will instruct the operator where to move the telescope between exposures.

The "Image Request" window allows the operators to use the ABC for other observations. They can change the RA and Dec, the shutter position, focus position,
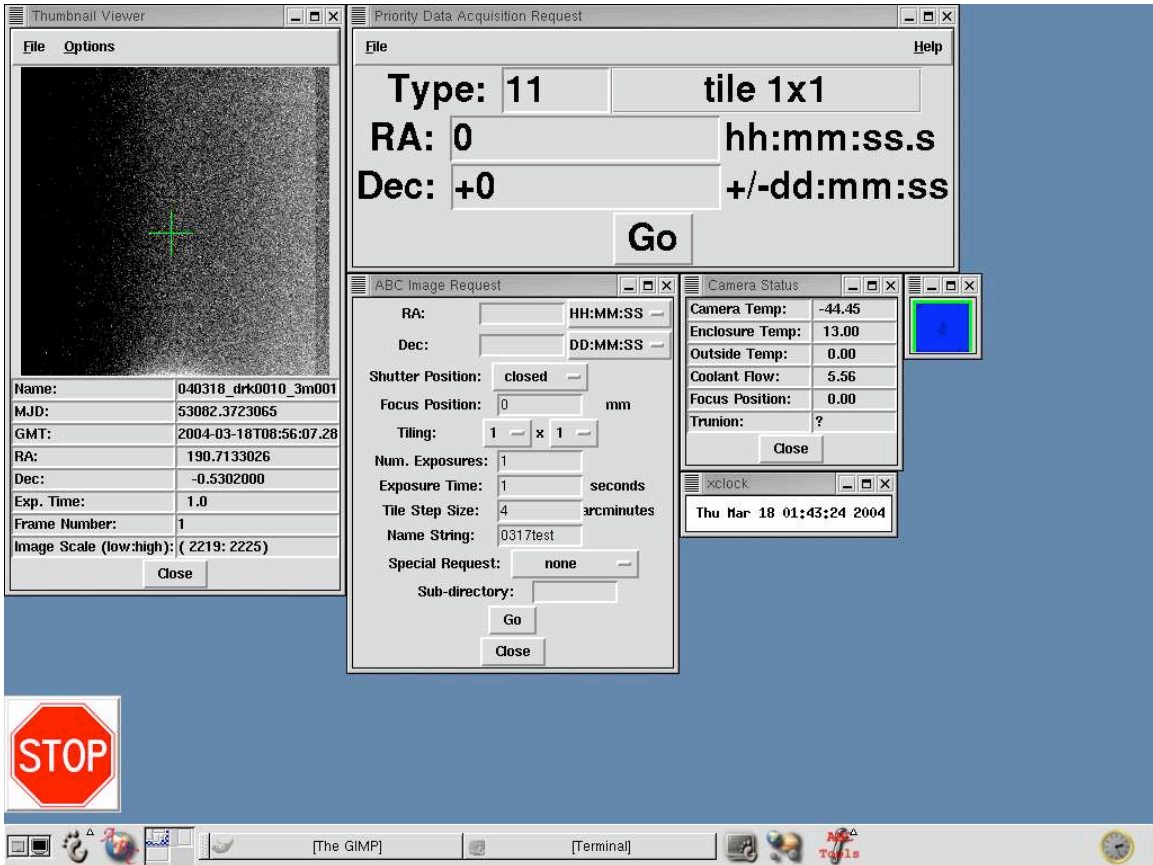
Figure 2.4 Screenshot of the ABC Interface, exactly as the operators use it. The "Priority Data Acquisition Request" window is what the operators use to get images of GRBs.

tiling, number of exposures, exposure length (from 0.1s to 180s), tile step size (for when there is tiling), name string, and sub-directory. Special request provides a drop down menu programmed with some of the common types of observations the operators like to make with presets for the other fields). The sub-directory and name string fields allow the operators to customize the names of the files so that they are easy to find and to store them in a sub-directory of their choosing.

The "Thumbnail Viewer" shows the most recent image taken by the ABC. This is updated automatically after each image is taken. The thumbnail allows the operators to verify that the focus is good, and that the image matches the finding chart supplied by the fax. This image is also available on the AEOS console through a video feed.

The "Camera Status" window allows the operators to monitor the ABC. It displays the temperature of the CCD camera, the temperature of the ABC enclosure, and the flow rate of the coolant for the ABC.

The stop sign button permits the operators to cancel any remaining images that are queued. This allows them to stop taking images, or to start a new set of exposures, with different parameters.

The "CD Creator" window, not shown, lets the operator quickly and easily create CDs of the ABC data. The raw images are copied to a specified location on the Control Computer, and the CD Creator calculates how many CDs are required to copy those files, and prompts the operator for CDs. Once the CDs are created, the operator can then mount the CDs on another computer that is connected to the Internet which can then send the data to a computer in Michigan.

CHAPTER III

ABC Data Analysis

3.1 Introduction

The previous chapter described the AEOS telescope and ABC, and how the ABC observed GRB afterglows just minutes after the GRB was detected. This chapter will describe what happens to the data once it is taken, how GRB optical afterglows are detected in the ABC data, and how the results are reported to the community.

Before the data can be analyzed, it must be transferred to the University of Michigan. The AEOS operators copy the data to CDs, and the CDs are inserted in a computer with Internet access so that the files can be downloaded to Michigan. It takes a day or more to get the data, to allow the operators to transfer the data to disks, and mount them on the FTP computer for remote access. The data consists of a series of 10-second image files that are not processed in any way. These images are formatted as Flexible Image Transport System (FITS) files, which accommodates a very customizable header and multiple arrays of data, that can be defined by the user.

Once the data is received in Michigan, the entire batch is processed through an analysis pipeline. Designed specifically for ABC images, it handles one field at a time and one day of data at a time. The pipeline is written in C, Perl and IDL, and

27

is reasonably fast, requiring an hour or two to analyze the data from a typical GRB response. The pipeline consists of several steps, which include image correction, source extraction, astrometry, photometry, and searching for the afterglow. Each of these steps are described in the following sections.

3.2   Image Correction

The first step in the pipeline is image correction. This usually consists of subtracting the dark image (an image of the same exposure length, but with the shutter closed) from a raw image, and dividing the difference by a flat field (see Equation 3.1).

$$(3.1) \qquad\qquad corrected = (raw - dark)/flat$$

Unlike ROTSE, which takes dark images every night, the ABC only performs this function once or twice a year. These exposures are counted against the ABC allotment of observing time. Despite these limitations, the dark images work quite well. To create the dark, the ABC takes a series of 10 images, with the shutter closed, of (usually) 10 second exposures, and median them together to produce the standard dark that is subtracted from the raw images. A set of darks of other exposure lengths also exists for use on other (non-GRB) observations, with different durations.

Two methods for creating a flat field for the ABC have been tried but with no success. In the first method, the operators take a series of images of random parts of the sky, and then take a median of those images to get a sky flat. Another way to make a flat is to take a series of images at twilight, and then take the median of those to get a twilight flat. The problem with using either of these flats is that there is a significant amount of stray light entering the ABC, and this stray light

changes throughout the observations, thus making it appear as though the flat field is changing with time. Using the same flat field on these images causes the magnitude calculations for various parts of the images to be much higher or much lower than their true magnitudes. Since this is already the case for the images (without a flat field correction), no flat is used.

The ABC image correction does not use a flat field, so the resulting formula for image correction is actually Equation 3.2. The resulting FITS image, the corrected image (regardless of formula used), is called a "c" file. By doing relative photometry on these images or by limiting the photometry to stars near the afterglow, both described in (Section 3.6), it is possible to get accurate photometry without a flat field.

$$(3.2) \qquad\qquad corrected = raw - dark$$

An example of an ABC image can be seen in Figure 3.1. This is an image, corrected by subtracting a dark frame. The contrast is inverted to make it easier to print. This is a very crowded field for the ABC; many of the PSFs of the stars overlap. Most of the stray light is visible as crescent shapes in ABC images. The quantity of stray light is highly variable between different fields and observations at different times. The crescent shapes and the variability of stray light is due to light that enters near the secondary mirror, which is not large enough in diameter to block this light. The vignetting, which looks like a slightly darker circle, is equally variable, depending on the sky brightness and other factors. Because of the problems with the variable stray light and vignetting, no flat fields are used. There are additional problems with the photometry because of this, which can be avoided by using only nearby stars for the photometry, or if the field allows, by using relative photometry.
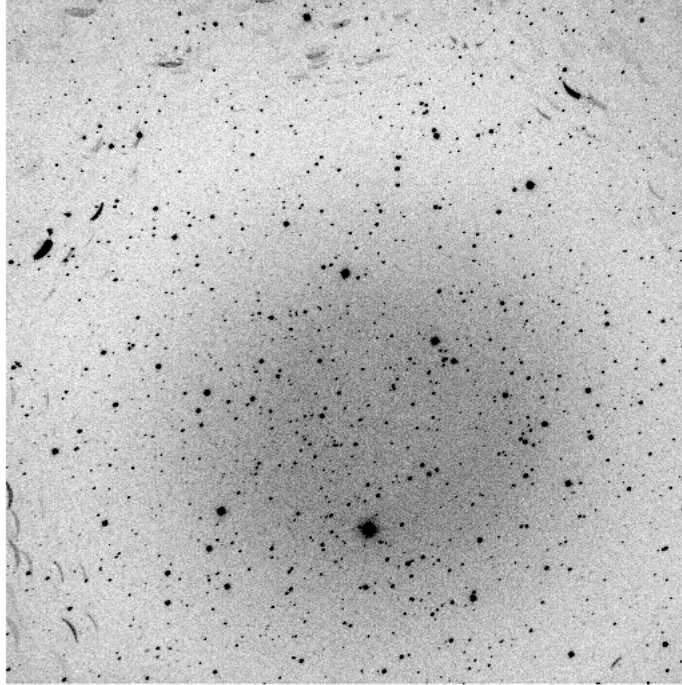
Figure 3.1 Example of a 10s image from the ABC, dark subtracted, and with the colors inverted. Stray light, in the form of crescent shapes, is visible on the edges of the image. Some of the stray light also looks like stars (point like objects). Vignetting is also present, causing the round shape that is slightly darker than the rest of the image.

This is explained in more detail in the Photometry Section (Section 3.6).

3.3   Source Extraction

The next step in the pipeline, once the images are corrected, is to find all the sources in the image. This is done using SExtractor (Source Extractor), a public code that is designed to find all the sources in an astronomical image. There are many ways to configure it, ways to modify how it find objects, and ways to configure the output files. The ABC configuration files are modified from the ROTSE configuration files.

The version of SExtractor that was used for ABC data is version 2.2.2, and it was configured to find all interesting objects in an ABC image, assuming that the FWHM is roughly 8 pixels. SExtractor finds everything: stars, galaxies, rocks, stray

light, hot pixels, cosmic rays hits, ice crystals, UFOs, etc. Once SExtractor has found the sources in the image, it creates two new FITS files: a "sky" FITS file, and an "sobj" FITS file. The sky file is a 64x65 pixel map of the background, as determined by SExtractor. The sobj file is the source object file, which for each star contains a list of x and y position, the flux and magnitude calculated by SExtractor, as well as other quantities such as the flux radius, elongation, ellipticity, etc. The x and y positions, flux and magnitudes are input for astrometry and photometry; the other information is used to discriminate real objects from stray light. Once SExtractor has created the sobj and sky files, it is time to move onto the next step, establishing the astrometry.

3.4   Astrometry

Finding the astrometry, the mapping between the x and y positions of the objects, and their RA and Dec is one of the trickier parts of the ABC analysis. This mapping (which is also known as a warp) is important, because the x and y positions of each star within the image is known, but the RA and Dec of each star is not, and is needed in order to compare to star catalogs. Complications occur because there are often not enough stars to do the astrometry in an automated way, there is too much stray light that looks suspiciously like real stars, or the telescope may not be centered on the correct RA and Dec. There are two steps to doing astrometry. The first step is to match the stars in the ABC images to a star catalog, using one of two methods: the automated way, in which the computer makes the matches, or the manual way, where the human does the work. The second step is to create a calibrated object ("cobj") file once the astrometry is found. Programs were written in IDL and Perl to accomplish each of these steps.

The easiest way to match to a star catalog is the automated method, however there are many cases for which it can fail. In the automated way, the 35 brightest point sources in an image with a small FWHM and small flux radius are selected, as well as the 35 brightest stars from a star catalog, within a 3' radii from the RA and DEC of the observations. These restrictions attempt to select objects that are mostly consist of stars, and not galaxies or stray light. These two lists of objects are fed into a triangle matching routine, which attempts to find similar triangles between sets of stars. Triangle matching is robust: only a 50% overlap between the 2 sets of objects is required for triangle matching to map the image's stars to a star catalog. Triangle matching is also fast: with 35 stars, it only takes a few seconds to find a match. Once the triangle matching routine is completed, if it was successful, there will be a mapping between the ABC stars and the catalog stars, and it is possible to calculate how to warp the ABC x and y coordinates to determine the RA and Dec of the ABC stars.

There are many instances where the automated astrometry routines do not work. This occurs when there is an abundance of stray light, making it difficult to differentiate between stray light and stars. If more than half of the bright objects selected are stray light, this method will not work. If there are not enough stars in the field (less than 10), there may not be enough to use triangle match. With a 6'x6' field of view, this happens about a third of the time. Also, if the field is unusually crowded, there may be problems as well, because for very crowded fields, the star catalogs are not as accurate, and what is listed as a bright star in the star catalog might be 5 (or more) fainter stars in the ABC image, and those would not make a brightness cut. Rather than tweak the automated routines to get special cases to work, a manual method of finding the astrometry was created.

The manual method of astrometry is slower because it requires matching pairs of stars in the star catalog and the ABC images to be selected by eye, but it always works. First, the manual astrometry program displays an image of the Digitized Sky Survey (DSS) field on the left, and the ABC image on the right. To find the astrometry, 3 stars are selected on the DSS field, and their ABC counterparts are selected on the ABC image. Once the three pairs of stars are selected, the software creates a 4th "star" by taking the average of the position of the 3 stars in the DSS field and in the ABC image. To create a warp between the RA and DEC and the x and y positions, there needs to be at least 4 points, and it is easier to create a star rather than to select a 4th star. This method is slower than the automated method, because it takes time to select the stars manually, but it will work on any of the images for which the automated way does not work.

Once a warp is found between the catalog stars and the ABC image, using either the automated way or the manual way, the next step is to create a cobj file. This file contains each object detected by SExtractor (real or not), and for each object, the RA, DEC (which are calculated from the warp), the x and y position, magnitude, magnitude error, FWHM, and a few other items from SExtractor. The magnitudes are offset by the median (usno magnitudes - ABC magnitudes), and the headers in the cobj file and c file are modified to have the correct RA and DEC and kx, ky (for warping).

3.5 Coadding images

Once the astrometry is done, it is usually a good time to determine if the images need to be coadded. There are several reasons why the images are coadded, and why longer exposures are not taken. The optical afterglow or surrounding stars may be

too faint to be well detected in single images, leading to large errors in the magnitude, and also difficulties extracting a magnitude. Coadding images together improves the limiting magnitude, improves the magnitude errors, and improves the detection of fainter objects. Such improvements can also be achieved by taking longer exposures, except that in the case of the ABC, the AEOS is an alt-az mount, so the stars rotate with time, and long exposures create star trails.

There are several steps to coadding an image. Before the files are coadded, the astrometry must be completed to rotate and move the images to line up the stars. From this set, one is selected to be the reference image, usually the first of the series. The others are then rotated and translated using the astrometry to match them to the reference image and then the corrected (dark subtracted) files are summed up. From there, it is necessary to rerun SExtractor, and recalculate the astrometry, because the images are deeper, and therefore there are more stars. Once those steps are done, the coadded image is ready for photometry.

3.6 Photometry

The next step in the pipeline is to perform the photometry to find the brightness of the objects in the image and to calibrate them to known stars. The photometry on the ABC images is difficult because there are often different problems with the images. The types of problems encountered determines the type of photometry that is done. There are two types of photometry programs for the ABC images: aperture photometry, and point spread function (PSF) photometry. Once the photometry is done, it is calibrated to the United States Naval Observatory (USNO) or Sloan Digital Sky Survey (SDSS) catalogs, and sometimes, after that calibration, relative photometry is done as well.

The ABC images present different challenges and it is impossible to find one specific method to analyze all the data. The problems include the FWHM of the stars, the numbers of stars, the stray light, and lack of calibration to star catalogs. The first problem is that the FWHM of different images can vary between 4 to 15 pixels. Not only is the seeing highly variable at Haleakala, but also the focus may still be tweaked by telescope operators during the early images. If the images contains many stars they will be blended together on some images, but not others. It also makes the photometry harder because the errors will be higher if the FWHM is larger, and fainter stars will disappear. Another complication is that there might not be enough stars to do good photometry. With a 6'x6' field of view, it is often the case that there are only 5-10 stars present on the entire image. Stray light is also an issue because it can often look like stars, making it difficult to find the astrometry, or to differentiate the stray light from the GRB afterglow. Stray light can also look like extended shapes, and this can make stars appear to be brighter than they actually are if the stars are mixed in with the stray light. Another obstacle is possible lack of good calibrated magnitudes from the USNO (or other catalogs). This happens in very crowded fields because the ABC has a much better spatial resolution than the USNO, so objects that appear to be stars in the USNO may actually be multiple stars in the ABC.

Aperture photometry is one of the ways to perform photometry with the ABC. This is done by summing up the flux in a circle surrounding a star, and subtracting off the sky. SExtractor does this calculation when it finds the sources in the image, but even if it is not done through SExtractor, this step is fast. Unfortunately, this type of photometry has problems when the images do not have a uniform background, because it overestimates or underestimates the background, which in turn causes the

calculated magnitude to be incorrect.

The other way to do photometry with the ABC is by doing point spread function (PSF) photometry. To do this, the PSF for a collection of stars is found. These are stars that are chosen because they are not too faint, or too bright, and they are not extended objects, like galaxies. A Gaussian is fit to each reference star, and from this the PSF is determined, and used to calculate the magnitudes for the other stars in the image. This method is slower, but yields much better results for fainter objects and crowded fields. We use the ROTSE Photometry (RPHOT) software, designed by Robert Quimby, for ROTSE images, but have made some small modifications so that it can handle ABC images. The preference is to use RPHOT for the ABC data, and if that fails, then to use aperture photometry.

Once the photometry is completed, the magnitudes of the objects need to be calibrated to a star catalog, usually either USNO or SDSS. The easiest way to calibrate to the USNO (or SDSS, if available), is to take bright, but unsaturated stars that are within an arcminute of where the afterglow is, find the median offset, and apply that offset. The offset is calculated by finding the USNO R band magnitudes of a set of stars, and subtracting from that the raw ABC magnitude of those same stars. Calibrating the magnitudes by applying a uniform offset to all is usually not the most accurate, for three reasons. First, there are usually not many stars available to use because the ABC images go much fainter than the USNO catalog and the field of the ABC is so small. Calculating the median offset is better when there are a lot of calibration stars in the field. Second, the ABC is an unfiltered camera but the magnitudes are calibrated to the R (or r) band. The unfiltered ABC images contain light from about 400 nm-900 nm, but the R band sees only light between 589 nm and 727 nm. Two stars with the same R magnitude may have completely different

magnitudes in other bands, so that on the ABC's unfiltered images, one star could be much brighter than the other, even though they both have the same R magnitude. Third, there may be large amounts of vignetting or stray light, making stars appear fainter or brighter than they should, which skews the offset.

One of the ways to address the difficulties with just calibrating all the star magnitudes to an offset is to use relative photometry. Unfortunately, the ABC fields are often too sparse to use this technique. For each image, all of the bright, non-saturated USNO stars within an arcminute are used. The USNO R magnitude for each of these stars is subtracted from the ABC magnitude, and then a linear function of x and y is fit, mapping the differences between the ABC magnitudes and the USNO magnitudes. This is good for when there are a lot of stars, and when the background near the afterglow can be approximated by a linear fit.

3.7   Afterglow Search

Once the astrometry and photometry is completed, it is time to search for the afterglow. There are two types of searches, depending on what's reported on the GCN before the data is analyzed. One type of search is appropriate when the location of the OT is known, and the other is initiated when there is no detection of an afterglow. This section discusses both of these searches, and explains what happens after the afterglow is found, or not found.

The easiest case is if the location of the afterglow is reported on the GCN. Once the astrometry is done, it is simple to find out if there is an object at (or near) the location reported in the GCN. This can be done by querying the cobj file to find out if SExtractor found any objects at that location. As a sanity check, we look at the image to determine if the OT is believable. Depending on what the detection looks

like, the images may be coadded to get deeper detections.

If there are no detections of the afterglow by the time the ABC data is analyzed, the error box is searched to determine if there is a measurable afterglow, or only a limiting magnitude. The search is limited to the BAT error circle, or if there is an XRT position, to the XRT error circle which is smaller and more accurate. First, we look for objects that are not in either the DSS or the SDSS (if there is SDSS data for this field). If no new objects are found, we calculate and report the limiting magnitude. If new objects are seen, we need to determine if they are the GRB afterglow or some other artifact. There are a number of checks to determine if the new object is a GRB afterglow, or something else. First, the new object can't move between frames. If it does, it is likely either stray light, rocks, a satellite, or some other moving object. Second, if the object is fainter than the faintest USNO stars for that field, it's likely not the OT, and observations a day or so later can verify its non-fading nature. Third, the new object must look star-like, and not extended (this excludes faint galaxies and stray light, which often takes interesting shapes). To date, no afterglows in the ABC data have been found that were not already reported on the GCN. This is because 24-48 hours have passed before we get the data (if not longer), and most astronomers report their findings, especially if they see an afterglow, within a few hours of the GRB detection.

Depending on what is found in the ABC data, a GRB Coordinates Network (GCN) circular is written, and sent out. The GCN circulars are short reports written by GRB observers which describe the telescope and details of follow-up GRB observations. If the afterglow is seen in the ABC data, the magnitude, time, and a decay rate, which is calculated from ABC data and other GCN data is written up as a circular and submitted. If no afterglow is seen in the ABC data, and the ABC observations are

deeper and earlier than other observations already reported, a circular is submitted stating the limiting magnitude of the observations and the times at which they occurred. Both of these types of circulars help other astronomers plan out their observations.

3.8   Lightcurve Construction

This step is done after the GRB afterglow is detected, and usually concurrent with, or after the afterglow is reported to the GCN. To create a light curve, the cobj files are used, as well as the magnitudes for the afterglow, and several nearby stars, as calculated by RPHOT. First the afterglow magnitude and the time at which it was observed is found in the files, and magnitude vs time is plotted. Nearby stars vs time are also plotted, to see if they vary, which they shouldn't. If the magnitudes of the nearby stars vary, the photometry analysis is redone, with more careful selection of reference stars. Nearby USNO stars are also checked, to make sure that they are properly calibrated, and have magnitudes close to what they should have. Some discrepancies are to be expected, as the ABC is unfiltered, and the star catalog is in the R band. If the nearby stars do not vary, and are reasonably close to the expected USNO magnitudes, the lightcurve undergoes other calculations. First, the decay rate(s) are calculated for ABC data combined with ROTSE (and sometimes other) data. The formula for this is $m \propto t^{-\alpha}$, where m is the magnitude, t is the seconds from when the GRB occurred, and α is the decay rate. Next, the magnitudes are converted to flux density, to make it easier to compare ABC observations to other bands (X-ray, Gamma-Ray, or other optical bands). Converting the ABC magnitudes to flux density is also useful for comparing ABC data to GRB afterglow theory.

3.9 Grating Analysis

For a few of the bursts, a blazed transmission grating was in place, and this changed some of the analysis steps. The images look different from the typical unfiltered images, as can be seen in Figure 4.1. The image correction and source extraction, and coadding steps are identical for both the grating images and the unfiltered images. The differences occur for finding the astrometry and the photometry, and there is an additional step for constructing a spectrum. Finding the OT and constructing a lightcurve, once the astrometry and photometry are done, are identical whether the images are taken with or without a grating.

3.9.1 Astrometry

The first difference between the grating and unfiltered analysis occurs with the astrometry. The automated method is not possible with the grating images, due to the difficulty of differentiating between the 0th and 1st order with certainty, and also because there is usually only a small (less than 10) number of 0th order stars, making it difficult to do astrometry on the 0th order stars.

The manual method for finding astrometry, already discussed previously, works without any modification. Three bright stars are chosen on the DSS side, and three corresponding 0th order counterparts are chosen on the ABC side from which the astrometry is calculated. To keep things simple, the astrometry is tied to the 0th order parts of the stars, because the 1st order shapes of the stars can vary, depending on the color of the stars. Basing the astrometry calculations on the 1st order part of the stars may cause slight shifts in the astrometry, particularly if 3 different stars are chosen for the astrometry. To prevent these complications, the 0th order parts of the stars are used for the astrometry.

3.9.2 Photometry

The next difference between the grating and unfiltered analysis occurs with the photometry.

As can be seen in Figure 4.1, each object consists of a "dot" and a "line". The "dot" is the 0th order part of the spectrum and the "line" is the 1st and 2nd order part of the spectrum. A magnitude can be calculated from each segment, however the 1st and 2nd order are more complicated, because the 2nd order, which is much fainter, overlaps with the 1st order. Because of the faintness, the 2nd order is ignored. Both 0th order and 1st order magnitude calculations have complications which prevent PSF magnitudes from being calculated, so aperture photometry is used. The 0th order is always much fainter, because the grating is blazed and designed so that the maximum efficiency peaks in the first order at 640 nm. Only the brightest stars have a 0th order, and there are often not enough stars present to calculate a PSF, therefore aperture photometry must be used for the 0th order. For the first order, there is significant variability between different stars, as the 1st order is a spectrum (but a low R 10 resolution) of the stars, so it is not possible to get a PSF of the star, so aperture photometry is the only way to find the magnitude of the 1st order.

It is a good check to verify that for a given object that both the 0th and 1st order magnitudes are similar, as can be seen for GRB 060708.

3.9.3 Extracting a Spectrum

The purpose of grating images is to construct a spectrum. A software package was written to extract a spectrum, and this package assumes that the astrometry is tied around the 0th order part of the object. The software first rotates the image so that the 0th and 1st order are horizontal. Since the grating sits in the ABC for extended

periods of time, the angle of the grating is known, and programmed directly into the software. The first step, once the image is rotated, is that a set number of pixels are summed up vertically, to get the intensity for each horizontal position (which translates into a wavelength). The background is calculated by summing up the background pixels far from the object, and subtracted from the intensity. Aperture photometry is then used to calculate the magnitude of the 0th order object, using the IDL astrolib routines.

To use the package, one tells the software the image name, RA, and Dec at a minimum, as well as a few other tweaks as needed. An image and spectrum is plotted as output, as seen in Figure 3.2. The RA and DEC of the object is printed on the top of the plot, for easy reference. The wavelength scale is plotted on the subimage, and the number of pixels from the 0th order are plotted on the spectrum. The 0th order magnitude is calculated, as well as an array of pixels vs intensity.
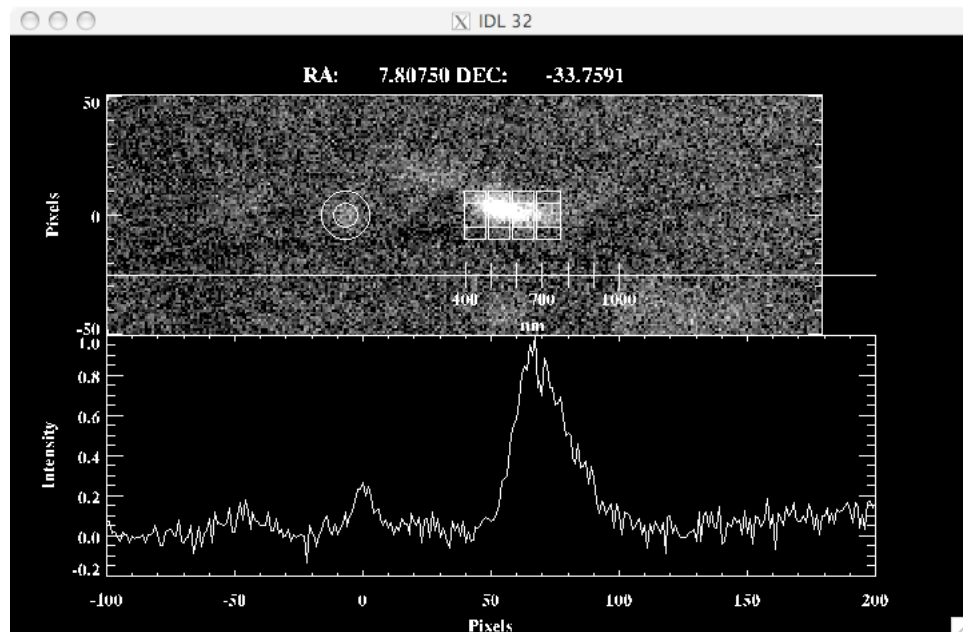
Figure 3.2 Example of a spectrum. The top portion has been rotated so that the star (0th and 1st order) is horizontal, the bottom portion is the spectrum.
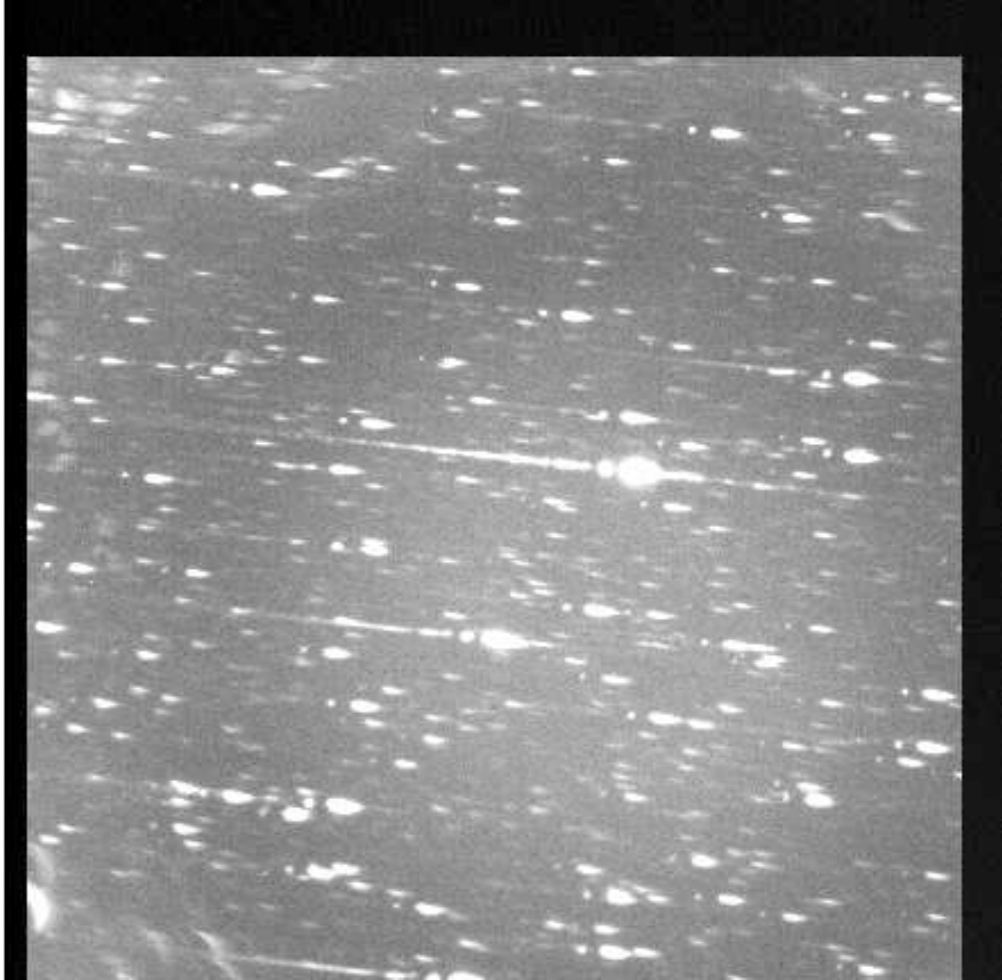
Figure 3.3 Example of a grating image, stars and other objects that look like exclamation points.

CHAPTER IV

ABC Observations

4.1 Introduction

Since the launch of $Swift$, ABC has taken data on 21 of the 50 faxed or "called-in" GRBs. Of the 29 unobserved GRB fields, bad weather prevented 19, equipment failure prevented 3, 5 were not observed because the AEOS is closed on the weekends, and 2 were not observed because this experimenter was not alerted, and the operators won't observe a GRB without confirmation that the fax was triggered by a bona fide event.

A table of the 21 GRBs for which there is ABC data is listed below. $Swift$ detected all but two of these GRBs; INTEGRAL detected the remaining. Of these observed GRBs, 10 had an afterglow visible to the ABC, described in Section 4.3, 4 had interesting upper limits, described in Section 4.5, and 7 were not interesting, either because the limits were not as deep as other limits or because there was an afterglow present, but the magnitude was fainter than the ABC's limiting magnitude.

4.2 Data Analysis

This chapter includes the data from both the ROTSE telescopes and the ABC instrument, but the data analysis is different between them. There are three cases

GRB	Satellite	Filter	First usable ABC image	ABC detection	OT detected
050906	Swift	grating	15m	no	no
050925	Swift	grating	13m	no	no
051117B	Swift	grating	14m	no	no
060108	Swift	grating	6m	no	yes
060110	Swift	unfiltered	77m	yes	yes
060116	Swift	unfiltered	7m	yes	yes
060202	Swift	grating	6m	no	yes
060428B	Swift	grating	5m	no	yes
060510B	Swift	grating	10m	no	yes
060708	Swift	grating	17m	yes	yes
060912	Swift	grating	11m	no	yes
060923C	Swift	unfiltered	11m	no	yes
060930	INTEGRAL	unfiltered	11m	no	no
070208	Swift	unfiltered	12m	yes	yes
070419A	Swift	unfiltered	58m	yes	yes
070518	Swift	unfiltered	30m	yes	yes
070529	Swift	unfiltered	6m	yes	yes
071003	Swift	unfiltered	8m	yes	yes
071011	Swift	unfiltered	49m	yes	yes
071021	Swift	unfiltered	10m	no	IR
080613A	INTEGRAL	unfiltered	17m	yes	yes

Table 4.1 GRBs with ABC data. First usable ABC image refers to the first useful image, not necessarily the first image. This happens when the OT is near the edge of the error circle, and not yet part of the ABC field of view.

to consider: unfiltered ABC data, ABC data with a grating, and ROTSE data.

The unfiltered ABC data was explained in detail in the previous chapter, so will only be briefly discussed here. The steps, once the data is transferred to Michigan, is to first subtract the darks from the raw images and then find the sources in the images using SExtractor, perform the astrometry and the photometry. The images are coadded after the astrometry step, if needed, in which case the steps involving SExtractor, astrometry, and photometry are redone.

The ABC images with a grating are a bit more difficult. These were also discussed in the previous chapter. The steps are identical until the astrometry step. This has to do with the differences of the PSFs on the grating images and unfiltered images. On an unfiltered image, a point source will look like a Gaussian. On a grating image, a point source will look like an exclamation point. Depending on the spectral distribution of the point source the position and length of the line will move, relative to the point. Standard astrometry and photometry methods will not work here.

The ROTSE analysis is similar to the unfiltered ABC image analysis. The ROTSE data is automatically analyzed with a software pipeline in realtime. The images are dark-subtracted and flat-fielded, and have been calibrated to the USNO A2.0 R catalog. More details of the data analysis is described in Eli Rykyoff's dissertation (Rykoff, 2005). The images are already processed, and are usually coadded by others and ready for photometry. Often, the analysis is already done and limits can be extended from the GCN. Photometry for detections can be redone using RPHOT (described in the previous chapter), to get more careful measurements, and to calibrate the magnitudes to the USNO B1.0 R2 catalog.

4.3 Detections

For the following text, each section of GRB data is laid out chronologically. First the $Swift$ BAT observations are discussed, which include the trigger number, the date and time of the detection, the BAT error circle, the T_{90} duration of the burst, and the fluence. Then, the $Swift$ XRT and UVOT observations are discussed, which include any fading XRT or UVOT counterparts that may have been found, or limits, and other interesting objects nearby. Next, other optical detections that were interesting (but not all of them) are reported, including a redshift, if one was detected, is reported. These observations are not reported in the order that they occurred on the GCN, but by wavelength (γ, X-ray, UVOT, optical). Finally, the ABC observations are reported, as those are usually some of the last observations to be reported on the GCN, so it seems fitting that they are the last to be described in each section. In each section is also a table and plot of ABC data, and in the next chapter is the theoretical explanation of the ABC data.

4.4 Initial GRB detection - gamma-ray data

All but one of the optically detected GRBs were detected by the $Swift$ satellite. For each of these bursts, the time (UT), trigger number, error circle radius, $T_{90}(s)$, fluence (15-150keV), and the references for this information are given in Table 4.2. The other burst (GRB 080613A) was detected by INTEGRAL, and details about its detection are included in the GRB 080613A section.

4.4.1 GRB 060110: The First ABC detection

Due to the moon observing constraint, there were no early XRT or UVOT observations. XRT observations started at 2.8 days, and a faint fading counterpart was

GRB	Time (UT)	trigger	error circle	$T_{90}(s)$	Fluence(15-150keV)	References
060110	08:01:17	176702	3'	17 ± 2	$1.4 \pm 0.1 \cdot 10^{-6} erg/cm^2$	1, 2
060116	08:37:27	177533	3'	113 ± 10	$2.6 \pm 0.3 \cdot 10^{-6} erg/cm^2$	3, 4
060708	12:15:59	217805	3'	9.8 ± 1.0	$5.0 \pm 0.4 \cdot 10^{-7} erg/cm^2$	5, 6
070208	09:10:34	259714	3'	48 ± 2	$4.3 \pm 1.0 \cdot 10^{-7} erg/cm^2$	7, 8
070419A	09:59:26	276205	3'	116 ± 6	$5.6 \pm 0.8 \cdot 10^{-7} erg/cm^2$	9, 10
070518	14:26:21	279592	3'	5.5 ± 0.2	$1.6 \pm 0.2 \cdot 10^{-7} erg/cm^2$	11, 12
070529	12:48:28	280706	3'	109 ± 3	$2.6 \pm 0.2 \cdot 10^{-6} erg/cm^2$	13, 14
071003	07:40:55	292934	3'	150 ± 10	$8.3 \pm 0.3 \cdot 10^{-6} erg/cm^2$	15, 16
071011	12:40:13	293924	3'	61 ± 1	$2.2 \pm 0.2 \cdot 10^{-6} erg/cm^2$	17, 18

Table 4.2 $Swift$ BAT information for GRBs observed with the ABC.
(1) (Zane et al., 2006), (2) (Zane et al., 2006), (3) (Campana et al., 2006a), (4) (Barthelmy et al., 2006), (5) (Moretti et al., 2006), (6) (Fenimore et al., 2006) , (7) (Sato et al., 2007), (8) (Markwardt et al., 2007), (9) (Stamatikos et al., 2007b), (10) (Stamatikos et al., 2007a), (11) (Guidorzi et al., 2007a), (12) (Krimm et al., 2007) , (13) (Holland et al., 2007), (14) (Parsons et al., 2007), (15) (Schady et al., 2007), (16) (Ukwatta et al., 2007) (17) (Marshall et al., 2007), (18) (Sakamoto et al., 2007b)

GRB	$\delta t(s)$	X-ray afterglow?	References
060110	242210	Y	(Page et al., 2006)
060116	154	Y	(Campana et al., 2006b)
060708	62	Y	(Fenimore et al., 2006)
070208	116	Y	(Markwardt et al., 2007)
070419A	113	Y	(Stamatikos et al., 2007b)
070518	70	Y	(Guidorzi et al., 2007a)
070529	131	Y	(Holland et al., 2007)
071003	22335	Y	(Starling & Schady, 2007)
071011	2963	Y	(Sbarufatti et al., 2007b,a)
080613A	24378	Y	(Guidorzi & Markwardt, 2008)

Table 4.3 $Swift$ XRT information for GRBs observed with the ABC. $\delta t(s)$ is when XRT observations started, counting from when the GRB was detected.

found (Page et al., 2006). PAIRITEL was the first to find the counterpart in the near IR (Bloom, 2006), with coordinates of α 04:50:57.85 and δ +28:25:55.7 (J2000.0). There were few other detections by other telescopes, mostly because of the brightness of the moon. ROTSE-IIIb, located at McDonald Observatory, Texas, responded to GRB 060110, with the first image starting at 08:01:44.8 UT (27.1 seconds after the burst). The unfiltered images were calibrated relative to USNO A2.0 R-band. The optical counterpart, which was originally detected by (Bloom, 2006), was seen in the ROTSE images, and reported in a GCN circular (Rujopakarn et al., 2006). The optical counterpart was only marginally detected because of the brightness of the moon.

The ABC started observing GRB 060110 at 08:05:19.18 UT ($\sim$ 5 minutes after the trigger) and ending at 09:37:53.68 UT. These are a series of 10s unfiltered exposures. The ABC images were centered on the BAT coordinates, but the optical counterpart was later found to be just outside of the 3' radius BAT error box. Because the AEOS is an alt-az mount, the field rotates with time, and unfortunately the first hour of images did not contain the optical counterpart. The ABC images were calibrated using the USNO B 1.0 R2 catalog. The optical counterpart was present in the ABC images, the magnitude was calculated, and a circular was sent out (Swan et al., 2006e). Table 4.4 shows the optical photometry for GRB 060110 from ROTSE-IIIb and ABC. The ROTSE photometry is from (Rujopakarn et al., 2006), the ABC photometry has been analyzed as described in Chapter III. Figure 4.1 shows the lightcurve for GRB 060110, containing both ROTSE and ABC data.

4.4.2 GRB 060116: The Dark Burst

$Swift$ XRT observations started at 154s after the burst was detected. Nothing was immediately detected (Campana et al., 2006a), ground analysis revealed an X-ray

Telescope	Filter	$t_{mid}(s)$	Magnitude
ROTSE-IIIb	None	61.5 ± 34.5	16.0 ± 0.2
ROTSE-IIIb	None	99.1 ± 10.0	15.2 ± 0.2
ABC	None	4626 ± 184	18.70 ± 0.12
ABC	None	5003 ± 184	18.64 ± 0.20
ABC	None	5379 ± 184	18.51 ± 0.15

Table 4.4 ABC and ROTSE optical photometry for GRB060110. All times are in seconds since the burst time, 08:01:17 UT. ROTSE photometry is from (Rujopakarn et al., 2006)
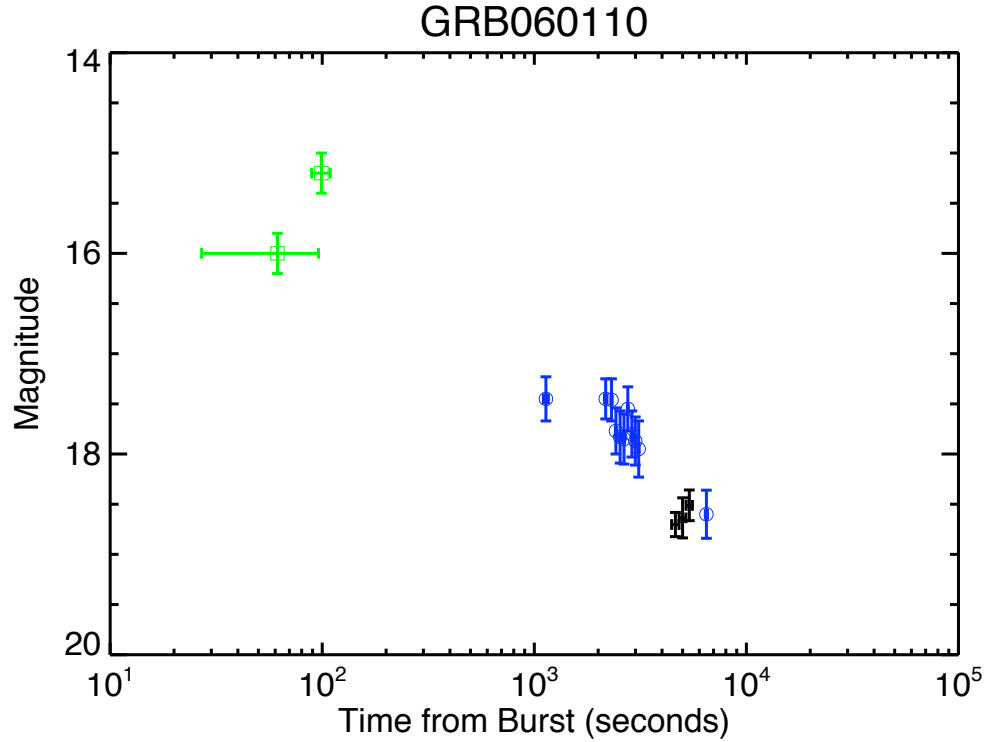
Figure 4.1 Lightcurve for 060110, including prompt data from ROTSE-IIIb and early data from the ABC. Black points represent ABC data, green points represent ROTSE data, blue points with error bars are from (Cenko et al., 2008), and the rest is from the GCN.

counterpart (Campana et al., 2006b). Later XRT observations and analysis showed the X-ray counterpart decayed as $t^{-\alpha}$, with $\alpha = -0.95 \pm 0.07$, and with no flare activity (Campana et al., 2006c). $Swift$ UVOT observations started at 153s after the burst was detected, no afterglow was found in a 200s V band exposure (Campana et al., 2006a).

The United Kingdom Infra-Red Telescope (UKIRT) at Mauna Kea was the first to detect the optical counterpart, with coordinates of $\alpha 05 : 38 : 46.280, \delta -05 : 26 : 13.14$ (J2000.0) (Kocevski et al., 2006). These observations started at 9:42:00UT, cited no variability, and reported a J band magnitude of $J = 18.3 \pm 0.1$. Other telescopes observed GRB 060116, and reported upper limits, but no confirmation of the UKIRT counterpart. ROTSE-IIIb had early upper limits of GRB 060116 (Rykoff et al., 2006c).

The ABC started observing GRB 060116 at 08:45:11 UT and ending at 09:09:38 UT, in a series of unfiltered 10 second images. This was about 7 minutes after the burst was detected by $Swift$, and due to the lack of an optical counterpart detection by other telescopes, the images were coadded. The ABC images were calibrated using the USNO B 1.0 R2 catalog. The optical counterpart was present in the ABC images, the magnitude was calculated, and a circular was sent out (Swan et al., 2006a).

Once the ABC had confirmed GRB 060116 in the optical, this prompted further investigations with ROTSE data. The counterpart is present in the ROTSE-IIIb data, when it is carefully coadded and analyzed. Several GCNs (Piranomonte et al., 2006) (Tanvir et al., 2006) (Grazian et al., 2006) report observations that have a large photometric redshift (z=6.6).

Table 4.5 shows the optical photometry for GRB 060116 from ROTSE-IIIb and

Telescope	Filter	$t_{mid}(s)$	Magnitude
ROTSE-IIIb	None	99.05 ± 20.27	17.760 ± 0.358
ROTSE-IIIb	...	113.27 ± 34.40	18.509 ± 0.597
ROTSE-IIIb	...	199.82 ± 39.40	18.215 ± 0.454
ROTSE-IIIb	...	229.17 ± 68.74	18.478 ± 0.521
ABC	None	553.13012 ± 89.6000	20.2689 ± 0.0700581
ABC	None	741.13016 ± 89.6000	20.8083 ± 0.107511
ABC	None	929.08019 ± 89.5500	20.9878 ± 0.0928131
ABC	None	1117.0302 ± 89.5999	21.0347 ± 0.113751
ABC	None	1399.6301 ± 184.200	21.4077 ± 0.132154
ABC	None	1766.6800 ± 174.050	21.7805 ± 0.219328

Table 4.5 ABC and ROTSE optical photometry for GRB060116. All times are in seconds since the burst time, 08:37:27 UT

ABC. The ROTSE photometry is described in Section 4.2, the ABC photometry has been analyzed as described in Chapter III. Figure 4.2 shows the lightcurve for GRB 060116, containing both ROTSE and ABC data.

4.4.3 GRB 060708: The Only ABC GRB with Color Information

$Swift$ XRT observations started at 12:17:01 UT, 62 seconds after the BAT trigger, and a bright fading X-ray source was located (Fenimore et al., 2006). UVOT observations started 72 seconds after the BAT trigger, and a candidate was located at α 00:31:13.85 δ -33:45:32.4, with an estimated white band magnitude of 17.4 ± 0.5. Further $Swift$ UVOT detections were obtained in all filters except M2 and W2, suggesting a photometric redshift of $z = 1.8$ (Schady & Moretti, 2006).

There were few optical observations of this burst. PROMPT reported optical limits of $z' > 19$ at 15.7 hours after the burst, $i' > 19.2$ at 18.6 hours, and $r' > 19.3$ at 15.7 hours (Parris et al., 2006). The other optical observations were with the VLT, which reports a mag of $R = 22.9$ at 1.778 days after the burst, and a redshift of $z < 2.3$. The nearby galaxy (8 arcsec south of the afterglow) was found to have a mag of $R = 19.5$, and a redshift of $z = 0.249$ (Jakobsson et al., 2006b).

The ABC started observing GRB 060708 at 12:33:14.2 and ending at 14:16:21.8
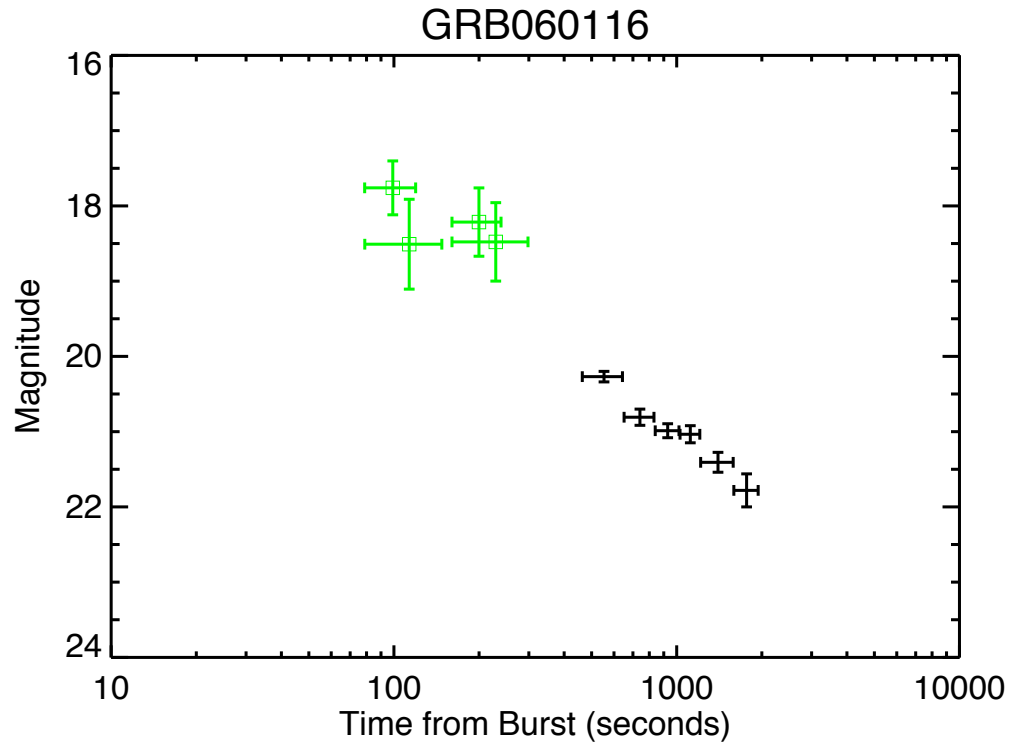
Figure 4.2 Lightcurve for 060116, including prompt data from ROTSE-IIIb (green) and early data from ABC(black).

UT. These are 10s images obtained with a low resolution diffraction grating. The images are coadded in sets of ten (except for the first set). ABC photometry was calibrated to the USNO B1.0 R2 magnitude of the nearby 14th magnitude star, due to the sparse nature of the field. The optical counterpart was detected and the results reported as a GCN circular (Swan et al., 2006d).

The photometry for GRB 060708 was done in a couple of different ways, due to the diffraction grating. The diffraction grating splits the light into different orders, but most goes into the 0th and 1st orders. Aperture photometry was done first on the 0th order (which looks like a typical Gaussian), and then on the 1st order (which looks like an elongated Gaussian). Next, a spectrum was constructed for the afterglow for each coadded image, to see if there was any variability in the spectrum.

Table 4.6 shows the optical photometry for GRB 060708 from the ABC, this is the 0th and 1st order photometry. Both 0th and 1st order photometry follow a similar decay rate and when calibrated to the nearby 14th mag star have similar magnitudes. The ABC photometry has been analyzed as described in Chapter III. Figure 4.3 shows the 0th and 1st order lightcurve for GRB 060708.

4.4.4 GRB 070208

$Swift$ XRT observations started 116s after the burst, and an X-ray counterpart was found (Markwardt et al., 2007). $Swift$ UVOT observations started 119s after the burst, with a 100s exposure in the white filter (160nm-650nm), but no afterglow was detected (Markwardt et al., 2007).

Of the ground based optical observations, ROTSE-IIIb was the first to report their findings on the GCN (Yuan et al., 2007). ROTSE-IIIb automatically responded to the GCN alert, but it was already too faint to be seen by ROTSE, despite the speed. The Faulkes North telescope was the first to report a fading afterglow, located at α

Telescope	Order	$t_{mid}(s)$	Magnitude
ABC	0th	1362 ± 327	17.68 ± 0.22
ABC	0th	1788 ± 90	17.42 ± 0.13
ABC	0th	3055 ± 90	18.33 ± 0.26
ABC	0th	3243 ± 90	17.76 ± 0.15
ABC	0th	3431 ± 90	18.28 ± 0.17
ABC	0th	3619 ± 90	17.82 ± 0.11
ABC	0th	3807 ± 90	18.61 ± 0.21
ABC	0th	3995 ± 90	18.56 ± 0.19
ABC	0th	6015 ± 90	18.48 ± 0.16
ABC	0th	6203 ± 90	18.81 ± 0.20
ABC	0th	6391 ± 90	18.40 ± 0.13
ABC	0th	6579 ± 90	18.71 ± 0.15
ABC	0th	6767 ± 90	18.53 ± 0.14
ABC	0th	6955 ± 90	18.58 ± 0.14
ABC	0th	7143 ± 90	18.68 ± 0.18
ABC	1st	1362 ± 327	17.64 ± 0.03
ABC	1st	1788 ± 90	17.88 ± 0.03
ABC	1st	2867 ± 90	18.11 ± 0.03
ABC	1st	3055 ± 90	18.21 ± 0.03
ABC	1st	3243 ± 90	18.27 ± 0.03
ABC	1st	3431 ± 90	18.24 ± 0.03
ABC	1st	3807 ± 90	18.32 ± 0.03
ABC	1st	3995 ± 90	18.37 ± 0.03
ABC	1st	6015 ± 90	18.61 ± 0.03
ABC	1st	6391 ± 90	18.66 ± 0.03
ABC	1st	6579 ± 90	18.72 ± 0.03
ABC	1st	6767 ± 90	18.74 ± 0.03
ABC	1st	6955 ± 90	18.87 ± 0.03

Table 4.6 ABC optical photometry for GRB060708. All times are in seconds since the burst time, 12:15:59 UT
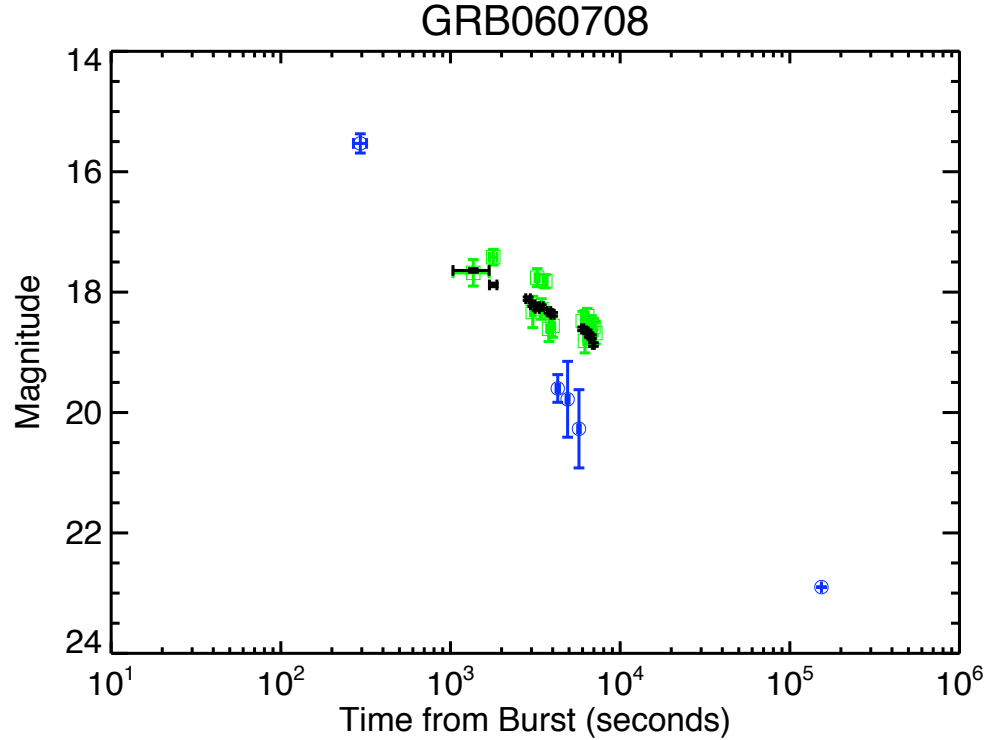
Figure 4.3 Lightcurve for GRB 060708, 0th (green) and 1st (black) order broadband data from ABC spanning from 1300 seconds to 7000 seconds, and the blue points are from the GCN.

13:11:32.51 δ +61:57:54.5 (J2000.0) (Guidorzi et al., 2007b). Palomar-60 confirmed Faulkes' findings (Fox et al., 2007), PAIRITEL saw an IR counterpart as well (Bloom, 2007), and there are many other optical observations (including the ABC's, explained below). Gemini-North observed this GRB with a spectrograph and found the redshift to be 1.165 (Cucchiara et al., 2007a).

ABC observations started at 09:22:38 UT (12 minutes after the burst) and ended about 45 minutes later. These consisted of 10 second unfiltered images, which were then coadded together. ABC photometry was calibrated to SDSS data, provided by (Cool et al., 2007). Due to the sparse nature of the field, the optical counterpart was calibrated to the nearby star at α 13:11:32.95 δ+61:57:57:41, which has a magnitude of $r = 19.301$. The optical counterpart was detected and reported as a GCN Circular (Swan et al., 2007e).

Telescope	Filter	$t_{mid}(s)$	Magnitude
ROTSE-IIIb	None	43.0 ± 2.5	< 16.0
ROTSE-IIIb	None	74.0 ± 33.5	< 17.5
ROTSE-IIIb	None	263.1 ± 147.5	< 18.2
ABC	None	814 ± 90	19.75 ± 0.05
ABC	None	1002 ± 90	19.75 ± 0.06
ABC	None	1190 ± 90	19.63 ± 0.05
ABC	None	1378 ± 90	19.74 ± 0.05
ABC	None	1566 ± 90	19.74 ± 0.06
ABC	None	1754 ± 90	19.76 ± 0.06
ABC	None	1951 ± 99	20.02 ± 0.06
ABC	None	3042 ± 90	20.44 ± 0.09
ABC	None	3239 ± 99	20.53 ± 0.11

Table 4.7 ABC and ROTSE optical photometry for GRB070208. All times are in seconds since the burst time, 09:10:34 UT

Table 4.7 shows the optical photometry for GRB 070208 from ROTSE-IIIb and ABC. The ROTSE upper limits are from (Yuan et al., 2007), and the ABC photometry has been analyzed as described in Chapter III. Figure 4.4 shows the lightcurve for GRB 070208, containing ABC data.

4.4.5 GRB 070419A

Swift XRT observations started at 113s after the burst, and found a bright, fading, and uncatalogued X-ray source, which they identify as the X-ray afterglow (Stamatikos et al., 2007b). *Swift* UVOT observations started at 115s after the burst, with a 400s V band exposure, but no afterglow was initially detected (Stamatikos et al., 2007b). Later analysis revealed a V magnitude of 20.2 ± 0.3 in a 394s exposure starting at 115s and ending at 515s (Landsman & Stamatikos, 2007).

The earliest optical observations, from ROTSE-IIIb, are images beginning at 81.2 s after the burst (Schaefer et al., 2007). These images were limiting magnitudes, with no counterpart detected. The optical counterpart was first detected by KAIT, in an unfiltered image starting at 10:05:19UT with coordinates α 12:10:58.82 δ +39:55:33.9 (J2000.0) (Chornock et al., 2007). Palomar-60 observed this counterpart fade by
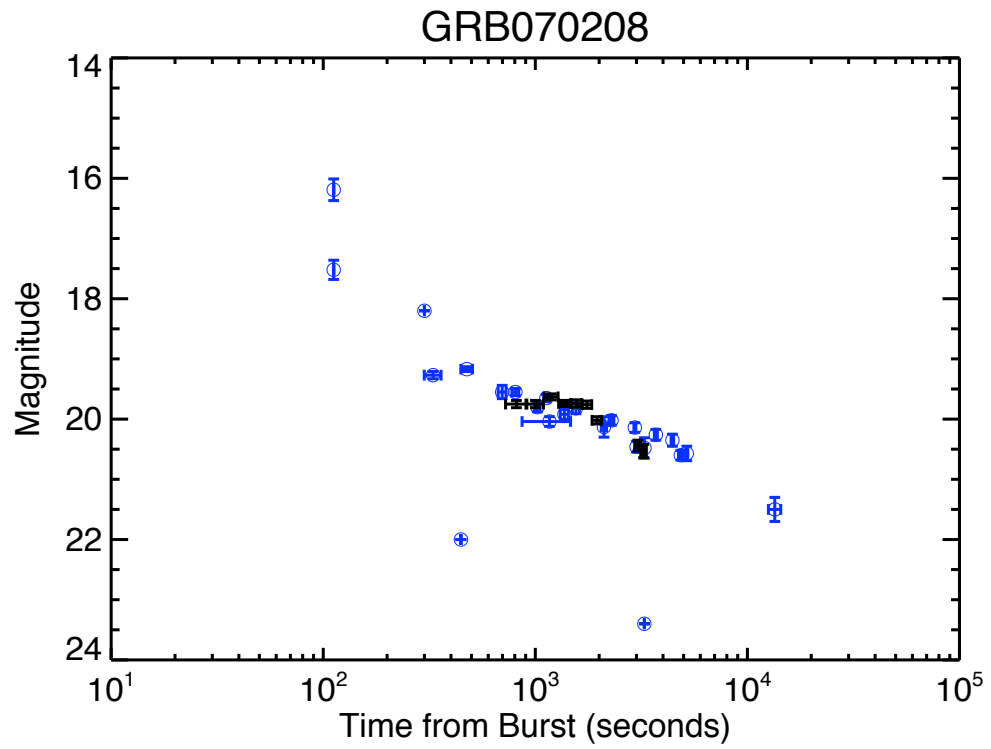
Figure 4.4 Lightcurve for 070208, with data from ABC spanning from 800 seconds to 3200 seconds. The black points represent the ABC data, and the blue points are from (Cenko et al., 2008) and the GCN.

one magnitude in the space of 5 minutes, confirming that it is the counterpart for GRB 070419A (Cenko & Fox, 2007). UKIRT observed the counterpart in the IR, starting 39 minutes after the burst, and it was detected in J, H, and K band (Rol et al., 2007). About 1.6 hours after the burst, a spectrum was taken with the Low-Resolution Imaging Spectrometer mounted on the 10-m Keck I telescope, and a redshift of $z = 0.91$ was found for the host galaxy of GRB 070419A (Cenko et al., 2007). There were many other observations for this GRB, these were the first and most notable observations.

The ABC observations started at 10:57:41UT ($\sim$ 58 minutes after the trigger) and ended at 11:53:52UT. These are 10s unfiltered exposures, and they were coadded into sets of 10 and sets of 20. These observations are calibrated to the SDSS. The optical counterpart was detected and reported to the GCN (Swan et al., 2007a).

Table 4.4.5 shows the optical photometry for GRB 070419A from ROTSE-IIIb and ABC. The ROTSE upper limits are from (Schaefer et al., 2007), the ABC photometry has been analyzed as described in Chapter III. Figure 4.5 shows the lightcurve for GRB 070419A, containing ABC data.

4.4.6 GRB 070518: The Twilight Burst

$Swift$ XRT observations started at 70s after the burst, and a counterpart was found and reported (Guidorzi et al., 2007a). UVOT observations started at 82s with the white filter, in a 100s exposure, and a counterpart was found (Guidorzi et al., 2007a). Refined analysis (Cucchiara et al., 2007b) show the afterglow to be clearly detected in all 7 filters, suggesting a redshift lower than 0.7.

The ground based optical observations started with a report from Xinglong (Xin et al., 2007a), which confirmed the UVOT detection. These observations started at 512s after the burst, and found the optical counterpart to have a a magnitude of $R =$

Telescope	Filter	$t_{mid}(s)$	Magnitude
ROTSE-IIIb	None	83.7 ± 2.5	< 16.0
ROTSE-IIIb	None	114.7 ± 33.5	< 17.8
ABC	None	3585 ± 90	20.54 ± 0.08
ABC	None	3773 ± 90	20.65 ± 0.07
ABC	None	3961 ± 90	20.56 ± 0.05
ABC	None	4150 ± 90	20.65 ± 0.07
ABC	None	4338 ± 90	20.72 ± 0.05
ABC	None	4526 ± 90	20.96 ± 0.10
ABC	None	4715 ± 90	20.92 ± 0.06
ABC	None	4903 ± 90	21.15 ± 0.09
ABC	None	5091 ± 90	21.01 ± 0.09
ABC	None	5280 ± 90	21.10 ± 0.09
ABC	None	5468 ± 90	21.13 ± 0.08
ABC	None	5656 ± 90	21.14 ± 0.09
ABC	None	5845 ± 90	21.70 ± 0.27
ABC	None	6033 ± 90	21.28 ± 0.11
ABC	None	6316 ± 184	21.24 ± 0.07
ABC	None	6692 ± 184	21.39 ± 0.07

Table 4.8 ABC optical photometry for GRB0070419A. All times are in seconds since the burst time, 09:59:26 UT. In this figure, the ABC data is represented as the black points, and the blue points are from the GCN and (Cenko et al., 2008).
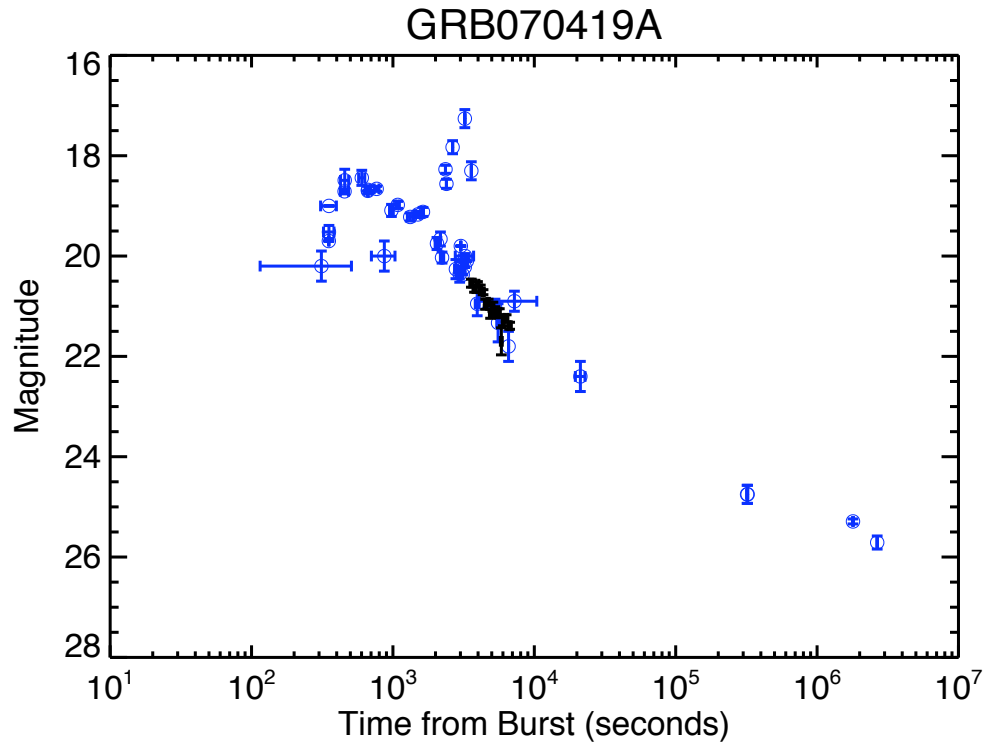
Figure 4.5 Lightcurve for 070419A, with data from ABC spanning from 3500 seconds to nearly 6900 seconds. Black points represent ABC data, and blue points represent data from the GCN and from (Cenko et al., 2008).

Telescope	Filter	$t_{mid}(s)$	Magnitude
ABC	None	1820 ± 52	19.58 ± 0.38
ABC	None	1933 ± 52	20.02 ± 0.15
ABC	None	2046 ± 52	20.30 ± 0.16
ABC	None	2231 ± 124	20.17 ± 0.15

Table 4.9 ABC optical photometry for GRB070518. All times are in seconds since the burst time, 14:26:21 UT

19.84 at 32.73 minutes after the burst. Observatorio Sierra Nevada (8.6hrs) (Jelinek et al., 2007), Telescopio Nazionale Galileo (35hrs) (Covino et al., 2007), MAGNUM telescope (10.6 minutes) (Price & Minezaki, 2007), and the Large Binocular Telescope (17hrs) (Garnavich et al., 2007) also observed GRB 070518.

ABC observations started during twilight, at 14:55:49 UT and ended at 15:04:00 UT. Because of twilight, the images were coadded to allow for detection of the afterglow, and were calibrated to USNO A2.0 R band star (R=18.7) located at α 16:56:47.44 δ +55:17:45.6. This star was chosen so as to be consistent with other GCN observations.

Table 4.4.6 shows the optical photometry for GRB 070518 from the ABC. The ABC photometry has been analyzed as described in Chapter III. Figure 4.6 shows the lightcurve for GRB 070518, containing ABC and GCN data.

4.4.7 GRB 070529

$Swift$ XRT began observing 131s after the burst was detected, and found a fading counterpart (Holland et al., 2007). The XRT began observing in AUTO state 131s after the BAT trigger in window timing mode, with a total exposure of 11.6s, switching to photon counting mode after 13s. Seven observations in photon counting mode followed, for a total exposure time of 120 ks, with monitoring of the X-ray afterglow lasting one week. The UVOT began observing 134s after the burst was detected, and found an afterglow candidate, located at α 18:54:58.19 δ 20:39:34.00

Figure 4.6 Lightcurve for 070518, there is only about 5 minutes of ABC data represented as the black points, data from the GCN (blue) is also included.
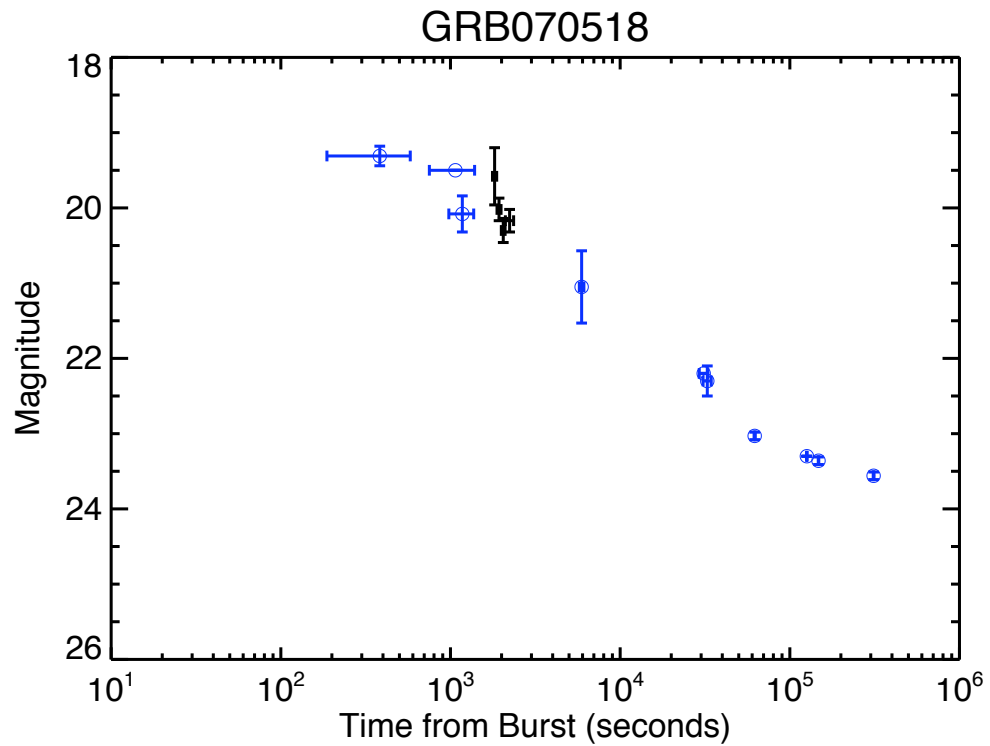
(Holland et al., 2007). The UVOT continued observations (in V,B, and U bands) for about a week, with a final detection occurring about 2.7 days after the burst (See Table 4.4.7)

GRB 070529 occurred in a very crowded part of the sky, making it difficult for most telescopes to observe it. Other than ABC and UVOT, only MIRO (a 1.2m telescope) reported a faint source in a crowded field (Baliyan et al., 2007). Gemini North took a spectrum of the afterglow, and found a redshift of $z = 2.4996$ (Berger et al., 2007).

ABC observations started at 12:53:53 UT and ended at 15:17:49 UT. These are 10s unfiltered exposures. The optical counterpart was seen, and reported on the GCN (Swan et al., 2007c). There are several issues to point out. The first issue is that the first few images are thrown out, because for the first few images, the GRB field happened to be right at zenith. There was too much rotation present, and the stars were streaked too much, and by variable amounts. The first usable image occurred at 12:55:04UT (396s after the burst). The second issue is that there are several gaps in the data. When an XRT position is found, if the Rice University CCD camera (RUCCD) is online, then data taking alternates between the ABC and the RUCCD. The RUCCD was taking data during the ABC gaps. Unfortunately, RUCCD did not see anything.

The ABC photometry has been analyzed as described in Chapter III, but this is by far the trickiest set of data to analyze. The ABC images were initially calibrated to USNO B1.0, however the crowding in the field presented some problems. To counteract this, stars which were reasonably well measured (not too faint, not too bright) were selected, and UVOT V band magnitudes were extracted for these stars. The ABC was then calibrated to these magnitudes. Another issue was the significant

vignetting and stray light present (and the quantity of stars and images for which to make quality checks). This is the only set of data for which relative photometry was possible and necessary.

Table 4.4.7 shows the optical photometry for GRB 070529 from the ABC, and Table 4.4.7 shows the photometry from the UVOT for GRB 070529. Figure 4.7 shows the lightcurve for GRB 070529, containing ABC and UVOT data.
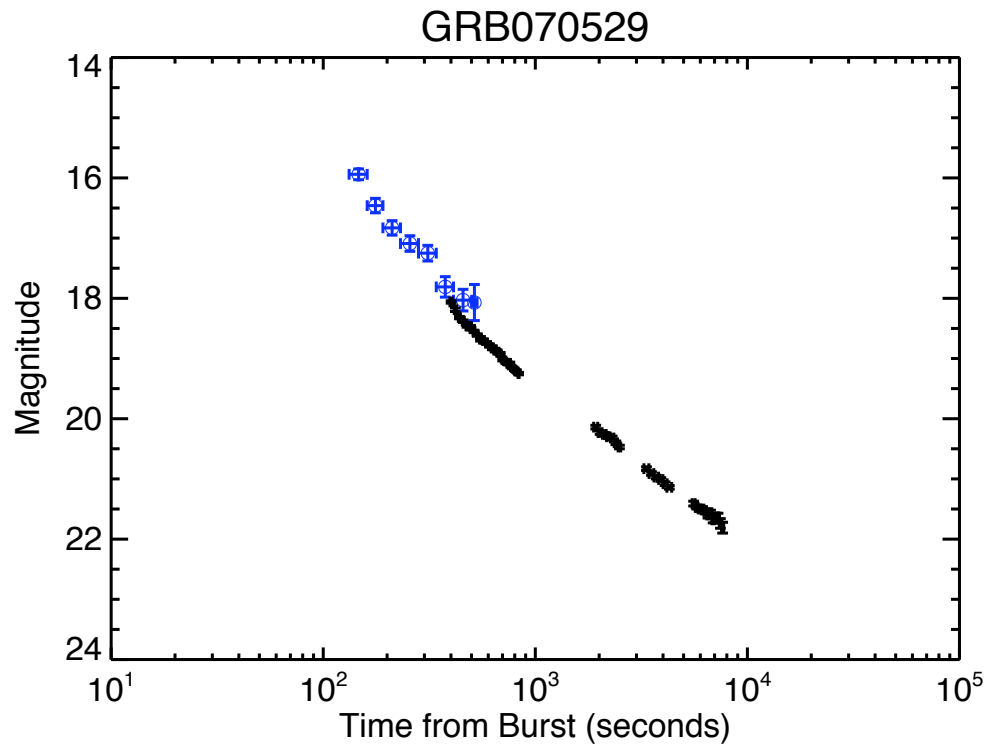
Figure 4.7 Lightcurve for 070529, several hours of ABC data. The ABC data is represented as the black points, and the UVOT V band is represented as the blue points. The U band and the upper limits are not plotted here.

4.4.8 GRB 071003: The Hockey Stick GRB

There were no prompt XRT or UVOT observations, because $Swift$ was returning to normal operations (Ukwatta et al., 2007). XRT observations started later than normal, at 22ks, and a faint afterglow was found (Starling & Schady, 2007).

KAIT was the first to detect and report an optical afterglow, with imaging starting

Telescope	Filter	$t_{mid}(s)$	Magnitude
ABC	none	400.9 ± 5.0	18.06 ± 0.02
ABC	none	419.7 ± 5.0	18.19 ± 0.03
ABC	none	438.6 ± 5.0	18.32 ± 0.02
ABC	none	457.5 ± 5.0	18.38 ± 0.02
ABC	none	476.3 ± 5.0	18.46 ± 0.02
ABC	none	495.1 ± 5.0	18.47 ± 0.02
ABC	none	513.9 ± 5.0	18.55 ± 0.02
ABC	none	532.8 ± 5.0	18.61 ± 0.02
ABC	none	551.7 ± 5.0	18.68 ± 0.03
ABC	none	570.5 ± 5.0	18.70 ± 0.02
ABC	none	589.3 ± 5.0	18.74 ± 0.02
ABC	none	608.1 ± 5.0	18.79 ± 0.02
ABC	none	626.8 ± 5.0	18.82 ± 0.03
ABC	none	645.6 ± 5.0	18.86 ± 0.03
ABC	none	664.4 ± 5.0	18.90 ± 0.02
ABC	none	683.2 ± 5.0	18.92 ± 0.02
ABC	none	702.0 ± 5.0	19.02 ± 0.02
ABC	none	720.8 ± 5.0	19.04 ± 0.02
ABC	none	739.6 ± 5.0	19.08 ± 0.02
ABC	none	758.4 ± 5.0	19.08 ± 0.02
ABC	none	777.3 ± 5.0	19.15 ± 0.02
ABC	none	796.1 ± 5.0	19.18 ± 0.02
ABC	none	814.9 ± 5.0	19.21 ± 0.02
ABC	none	833.8 ± 5.0	19.25 ± 0.02
ABC	none	1926.5 ± 42.7	20.14 ± 0.03
ABC	none	2020.7 ± 42.7	20.23 ± 0.03
ABC	none	2114.8 ± 42.7	20.26 ± 0.03
ABC	none	2209.0 ± 42.7	20.30 ± 0.03
ABC	none	2303.2 ± 42.8	20.32 ± 0.03
ABC	none	2397.6 ± 42.7	20.40 ± 0.03
ABC	none	2491.8 ± 33.2	20.47 ± 0.03
ABC	none	3341.5 ± 89.7	20.83 ± 0.03
ABC	none	3529.9 ± 89.7	20.91 ± 0.03
ABC	none	3718.1 ± 89.8	20.97 ± 0.03
ABC	none	3906.5 ± 89.8	21.01 ± 0.03
ABC	none	4095.0 ± 89.8	21.08 ± 0.03
ABC	none	4283.3 ± 110.8	21.14 ± 0.03
ABC	none	5577.7 ± 89.6	21.41 ± 0.04
ABC	none	5765.8 ± 89.6	21.47 ± 0.03
ABC	none	5953.8 ± 89.6	21.50 ± 0.04
ABC	none	6141.7 ± 89.6	21.50 ± 0.04
ABC	none	6329.7 ± 89.6	21.54 ± 0.04
ABC	none	6517.7 ± 89.6	21.60 ± 0.05
ABC	none	6705.7 ± 89.6	21.56 ± 0.04
ABC	none	6893.7 ± 89.6	21.68 ± 0.05
ABC	none	7081.7 ± 89.6	21.67 ± 0.05
ABC	none	7269.7 ± 89.6	21.63 ± 0.06
ABC	none	7457.7 ± 89.6	21.74 ± 0.08
ABC	none	7645.7 ± 89.7	21.81 ± 0.09

Table 4.10 ABC optical photometry for GRB070529. All times are in seconds since the burst time, 12:48:28 UT

Telescope	Filter	$t_{mid}(s)$	Magnitude
UVOT	V	146.8 ± 14.4	15.94 ± 0.09
UVOT	V	176.2 ± 15.0	16.46 ± 0.12
UVOT	V	211.2 ± 20.0	16.83 ± 0.12
UVOT	V	256.2 ± 25.0	17.09 ± 0.13
UVOT	V	311.2 ± 30.0	17.25 ± 0.13
UVOT	V	376.2 ± 35.0	17.81 ± 0.17
UVOT	V	456.2 ± 45.0	18.03 ± 0.18
UVOT	V	516.2 ± 15.0	18.07 ± 0.30
UVOT	V	660.2 ± 9.5	> 18.78
UVOT	V	797.2 ± 9.5	> 18.95
UVOT	V	1054.2 ± 190.5	19.15 ± 0.20
UVOT	V	10544.2 ± 335.5	20.88 ± 0.43
UVOT	V	12615.7 ± 197.0	> 20.23
UVOT	V	17302.2 ± 1295.5	> 20.92
UVOT	V	23079.7 ± 1301.0	20.50 ± 0.35
UVOT	V	28988.2 ± 1177.5	> 20.92
UVOT	V	37056.2 ± 3227.5	20.72 ± 0.32
UVOT	V	44436.7 ± 3080.0	> 20.60
UVOT	V	57772.2 ± 4833.5	20.42 ± 0.30
UVOT	V	70120.2 ± 5621.5	20.92 ± 0.19
UVOT	V	89979.7 ± 8922.0	20.28 ± 0.17
UVOT	V	112734.7 ± 9489.0	20.83 ± 0.17
UVOT	V	139081.7 ± 12434.0	20.35 ± 0.14
UVOT	V	170065.7 ± 15105.0	21.52 ± 0.27
UVOT	V	199141.7 ± 9429.0	20.78 ± 0.16
UVOT	B	616.2 ± 4.5	> 19.21
UVOT	B	752.2 ± 4.5	> 19.17
UVOT	U	596.2 ± 9.5	20.12 ± 0.36
UVOT	U	733.2 ± 9.5	20.17 ± 0.41
UVOT	U	234548.7 ± 21074.0	23.68 ± 0.33
UVOT	U	278347.2 ± 17470.5	> 23.92
UVOT	U	601823.2 ± 41264.5	> 24.53

Table 4.11 UVOT optical photometry for GRB070529. All times are in seconds since the burst time, 12:48:28 UT

42 seconds after the burst. The afterglow position is located at α 20:07:24.12 δ 10:56:51.8 (J2000.0), with an unfiltered magnitude of 12.8 at 42s after the BAT trigger (Li et al., 2007). This data was later analyzed and submitted as a paper in (Perley et al., 2008)

Many other telescopes detected this burst. Notable detections include Keck I, with observations occurring between 9523s and 682940s, Gemini-S, with detections around 231174s, and P60, with observations between 176s and 2618s (Perley et al., 2008).

ABC observations started at 07:49:31.56 UT, roughly 9 minutes after the GRB was detected, and ended at 09:05:37.20 UT. Additional images were obtained starting at 11:07:31.57 UT, but the seeing had degraded to the point that the optical counterpart was no longer visible. Photometry was difficult because of the proximity of a nearby 10th magnitude star. Observations are calibrated to USNO B1.0 R2 band. The initial findings were submitted as a GCN circular (Swan et al., 2007d).

Tables 4.4.8, 4.4.8 , 4.4.8 , 4.4.8 and 4.4.8 show the optical photometry for GRB 071003 from the ABC. The ABC photometry has been analyzed as described in Chapter III. Figure 4.8 shows the lightcurve for GRB 071003.

4.4.9   GRB 071011

$Swift$ XRT observations did not start until 13:28:40UT, because of an Earth limb constraint. An X-ray afterglow was detected for GRB 071011, and was later found to fade with a powerlaw decay with slope -1.0 ± 0.7, (Sbarufatti et al., 2007b,a). There were no UVOT observations for this burst, as the UVOT was in safe mode (Marshall et al., 2007).

The Palomar 60' telescope was the first to find the optical counterpart for this afterglow (Cenko, 2007), with an $R = 17.92$ at 12:43:38 UT. LRIS confirms the

Telescope	Filter	$t_{mid}(s)$	Magnitude
ABC	None	522 ± 5	16.08 ± 0.01
ABC	None	540 ± 5	16.14 ± 0.01
ABC	None	559 ± 5	16.22 ± 0.01
ABC	None	578 ± 5	16.28 ± 0.01
ABC	None	597 ± 5	16.33 ± 0.01
ABC	None	616 ± 5	16.38 ± 0.02
ABC	None	634 ± 5	16.44 ± 0.01
ABC	None	653 ± 5	16.49 ± 0.02
ABC	None	672 ± 5	16.54 ± 0.02
ABC	None	691 ± 5	16.60 ± 0.02
ABC	None	709 ± 5	16.62 ± 0.02
ABC	None	728 ± 5	16.67 ± 0.02
ABC	None	747 ± 5	16.73 ± 0.02
ABC	None	766 ± 5	16.77 ± 0.02
ABC	None	785 ± 5	16.81 ± 0.02
ABC	None	803 ± 5	16.86 ± 0.02
ABC	None	822 ± 5	16.89 ± 0.02
ABC	None	841 ± 5	16.93 ± 0.02
ABC	None	860 ± 5	16.97 ± 0.02
ABC	None	879 ± 5	17.03 ± 0.02
ABC	None	897 ± 5	17.02 ± 0.02
ABC	None	916 ± 5	17.05 ± 0.02
ABC	None	935 ± 5	17.10 ± 0.02
ABC	None	954 ± 5	17.12 ± 0.02
ABC	None	973 ± 5	17.15 ± 0.02
ABC	None	991 ± 5	17.17 ± 0.02
ABC	None	1010 ± 5	17.21 ± 0.02
ABC	None	1029 ± 5	17.24 ± 0.02
ABC	None	1048 ± 5	17.26 ± 0.02
ABC	None	1067 ± 5	17.27 ± 0.02
ABC	None	1085 ± 5	17.30 ± 0.02
ABC	None	1104 ± 5	17.35 ± 0.02
ABC	None	1123 ± 5	17.37 ± 0.03
ABC	None	1142 ± 5	17.39 ± 0.03
ABC	None	1160 ± 5	17.43 ± 0.02
ABC	None	1179 ± 5	17.44 ± 0.03
ABC	None	1198 ± 5	17.47 ± 0.03
ABC	None	1217 ± 5	17.50 ± 0.03
ABC	None	1236 ± 5	17.51 ± 0.03
ABC	None	1254 ± 5	17.54 ± 0.03
ABC	None	1273 ± 5	17.58 ± 0.03
ABC	None	1292 ± 5	17.57 ± 0.03
ABC	None	1311 ± 5	17.58 ± 0.03
ABC	None	1330 ± 5	17.61 ± 0.03
ABC	None	1348 ± 5	17.62 ± 0.03
ABC	None	1367 ± 5	17.64 ± 0.03
ABC	None	1386 ± 5	17.67 ± 0.03
ABC	None	1405 ± 5	17.70 ± 0.03
ABC	None	1424 ± 5	17.70 ± 0.03
ABC	None	1442 ± 5	17.73 ± 0.03

Table 4.12 ABC optical photometry for GRB071003. All times are in seconds since the burst time, 07:40:55 UT

Telescope	Filter	$t_{mid}(s)$	Magnitude
ABC	None	1461 ± 5	17.70 ± 0.03
ABC	None	1480 ± 5	17.72 ± 0.03
ABC	None	1499 ± 5	17.77 ± 0.03
ABC	None	1518 ± 5	17.78 ± 0.03
ABC	None	1536 ± 5	17.81 ± 0.03
ABC	None	1555 ± 5	17.83 ± 0.03
ABC	None	1574 ± 5	17.81 ± 0.03
ABC	None	1593 ± 5	17.84 ± 0.04
ABC	None	1612 ± 5	17.85 ± 0.03
ABC	None	1630 ± 5	17.89 ± 0.03
ABC	None	1649 ± 5	17.88 ± 0.03
ABC	None	1668 ± 5	17.89 ± 0.03
ABC	None	1687 ± 5	17.90 ± 0.03
ABC	None	1706 ± 5	17.93 ± 0.03
ABC	None	1725 ± 5	17.95 ± 0.03
ABC	None	1743 ± 5	17.95 ± 0.03
ABC	None	1762 ± 5	17.97 ± 0.03
ABC	None	1781 ± 5	17.96 ± 0.04
ABC	None	1800 ± 5	18.01 ± 0.04
ABC	None	1819 ± 5	18.01 ± 0.04
ABC	None	1837 ± 5	18.01 ± 0.04
ABC	None	1856 ± 5	18.07 ± 0.04
ABC	None	1875 ± 5	18.04 ± 0.04
ABC	None	1894 ± 5	18.07 ± 0.04
ABC	None	1913 ± 5	18.08 ± 0.04
ABC	None	1931 ± 5	18.08 ± 0.04
ABC	None	1950 ± 5	18.11 ± 0.03
ABC	None	1969 ± 5	18.10 ± 0.04
ABC	None	1988 ± 5	18.17 ± 0.04
ABC	None	2007 ± 5	18.14 ± 0.04
ABC	None	2025 ± 5	18.10 ± 0.04
ABC	None	2044 ± 5	18.14 ± 0.04
ABC	None	2063 ± 5	18.16 ± 0.04
ABC	None	2082 ± 5	18.15 ± 0.04
ABC	None	2101 ± 5	18.16 ± 0.04
ABC	None	2119 ± 5	18.20 ± 0.04
ABC	None	2138 ± 5	18.17 ± 0.04
ABC	None	2157 ± 5	18.17 ± 0.04
ABC	None	2176 ± 5	18.18 ± 0.04
ABC	None	2195 ± 5	18.19 ± 0.04
ABC	None	2213 ± 5	18.15 ± 0.05
ABC	None	2232 ± 5	18.22 ± 0.04
ABC	None	2251 ± 5	18.26 ± 0.04
ABC	None	2270 ± 5	18.25 ± 0.04
ABC	None	2289 ± 5	18.23 ± 0.04
ABC	None	2307 ± 5	18.26 ± 0.04
ABC	None	2326 ± 5	18.19 ± 0.04
ABC	None	2345 ± 5	18.28 ± 0.04
ABC	None	2364 ± 5	18.24 ± 0.04
ABC	None	2383 ± 5	18.29 ± 0.04

Table 4.13 ABC optical photometry for GRB071003. All times are in seconds since the burst time, 07:40:55 UT

Telescope	Filter	$t_{mid}(s)$	Magnitude
ABC	None	2401 ± 5	18.27 ± 0.04
ABC	None	2420 ± 5	18.23 ± 0.05
ABC	None	2439 ± 5	18.30 ± 0.04
ABC	None	2458 ± 5	18.19 ± 0.05
ABC	None	2477 ± 5	18.20 ± 0.05
ABC	None	2495 ± 5	18.22 ± 0.05
ABC	None	2514 ± 5	18.31 ± 0.04
ABC	None	2533 ± 5	18.16 ± 0.06
ABC	None	2552 ± 5	18.29 ± 0.04
ABC	None	2571 ± 5	18.29 ± 0.04
ABC	None	2589 ± 5	18.31 ± 0.04
ABC	None	2608 ± 5	18.31 ± 0.04
ABC	None	2627 ± 5	18.32 ± 0.04
ABC	None	2646 ± 5	18.49 ± 0.02
ABC	None	2664 ± 5	18.35 ± 0.04
ABC	None	2683 ± 5	18.35 ± 0.04
ABC	None	2702 ± 5	18.32 ± 0.04
ABC	None	2721 ± 5	18.35 ± 0.04
ABC	None	2740 ± 5	18.38 ± 0.04
ABC	None	2758 ± 5	18.33 ± 0.04
ABC	None	2777 ± 5	18.37 ± 0.04
ABC	None	2796 ± 5	18.37 ± 0.05
ABC	None	2815 ± 5	18.45 ± 0.04
ABC	None	2834 ± 5	18.36 ± 0.04
ABC	None	2852 ± 5	18.38 ± 0.05
ABC	None	2871 ± 5	18.37 ± 0.05
ABC	None	2890 ± 5	18.39 ± 0.05
ABC	None	2909 ± 5	18.36 ± 0.04
ABC	None	2928 ± 5	18.39 ± 0.04
ABC	None	2946 ± 5	18.38 ± 0.05
ABC	None	2965 ± 5	18.40 ± 0.04
ABC	None	2984 ± 5	18.36 ± 0.04
ABC	None	3003 ± 5	18.39 ± 0.04
ABC	None	3022 ± 5	18.44 ± 0.04
ABC	None	3040 ± 5	18.41 ± 0.04
ABC	None	3059 ± 5	18.40 ± 0.05
ABC	None	3078 ± 5	18.38 ± 0.05
ABC	None	3097 ± 5	18.37 ± 0.05
ABC	None	3116 ± 5	18.41 ± 0.05
ABC	None	3134 ± 5	18.51 ± 0.04
ABC	None	3153 ± 5	18.45 ± 0.04
ABC	None	3172 ± 5	18.40 ± 0.05
ABC	None	3191 ± 5	18.38 ± 0.05
ABC	None	3210 ± 5	18.45 ± 0.05
ABC	None	3228 ± 5	18.42 ± 0.04
ABC	None	3247 ± 5	18.35 ± 0.05
ABC	None	3266 ± 5	18.42 ± 0.05
ABC	None	3285 ± 5	18.46 ± 0.05
ABC	None	3304 ± 5	18.46 ± 0.05
ABC	None	3322 ± 5	18.51 ± 0.05

Table 4.14 ABC optical photometry for GRB071003. All times are in seconds since the burst time, 07:40:55 UT

Telescope	Filter	$t_{mid}(s)$	Magnitude
ABC	None	3341 ± 5	18.43 ± 0.05
ABC	None	3360 ± 5	18.44 ± 0.04
ABC	None	3379 ± 5	18.44 ± 0.05
ABC	None	3398 ± 5	18.44 ± 0.04
ABC	None	3416 ± 5	18.42 ± 0.05
ABC	None	3435 ± 5	18.41 ± 0.05
ABC	None	3454 ± 5	18.37 ± 0.05
ABC	None	3473 ± 5	18.39 ± 0.05
ABC	None	3492 ± 5	18.44 ± 0.05
ABC	None	3510 ± 5	18.45 ± 0.04
ABC	None	3529 ± 5	18.42 ± 0.05
ABC	None	3548 ± 5	18.43 ± 0.05
ABC	None	3567 ± 5	18.43 ± 0.05
ABC	None	3586 ± 5	18.40 ± 0.05
ABC	None	3604 ± 5	18.44 ± 0.05
ABC	None	3623 ± 5	18.42 ± 0.05
ABC	None	3642 ± 5	18.27 ± 0.05
ABC	None	3661 ± 5	18.45 ± 0.05
ABC	None	3680 ± 5	18.46 ± 0.05
ABC	None	3698 ± 5	18.40 ± 0.05
ABC	None	3717 ± 5	18.45 ± 0.04
ABC	None	3736 ± 5	18.46 ± 0.05
ABC	None	3755 ± 5	18.44 ± 0.05
ABC	None	3773 ± 5	18.46 ± 0.05
ABC	None	3792 ± 5	18.45 ± 0.04
ABC	None	3811 ± 5	18.44 ± 0.05
ABC	None	3830 ± 5	18.49 ± 0.05
ABC	None	3849 ± 5	18.57 ± 0.04
ABC	None	3867 ± 5	18.43 ± 0.05
ABC	None	3886 ± 5	18.45 ± 0.06
ABC	None	4015 ± 5	18.50 ± 0.05
ABC	None	4034 ± 5	18.53 ± 0.04
ABC	None	4053 ± 5	18.48 ± 0.05
ABC	None	4072 ± 5	18.45 ± 0.05
ABC	None	4091 ± 5	18.45 ± 0.04
ABC	None	4109 ± 5	18.43 ± 0.05
ABC	None	4128 ± 5	18.43 ± 0.05
ABC	None	4147 ± 5	18.47 ± 0.05
ABC	None	4166 ± 5	18.47 ± 0.05
ABC	None	4185 ± 5	18.46 ± 0.04
ABC	None	4203 ± 5	18.45 ± 0.05
ABC	None	4222 ± 5	18.44 ± 0.05
ABC	None	4241 ± 5	18.46 ± 0.04
ABC	None	4260 ± 5	18.48 ± 0.05
ABC	None	4279 ± 5	18.46 ± 0.04
ABC	None	4298 ± 5	18.47 ± 0.05
ABC	None	4316 ± 5	18.43 ± 0.05
ABC	None	4335 ± 5	18.46 ± 0.05
ABC	None	4354 ± 5	18.48 ± 0.05
ABC	None	4373 ± 5	18.46 ± 0.05

Table 4.15 ABC optical photometry for GRB071003. All times are in seconds since the burst time, 07:40:55 UT

Telescope	Filter	$t_{mid}(s)$	Magnitude
ABC	None	4392 ± 5	18.46 ± 0.05
ABC	None	4410 ± 5	18.47 ± 0.04
ABC	None	4429 ± 5	18.46 ± 0.05
ABC	None	4448 ± 5	18.43 ± 0.04
ABC	None	4467 ± 5	18.46 ± 0.05
ABC	None	4486 ± 5	18.43 ± 0.05
ABC	None	4504 ± 5	18.43 ± 0.04
ABC	None	4523 ± 5	18.45 ± 0.04
ABC	None	4542 ± 5	18.41 ± 0.04
ABC	None	4561 ± 5	18.45 ± 0.04
ABC	None	4580 ± 5	18.42 ± 0.04
ABC	None	4598 ± 5	18.44 ± 0.05
ABC	None	4617 ± 5	18.41 ± 0.05
ABC	None	4636 ± 5	18.41 ± 0.04
ABC	None	4655 ± 5	18.43 ± 0.04
ABC	None	4674 ± 5	18.39 ± 0.04
ABC	None	4692 ± 5	18.44 ± 0.04
ABC	None	4711 ± 5	18.43 ± 0.05
ABC	None	4730 ± 5	18.43 ± 0.04
ABC	None	4749 ± 5	18.42 ± 0.05
ABC	None	4768 ± 5	18.43 ± 0.04
ABC	None	4786 ± 5	18.46 ± 0.05
ABC	None	4805 ± 5	18.42 ± 0.05
ABC	None	4824 ± 5	18.44 ± 0.05
ABC	None	4843 ± 5	18.45 ± 0.05
ABC	None	4862 ± 5	18.47 ± 0.05
ABC	None	4880 ± 5	18.43 ± 0.04
ABC	None	4899 ± 5	18.43 ± 0.05
ABC	None	4918 ± 5	18.41 ± 0.05
ABC	None	4937 ± 5	18.41 ± 0.04
ABC	None	4956 ± 5	18.43 ± 0.04
ABC	None	4974 ± 5	18.43 ± 0.04
ABC	None	4993 ± 5	18.44 ± 0.05
ABC	None	5012 ± 5	18.42 ± 0.04
ABC	None	5031 ± 5	18.41 ± 0.05
ABC	None	5050 ± 5	18.39 ± 0.05
ABC	None	5068 ± 5	18.41 ± 0.04
ABC	None	5087 ± 5	18.40 ± 0.05

Table 4.16 ABC optical photometry for GRB071003. All times are in seconds since the burst time, 07:40:55 UT

GRB071003
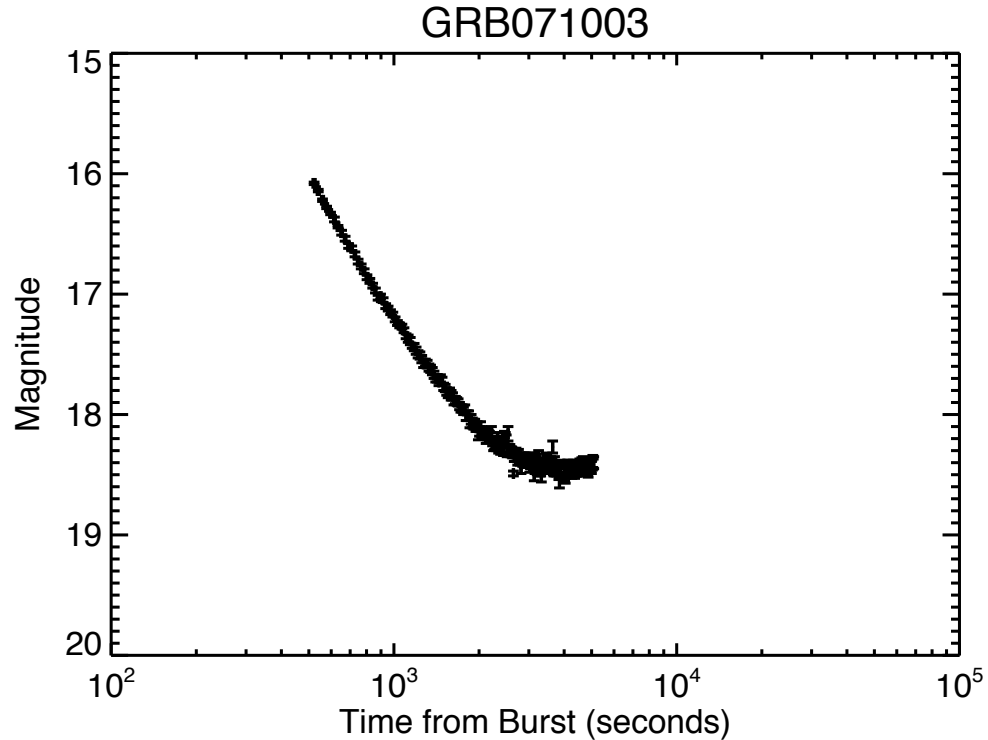
Figure 4.8 Lightcurve for 071003, containing several hours of ABC data.

Palomar 60 afterglow (Perley et al., 2007). NainiTal (Pandey et al., 2007), NAYUTA (Iizuka & Maeno, 2007), Xinglong TNT (Xin et al., 2007b) , MITSuME (Kuroda et al., 2007) also detected the afterglow, no other telescopes report detections. No redshift was detected for this GRB.

ABC observations started at 12:46:06.53 UT (6 minutes after the burst), and continued for 3 hours. These consisted of 10 s unfiltered images, which were then coadded together. ABC photometry was calibrated to the USNO B1.0 R2 catalog. Because of the location of the afterglow, which was near the edge of the initial BAT error circle, there are only 4 coadded ABC images with the afterglow present. Photometry was difficult, because of the presence of a large amount of stray light and vignetting. The afterglow was calibrated to a number of nearby stars using RPHOT.

Table 4.4.9 shows the optical photometry for GRB 0701011 from the ABC. The

Telescope	Filter	$t_{mid}(s)$	Magnitude
ABC	None	3075 ± 90	20.55 ± 0.47
ABC	None	3263 ± 90	20.68 ± 0.47
ABC	None	3451 ± 90	20.25 ± 0.48
ABC	None	3639 ± 90	20.05 ± 0.54

Table 4.17 ABC optical photometry for GRB071011. All times are in seconds since the burst time, 12:40:13 UT

ABC photometry has been analyzed as described in Chapter III. Figure 4.9 shows the lightcurve for GRB 071011, containing ABC data.
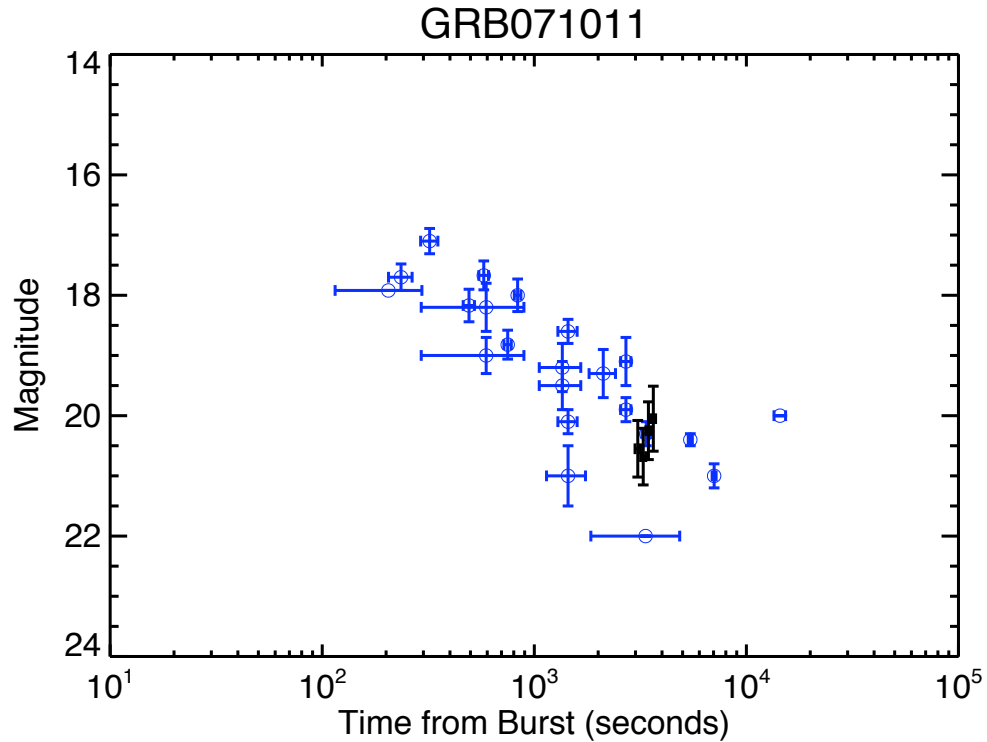
Figure 4.9 Lightcurve for GRB071011. ABC data, GCN data, and data from Cenko et al. (2008) are included. ABC data is black, the rest of the data is blue.

4.4.10   GRB080613A:The INTEGRAL Burst

GRB 080613A was detected on June 13th, 2008 by INTEGRAL at 09:35:21 UT, with a 1.5' error radius (Gotz et al., 2008). The T_{90} duration of the burst was 30s, and the fluence (20-200keV) was $1.3 \cdot 10^{-6} erg/cm^2$ (Gotz et al., 2008).

$Swift$ XRT observed GRB 080613A starting 24.2ks after the INTEGRAL trigger,

Telescope	Filter	$t_{mid}(s)$	Magnitude
ABC	None	1107 ± 108	19.29 ± 0.04
ABC	None	1333 ± 108	19.51 ± 0.04
ABC	None	1559 ± 108	19.58 ± 0.04
ABC	None	1784 ± 108	19.32 ± 0.04
ABC	None	2010 ± 108	19.33 ± 0.04
ABC	None	2235 ± 108	19.44 ± 0.04
ABC	None	2461 ± 108	19.63 ± 0.04
ABC	None	2687 ± 108	19.78 ± 0.05

Table 4.18 ABC optical photometry for GRB080613A. All times are in seconds since the burst time, 09:35:21UT

and obtained 3.6ks of data in photon counting mode. They detected an X-ray source in the error circle 4.9" from the optical detection (Guidorzi & Markwardt, 2008).

Faulkes North detected a fading counterpart at α 14:13:05.02 δ +05:10:23.5, from observations starting at 3.9 minutes after the trigger time (7872). *Swift* UVOT has upper limits for this burst (Hoversten & Holland, 2008). GROND has limits for this afterglow, starting at 14.8 hours after the trigger, (Clemens et al., 2008), which confirms the fading nature of the afterglow.

ABC observations started at 09:51:59.99 UT (16 minutes after the burst) and ended about 30 minutes later. These consisted of 10 second unfiltered images, which were then coadded together. ABC photometry was calibrated to the USNO B1.0 R2 catalog. Due to the sparse nature of the field, the optical counterpart was calibrated to the nearby $R = 18.18$ mag star at α 14:13:8.46 δ+05:10:35.3. The optical counterpart was detected, and was found to fade and rebrighten (see Figure 4.10).

Table 4.4.10 shows the optical photometry for GRB 080613A from the ABC. The ABC photometry has been analyzed as described in Chapter III. Figure 4.10 shows the lightcurve for GRB 080613A.

GRB080613A
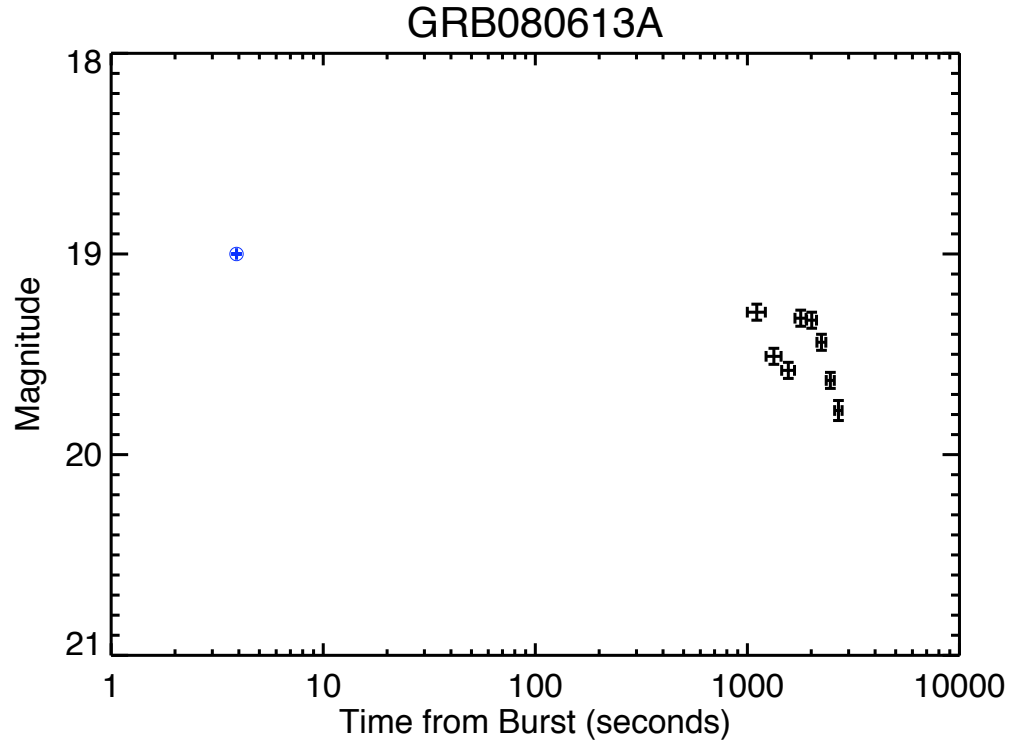
Figure 4.10 Lightcurve for 080613A.

4.5 Deep Non-Detections

4.5.1 Introduction

Each section of GRB data is constructed in the following way, in order of when the burst was detected (earlier bursts first, followed by later bursts). First the gamma-ray observations are discussed, which include the satellite, trigger number, date and time of the detection, error circle, T_{90} duration of the burst, and the fluence. Then, the *Swift* XRT and UVOT observations are discussed, which include any fading XRT or UVOT counterparts that may have been found, or limits, and other interesting objects nearby. Next, other optical (or IR) observations that were interesting (but not all of them) are reported. If any other interesting observations occurred (for example radio detections, or redshift determinations), these might also be reported as well. These observations are not reported in the order that they occurred on

the GCN, but by wavelength (γ, X-ray, optical). Finally, the ABC observations are reported, as those are usually some of the last observations to be reported on the GCN, so it seems fitting that they are the last to be described in each section. This section only reports the four interesting non-detections, which does not include the ABC non-detections when the ABC's limiting magnitude was not as deep as other telescopes at similar times.

4.5.2 GRB 050906:A Short Dark Burst

GRB 050906 was detected on September 6th, 2005 by $Swift$ BAT at 10:32:05 UT (trigger = 153866), with a 3' error radius (Krimm et al., 2005). The T_{90} duration of the burst was 128 ± 16 milliseconds, and the fluence (15-150keV) was $5.9 \pm 3.2 \cdot 10^{-8} erg/cm^2$ (Parsons et al., 2005b). This makes this a short dark burst.

$Swift$ UVOT was in safe mode, so there are no observations from UVOT. $Swift$ XRT observations started at 79 seconds after GRB trigger, with no sources detected by the on board algorithm (Krimm et al., 2005). Further XRT observations in 5.2ks of data reveal 2 faint sources, but neither are in the BAT error circle, near galaxy IC328, or near the radio source (Pagani et al., 2005). There is a slight excess of counts during the first orbit only at α 03:31:15.6 and δ -14:36:37, the $Swift$ team is not sure if the excess represents the detection of an astrophysical source, but if it did, they think it is the most likely X-ray counterpart to GRB 050906 (Fox et al., 2005b)

Palomar 60 began imaging 114s after the GRB trigger, but no new sources were detected, down to a limiting magnitude of $R > 20.4$ at 11:04:32 UT (Fox et al., 2005a). A radio source was detected at α 03:31:11.75 δ -14:37:18.1 with the VLA at a frequency of 8.46 GHz, on Sept 6.52 UT and Sept 6.58 UT (Cameron & Frail, 2005). The 8.2m Antu Telescope at ESO/Paranal sees a faint red V=26.2, R=24.5,

I=23.0 magnitude object located at the radio coordinates on Sept 7.4 (Jakobsson et al., 2005).

The ABC took images between 10:47 UT and 10:59 UT, starting 15 minutes after the BAT trigger. These are 1s and 10s images, taken with a diffraction grating. These are calibrated to USNO B1.0 R2. The ABC fov covers half of the BAT error box, and includes IC 328. Comparison of the 10s images, which start at 10:55 UT, to the DSS reveals no new sources to a limiting magnitude of 19. A GCN circular of these observations was submitted (Swan & Smith, 2005).

4.5.3 GRB 051117B

GRB 051117B was detected on November 11th, 2005 by $Swift$ BAT at 13:22:54 UT (trigger = 164279), with a 3' error radius (Band et al., 2005). The T_{90} duration of the burst was 8 ± 1 seconds, and the fluence (15-150keV) was $1.4 \pm 0.3 \cdot 10^{-7} erg/cm^2$ (Parsons et al., 2005a).

$Swift$ XRT began observing the field 135 s after the BAT trigger (Band et al., 2005). An X-ray candidate was found at α 05:40:43.0 δ -19:16:26.2. (Beardmore et al., 2005). $Swift$ UVOT began observing at 133s after the BAT trigger, with a 200s V filter, no afterglow candidate found, with a limit of about 17th magnitude (Band et al., 2005).

Other deep and early observations include ROTSE-IIIa, Lulin, and Siding Spring. ROTSE-IIIa images started at 18s, with unfiltered limiting magnitudes of 14.2 for a 5s exposure and 15.8 for a 175s coadd (Rujopakarn et al., 2005). The 40 inch at Siding Spring Observatory started a series of unfiltered exposures at 14:12 UT, with a limiting magnitude estimate of $R < 18.8$ (Fox, 2005). Lulin's 1m telescope started images at 14:11 UT, with limiting magnitudes of $R < 20.8$ (Chen et al., 2005). There was an extended source near the edge of the XRT circle, but no brightness variations

or other interesting things were seen by others.

The ABC took images between 13:40 UT and 13:54 UT, under scattered cloud conditions. These are 10s images, taken with a low resolution diffraction grating. The first image was taken 14 minutes after the burst. These are calibrated to USNO B1.0 R2. There are no new sources to a limiting magnitude of $R < 19.4$, and a GCN circular of these observations was submitted (Swan et al., 2005).

4.5.4 GRB 060930: A Non Swift Burst

GRB 060930 was detected on September 30th, 2006 by INTEGRAL at 09:04:09 UT, with a 2.5' error radius (Gotz et al., 2006). The T_{90} duration of the burst was 20 seconds, and the fluence (20-200keV) was $2.5 \cdot 10^{-7} erg/cm^2$ (Gotz et al., 2006).

ROTSE-IIIa had early (images starting 6.3s after the GRB) unfiltered limiting magnitudes of 15.8 for a 5s exposure, and 17.1 for a 156s coadded exposure (Swan et al., 2006c). Faulkes has a stacked image from 1.98-4.97mins after the burst, with a limiting R mag of 19.5, no new objects detected (Guidorzi et al., 2006a).

The ABC began imaging at 09:15:47.3 UT, about 11 minutes after the burst, and obtained 2 hours of 10s images. These images are calibrated to USNO B1.0 R2, and are coadded in sets of 20. Comparison of these images with images taken on Oct 5, 2006, revealed no optical counterpart within the 2.5 arcmin errorbox with a limiting magnitude of 21.0, and results were reported on the GCN (Swan et al., 2006b)

4.5.5 GRB 071021: A High Redshift Burst

GRB 071021 was detected on October 21th, 2007 by $Swift$ BAT at 09:41:33 UT (trigger = 294974), with a 3' error radius (Sakamoto et al., 2007a). The T_{90} duration of the burst was 225 ± 10 seconds, and the fluence (15-150keV) was $1.3 \pm 0.2 \cdot 10^{-6} erg/cm^2$ (Barbier et al., 2007). There were features in this GRB which

indicated that this was a high redshift burst. These include a long T_{90} duration with few significant peaks, a peak flux (1 s) < 1.0 ph/cm2/s, and a power-law photon index $1.70 < 2$ (Sakamoto et al., 2007c; Barbier et al., 2007).

$Swift$ XRT began observing the field 130 seconds after the BAT trigger, and found a bright, uncatalogued X-ray source (Sakamoto et al., 2007a). The X-ray light curve was flat for about 230 seconds after the trigger, then there was a steep decay, followed by a series of strong flares (Page et al., 2007) There were no UVOT observations for this burst, as it was still in engineering mode after the gyro restorations.

No optical counterparts were found for this burst. The deepest and earliest limits were found by the ABC, which is described in the following paragraph. A near infrared counterpart was found by (Castro-Tirado et al., 2007b), at 11.25 hrs after the event. The object is very faint, and barely detected in H and K bands, but not in J, and is located at α 22:42:34.31 δ 23:43:06.5 (Castro-Tirado et al., 2007a). Observations with the 8.2m VLT+FORS2 and the z_Gunn filter gives a detection, which suggests a redshift less than roughly 6.5 (Malesani et al., 2007). (Urata et al., 2007) marginally detects the afterglow in Ks band around October 23, 05:42UT, with a magnitude of 21.

The ABC began imaging the GRB about 10 minutes after the trigger, and ended about 2 hours later. The images are calibrated to USNO B1.0 R2 catalog. There are two very deep coadded limits for the ABC, both starting at 09:51:24.7 UT. The limits are 22.6th magnitude for a 367.5s coadded exposure and 23.7th magnitude for a 8262.3s coadded exposure. The NIR counterpart observed by (Castro-Tirado et al., 2007c) was not seen to the above limits. The ABC is an unfiltered camera, with enhanced sensitivity in the red end of the spectrum. This sensitivity to the red end of the spectrum allows us to see high ($z < 6$) bursts. These results were reported

on the GCN (Swan et al., 2007b)

CHAPTER V

Afterglow Models

5.1 Introduction to Theory

The most successful theory to explain GRBs is the fireball model, and this is the model that will be tested with ABC data. In the fireball model, emission is via synchrotron radiation, and consists of two components, internal shocks and external shocks. The afterglow (X-rays, optical, radio) comes from the external shocks, and the GRB prompt emission, which consists of gamma-rays and some of the X-rays, comes from the internal shocks. In this model, both the prompt emission and the afterglow emission is synchrotron emission, radiated by electrons in a magnetic field.

This chapter first describes the fireball model, and the reasoning behind various aspects of the theory. The purpose of this chapter is not to derive all aspects of the theory, but rather to explain the basics of the fireball model, and to cite references so that the reader can read more if interested. The final results are included, as those are used to determine if the ABC data fits the fireball model. The next part of the chapter attempts to fit the GRB data that the ABC obtained to the fireball model. In this chapter and the next, the flux density is parameterized as $F_\nu \propto t^{-\alpha}\nu^{-\beta}$, with the power law index defined as α and the spectral decay index defined as β.

5.2   Fireball Model Requirements and Assumptions

There are several requirements and assumptions that go into the fireball model. Most of these are based on observations and some are to make the calculations easier. These assumptions are that the fireball is isotropic, the surrounding density is constant, the fireball is relativistic, and the radiation is caused by synchrotron emission of electrons.

In the following sections, the reasoning behind why the fireball must be relativistic and why the radiation is synchrotron is explained. Throughout all of this, it is assumed that the medium surrounding the fireball is uniform. In Section 5.3.3, the medium is modified so that it is no longer constant, but reflects a wind environment influenced by gas emitted by the progenitor. There are other modifications that can be made to the simple fireball model, and these are addressed in Section 5.3.4.

5.2.1   Compactness Problem

One problem that any GRB model must solve is the compactness problem (Ruderman, 1975), which has to do with the short (millisecond) timescale variability of GRBs and the large energies involved, making the emitting region of the GRB opaque to photon-photon pair production. A typical GRB gamma-ray fluence is $F \sim 10^{-6} ergs/cm^2$, and a typical distance is $D \sim 3$ Gpc. The total isotropic gamma-ray energy is $E = 4\pi D^2 F \sim 10^{51}$ergs, assuming no relativistic motion, and the scale of emission is $c\delta t \sim 3 \cdot 10^8 cm$, since $\delta t \sim 10$ ms. For 2 photon pair production ($\gamma\gamma \rightarrow e^+ e^-$), the pair production optical depth is huge, since $\tau_{\gamma\gamma} = f_p \sigma_T F D^2 /(c\delta t)^2 m_e c^2 = 10^{15} f_p (\frac{F}{10^{-6}\frac{erg}{cm^2}})(\frac{D}{3Gpc})^2(\frac{\delta t}{10ms})^2$, f_p is the fraction of photons above the 2 photon pair production threshold, m_e is the electron mass, and $\sigma_T = 6.25 \cdot 10^{-25} cm^2$ is the Thomson cross section. Assuming no relativistic mo-

tion, the gamma-rays are attenuated in the source, long before reaching the Earth. Invoking relativistic bulk motion, where the GRB emitting region moves toward us with a high Lorentz factor, decreases the optical depth, allowing gamma-rays to be observed here on Earth. Assuming relativistic bulk motion helps the optical depth in two ways. First, the gamma-rays are blue-shifted by a factor of Γ, in the shell comoving frame, so the bulk of the gamma-rays are observed as X-rays in the jet frame, which decreases the number of photons above the pair production threshold, thus f_p drops by a factor of $\Gamma^{2(\alpha-1)}$, with α, the photon number spectral index ≈ 2. Second, the physical scale of the emission is $\Gamma c \delta t$ for relativistic motion, not $c \delta t$. The optical depth τ_{TT} drops by a factor $\Gamma^{2(\alpha-1)}\Gamma^4$, with typical values of $\Gamma \geq 100$ for $\tau_{TT} < 1$. These large values of Γ make GRBs one of the most relativistic objects observed so far.

5.3   Internal-External Shocks and the Fireball Model

The fireball model consists of internal and external shocks. These shocks are created when shells of ejecta, from the inner engine, collide with each other or with the interstellar medium (ISM). The internal shocks are created when the shells of ejecta, which have different Lorentz factors, crash into each other, causing the prompt gamma-ray emission. As the shells of ejecta collide, they create a shock front. The external shocks occur when the shock front collides with the ISM (or wind), which creates a forward shock and a reverse shock. The forward shock propagates through the ISM and is responsible for the afterglow, via synchrotron emission, and is seen for extended periods of time in IR, optical, radio, and in X-rays. The reverse shock propagates through the shell, is short lived, is driven by synchrotron emission, and is seen only in the IR or optical. In this section, details of the internal and exter-

nal shocks are described, including the expected lightcurve parameters for various models.

5.3.1 Internal Shocks

The central engine creates several shells of ejecta, with different Lorentz factors. When a faster shell collides into a slower moving shell, an internal shock is created, which in turn causes prompt gamma-ray emission. The wide variability in GRB emission can be explained by the different behaviors of the internal engine. There are 2 mechanisms that can explain the GRB prompt emission, synchrotron emission, and Inverse Compton scattering. See (Piran, 2005), (Piran, 1999), (Piran, 2000) for more information on internal shocks.

5.3.2 External Shocks

As the shells of ejecta pile up into each other, they form a single relativistic shell which plows into the ISM, creating two external shocks: a forward shock, and a reverse shock. The reverse shock, which is responsible for the bright optical flash that is sometimes observed, is short lived, as it lasts only as long as it passes through the shell, while the forward shock lasts much longer, and is responsible for the afterglow that is observed in many wavelengths.

Forward Shock

As the relativistically moving shock front crosses the ISM, the matter is heated to extreme temperatures, encounters a strong magnetic field, and then radiates its energy via synchrotron radiation. This is dominated by electrons, because electrons can move and radiate much faster than other particles. Other particles, such as protons, are ignored in these calculations.

The discussion here follows (Sari et al., 1998), and also (Zhang & Mészáros, 2004),

which derives the expected spectra and lightcurve assuming the afterglow emission is caused by relativistic shocks and synchrotron radiation. The forward shock is propagating through a cold constant medium density matter (ISM) with particle density n, and behind the shock, the particle density is $4\gamma n$ and the energy density is $4\gamma^2 n m_p c^2$, where γ is the Lorentz factor of the shocked material. The electrons are assumed to be Fermi accelerated with power law index p, and a minimum cutoff energy γ_m, $N(\gamma_e)d\gamma_e \propto \gamma_e^{-p} d\gamma_e$, with $\gamma_e \geq \gamma_m$. For these calculations, $p > 2$, to keep the energy of the electrons finite. Assuming that a constant fraction ϵ_e of the shock energy goes into the electrons, then the minimum Lorentz factor is:

$$(5.1) \qquad \gamma_m = \epsilon_e (\frac{p-2}{p-1}) \frac{m_p}{m_e} \gamma$$

Assuming that the magnetic energy density behind the shock is a constant fraction ϵ_B of the shock energy gives a magnetic field strength in the fluid frame of:

$$(5.2) \qquad B = (32\pi m_p \epsilon_B n)^{1/2} \gamma c$$

The radiation power and synchrotron frequency for an electron with a high Lorentz factor is the following, in the frame of the observer:

$$(5.3) \qquad P(\gamma_e) = \frac{4}{3} \sigma_T c \gamma^2 \gamma_e^2 \frac{B^2}{8\pi}$$

$$(5.4) \qquad \nu(\gamma_e) = \gamma \gamma_e^2 \frac{q_e B}{2\pi m_e c}$$

The spectral power (P_ν) varies as $\nu^{1/3}$ for $\nu < \nu(\gamma_e)$, and cuts off exponentially for $\nu > \nu(\gamma_e)$. The peak spectral power occurs at:

$$(5.5) \qquad P_{\nu,max} \approx \frac{P(\gamma_e)}{\nu(\gamma_e)} = \frac{m_e c^2 \sigma_T}{3 q_e} \gamma B$$

This description is suitable when the electron does not lose a significant fraction of its energy to radiation. There is a critical value γ_c given by $\gamma \gamma_c m_e c^2 = P(\gamma_c)t$, and solving for γ_c gives:

$$(5.6) \qquad \gamma_c = \frac{6\pi m_e c}{\sigma_T \gamma B^2 t}$$

An electron with an initial Lorentz factor $\gamma_e > \gamma_c$ cools down to γ_c in time t. During this time, the frequency of the synchrotron emission varies as $\nu \propto \gamma_e^2$, the electron energy varies as γ_e, and the spectral power P_ν varies as $\nu^{-1/2}$ between $\nu_c < \nu < \nu(\gamma_e)$. In addition, self absorption comes into play at low frequencies, and this causes a ν^2 dependence on the flux density.

The spectrum can now be calculated from the distribution defined earlier, but there are two cases, depending on whether $\nu_c < \nu_m$ or $\nu_m < \nu_c$. For $\nu_m < \nu_c$, called the "slow cooling case", the spectrum is:

$$(5.7) \qquad F = F_{\nu,m} \begin{cases} (\nu_a/\nu_m)^{1/3}(\nu/\nu_a)^2 & \nu < \nu_a \\ (\nu/\nu_m)^{1/3} & \nu_a \leq \nu < \nu_m \\ (\nu/\nu_m)^{-(p-1)/2} & \nu_m \leq \nu < \nu_c \\ (\nu_c/\nu_m)^{-(p-1)/2}(\nu/\nu_c)^{-p/2} & \nu_c \leq \nu \leq \nu_M \end{cases}$$

The "fast cooling case" occurs when $\nu_m > \nu_c$, with the spectrum given by:
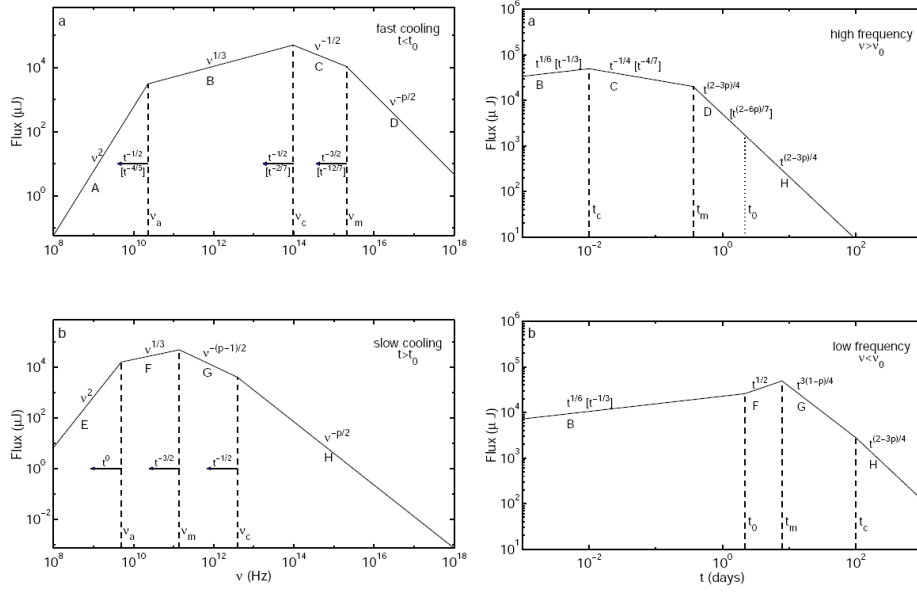
Figure 5.1 Synchrotron spectrum, from Zhang & Mészáros (2004)

$$(5.8) \qquad F = F_{\nu,m} \begin{cases} (\nu_a/\nu_c)^{1/3}(\nu/\nu_a)^2 & \nu < \nu_a \\ (\nu/\nu_c)^{1/3} & \nu_a \le \nu < \nu_c \\ (\nu/\nu_c)^{-1/2} & \nu_c \le \nu < \nu_m \\ (\nu_m/\nu_c)^{-1/2}(\nu/\nu_m)^{-p/2} & \nu_m \le \nu \le \nu_M \end{cases}$$

Assuming the afterglow is fully adiabatic, it is possible to calculate the expected light curves, knowing the break frequencies ν_m, ν_c, the peak flux $F_{\nu,max}$, and using hydrodynamic evolution. The shock is assumed to be spherical, and because it is also assumed to be adiabatic, the energy is constant, and given by $E = 16\pi\gamma^2 R^3 n m_p c^2/17$. There is a relation for t, R, and γ, $t \cong R/4\gamma^2 c$. From these relations, Sari et al. (1998) has calculated the lightcurves for different spectral and temporal regimes. The flux density obeys a power law $F_\nu \sim t^{-\beta}$ and also $F_\nu \sim t^{-\alpha}$, with specific values of α (for the temporal index) and β (for the spectral index) predicted by the fireball model.

Table 5.1 lists the closure relations for α and β for both ISM and wind fireball models, and for models including energy injection. A way to test the models is to measure β and α from the data, and then find which models best fit the data. These calculations assumed that the fireball was adiabatic and no energy was lost, which is probably not the case for an actual GRB.

External Reverse Shock

The emission from the reverse shock comes from the early phase of the fireball-ISM interaction, and the reverse shock propagates back into the fireball. The reverse shock emits synchrotron radiation, heats the shell, and accelerates electrons. This is short lived, and ends when the reverse shock crosses the shell. The density of the shell is higher than of the external medium, because the shell has swept up material by. Because the density of the shell is higher, the reverse shock emission should peak in the IR/optical, the details of which are discussed in (Sari & Piran, 1999) and (Lazzati & Begelman, 2006).

5.3.3 Modifications: Wind Environment

Up to this point, the assumption has been that the ejecta collides into the ISM, which is assumed to have constant density. One modification is to assume that the ejecta collides in a medium with $n(R) \propto R^{-k}$. The case of $k = 2$ is considered here, as this occurs when there is a stellar wind, which happens if the central engine is a massive star that collapsed prior to becoming a GRB (Section 5.3.5 discusses GRB progenitors).

(Chevalier & Li, 2000) give extensive derivations and calculations of the fireball model with a wind environment, and (Zhang et al., 2006) summarize the results, listed in Table 5.1. Differences between the ISM and wind models can be seen in how

ν_m and ν_c vary with time. For both models, $\nu_m \propto t^{-3/2}$. With the ISM, $\nu_c \propto t^{-1/2}$, while in a wind environment, $\nu_c \propto t^{1/2}$. This changes how the afterglow evolves with time, and changes the values of α and β for the different spectral regimes.

5.3.4 Modifications: Fireball Model with Energy Injection

Energy can be injected into the fireball during the deceleration phase, the forward shock is "refreshed", and decelerates less rapidly than with no energy injection. This explains the X-ray afterglow during the flatter segment (in Figure 1.1, the part explained by energy injection is segment II).

There are several different origins for refreshed shocks (see for example (Rees & Meszaros, 1998), (Sari & Mészáros, 2000), (Thompson, 1994), (Meszaros & Rees, 1997)), the most popular is that the central engine is longer lasting (Zhang & Mészáros, 2001), and behaves as

$$(5.9) \qquad\qquad L(t) = L_0(t/t_b)^{-q}$$

One specific example is that the energy injection from the spin-down from a millisecond pulsar (or millisecond magnetar) with q=0. In general, energy injection can come from matter falling onto a black hole. Zhang & Mészáros (2001) and Zhang et al. (2006) derive the synchrotron frequencies and the peak flux densities for the ISM and wind cases, and also derive the temporal indices (α) and spectral indices (β), which are listed in Table 5.1. With energy injection, as long as $q < 1$, $E_{iso} \propto t^{1-q}$ for both the ISM and wind models. For both the wind and ISM models, $\nu_m \propto t^{-(2+q)/2}$. For the ISM case, $\nu_c \propto t^{(q-2)/2}$ and $F_{\nu,max} \propto t^{1-q}$ and for the wind case, $\nu_c \propto t^{(2-q)/2}$ and $F_{\nu,max} \propto t^{-q/2}$.

5.3.5 Inner Engines/Progenitors

Up to now, the discussions have been about the fireball produced by the inner engine and how that fireball interacts with the surrounding medium to create the afterglow. Nothing has been said about the inner engine, or about the progenitor for GRBs. There are two different classes of GRBs, short/hard GRBs and long/soft GRBs, and there are different leading theories for each of these classes of GRBs. The leading theories are that short GRBs are caused by Neutron Star - Neutron Star (NS-NS) mergers, and that long GRBs are caused by the collapse of massive stars, in a theory known as the collapsar model.

The leading theory for short GRBs is that they come from NS-NS mergers. Excellent references on Neutron Star - Neutron Star mergers are Eichler et al. (1989) and Narayan et al. (1991). The leading theory for long GRBs is the collapsar model which is based on the collapse of a massive star (MacFadyen & Woosley, 1999).

Any model for the inner engine must satisfy the following requirements. First, the energy requirements are large (10^{51} ergs). Second, GRBs are collimated, with opening angles of $1° < \theta < 20°$. GRBs take place at once per $3 \cdot 10^5$ yr per galaxy, which is about 1/3000 of the rate of supernova. The variability of the prompt emission is as short as 1ms, suggesting a compact object, while the length of the GRB is 2-50s, suggesting prolonged activity, and not something that releases the energy in a single explosion.

The accretion of a massive ($\sim 0.1 M_\odot$) disk onto a compact object, like a black hole, would fit these requirements. The massive disk is needed because of the large amount of energy involved in GRBs. Accretion is needed to explain the short time scale variability and the long duration of the bursts. Observationally, some long GRBs are also supernovas, implying that long GRBs are associated with the deaths

	β	no injection α	$\alpha(\beta)$	injection α	$\alpha(\beta)$
ISM	slow cooling				
$\nu < \nu_m$	$-\frac{1}{3}$	$-\frac{1}{2}$	$\alpha = \frac{3\beta}{2}$	$\frac{5q-8}{6}$	$\alpha = (q-1) + \frac{(2+q)\beta}{2}$
$\nu_m < \nu < \nu_c$	$\frac{p-1}{2}$	$\frac{3(p-1)}{4}$	$\alpha = \frac{3\beta}{2}$	$\frac{(2p-6)+(p+3)q}{4}$	$\alpha = (q-1) + \frac{(2+q)\beta}{2}$
$\nu > \nu_c$	$\frac{p}{2}$	$\frac{3p-2}{4}$	$\alpha = \frac{3\beta-1}{2}$	$\frac{(2p-4)+(p+2)q}{4}$	$\alpha = \frac{q-2}{2} + \frac{(2+q)\beta}{2}$
ISM	fast cooling				
$\nu < \nu_c$	$-\frac{1}{3}$	$-\frac{1}{6}$	$\alpha = \frac{\beta}{2}$	$\frac{7q-8}{6}$	$\alpha = (q-1) + \frac{(2-q)\beta}{2}$
$\nu_c < \nu < \nu_m$	$\frac{1}{2}$	$\frac{1}{4}$	$\alpha = \frac{\beta}{2}$	$\frac{3q-2}{4}$	$\alpha = (q-1) + \frac{(2-q)\beta}{2}$
$\nu > \nu_m$	$\frac{p}{2}$	$\frac{3p-2}{4}$	$\alpha = \frac{3\beta-1}{2}$	$\frac{(2p-4)+(p+2)q}{4}$	$\alpha = \frac{q-2}{2} + \frac{(2+q)\beta}{2}$
Wind	slow cooling				
$\nu < \nu_m$	$\frac{1}{3}$	0	$\alpha = \frac{3\beta+1}{2}$	$\frac{q-1}{3}$	$\alpha = \frac{q}{2} + \frac{(2+q)\beta}{2}$
$\nu_m < \nu < \nu_c$	$\frac{p-1}{2}$	$\frac{3p-1}{4}$	$\alpha = \frac{3\beta+1}{2}$	$\frac{(2p-2)+(p+1)q}{4}$	$\alpha = \frac{q}{2} + \frac{(2+q)\beta}{2}$
$\nu > \nu_c$	$\frac{p}{2}$	$\frac{3p-2}{4}$	$\alpha = \frac{3\beta-1}{2}$	$\frac{(2p-4)+(p+2)q}{4}$	$\alpha = \frac{q-2}{2} + \frac{(2+q)\beta}{2}$
Wind	fast cooling				
$\nu < \nu_c$	$-\frac{1}{3}$	$\frac{2}{3}$	$\alpha = \frac{1-\beta}{2}$	$\frac{1+q}{3}$	$\alpha = \frac{q}{2} - \frac{(2-q)\beta}{2}$
$\nu_c < \nu < \nu_m$	$\frac{1}{2}$	$\frac{1}{4}$	$\alpha = \frac{1-\beta}{2}$	$\frac{3q-2}{4}$	$\alpha = \frac{q}{2} - \frac{(2-q)\beta}{2}$
$\nu > \nu_m$	$\frac{p}{2}$	$\frac{3p-2}{4}$	$\alpha = \frac{3\beta-1}{2}$	$\frac{(2p-4)+(p+2)q}{4}$	$\alpha = \frac{q-2}{2} + \frac{(2+q)\beta}{2}$

Table 5.1 Afterglow table from Zhang et al. (2006). These are the closure relations to determine which of the fireball models fit the data.

of massive stars. Also, long GRBs are found in star forming regions. Any model to explain the inner engine should meet all of these requirements.

In the collapsar model, GRBs arise from the collapse of a Wolf-Rayet star with fast rotation. Wolf-Rayet stars are massive, greater than $20M_\odot$ stars, that generally become type Ib or Ic supernova. In the collapsar model, the GRB arises from a failed type Ib supernova. The star ($M > 30M_\odot$), has burned down to an iron core, and collapses to a black hole. An accretion disk forms around the black hole, and a funnel forms around the rotation axis. The mass of the accretion disk is $\sim 0.1M_\odot$, allowing the accretion of the disk onto the black hole to take place for many seconds, which powers the GRB. Energy deposited in the surrounding matter will leak out onto the rotation axis and produce jets with angles of $< 10°$.

5.4   Modeling ABC GRBs

5.4.1   Introduction

The modeling of ABC GRBs will require a few things. Bursts will need both optical and X-ray data at roughly similar times. As a result of these requirements, 060110 and 080613A will not be discussed extensively, because they lack early X-ray data. GRB 071003 does not have X-ray data at early times. However, it has an extensive and unique optical lightcurve, and it has enough data to determine if it fits various models.

5.4.2   Fitting Optical and X-ray Decay Rates

The first step to compare the data to the model is to find the optical and X-ray decay rates. To do this, the optical magnitudes and the X-ray data are converted to a flux density, and the optical data and X-ray are fit with 1, 2 , or 3 power laws, using Eli Rykoff's plawfit.pro program. Each optical afterglow and X-ray afterglow was fit to either a single powerlaw, a broken power law, or a broken power law with 2 breaks:

$$(5.10) \qquad\qquad\qquad\qquad f_1 = at^{-\alpha}$$

$$(5.11) \qquad\qquad f_2 = a\left(\frac{t}{t_b}\right)^{\alpha_1}\left[1 + \left(\frac{t}{t_b}\right)^{(-s(\alpha_2-\alpha_1))}\right]^{(-1/s)}$$

$$(5.12) \quad f_3 = a\left(\frac{t}{t_{b_1}}\right)^{\alpha_1}\left[1 + \left(\frac{t}{t_{b_1}}\right)^{(-s_1(\alpha_2-\alpha_1))}\right]^{(-1/s_1)}\left[1 + \left(\frac{t}{t_{b_2}}\right)^{(-s_2(\alpha_3-\alpha_2))}\right]^{(-1/s_2)}$$

Here, f_1 is the single power law, f_2 the broken power law, f_3 the broken power law with 2 breaks. In these functions, s, s_1, s_2 are the smoothing parameters, these are set to 10. The various forms of t_b are the break times, and α_1, α_2, α_3, α are the power laws. The form used to fit was determined by eye. Ambiguous cases were

determined by fitting the data with 2 forms (a single power law and a broken power law), and for these bursts, one form was always a much better fit than another, both when the fits were plotted over the data and when χ^2 was calculated.

The optical data consists of ABC, ROTSE, GCN data, and published literature data (R and unfiltered only). GCN data without errors in time or magnitude are excluded, as this is often not carefully analyzed. The X-ray data consists of $Swift$ XRT data. Early X-ray and optical points are sometimes excluded in the fits, as these may contain flaring activity, or other anomalous features that are not explained by the fireball model. Late points may also be excluded as well, because there may not be enough data to extract another decay rate, but it is clear that they do not fit with a single power law. Listed below are the GRBs which presented difficulties during the fitting, the rest of the GRBs presented no problems. The optical and X-ray fits are listed in Table 5.2.

060110

The first ROTSE data point was excluded for the fit that is included in the table. When all the data, including the first ROTSE point, was fit to 2 power laws, the later power law was identical to the fit with 1 power law with the first ROTSE point excluded.

060708

The last data point for the 1st order ABC data, and all of the 0th order ABC data is excluded for the fit that is included in the table. Fitting the 0th order data only to a single power law decay, and fitting both the 0th and first order data to a single power law decay finds similar numbers for α, but with a much higher χ^2/dof due to the larger uncertainties and scatter in the measurements for the 0th order

data.

070208

This burst was fit with a single power law and a broken power law, but this did not change the value of χ^2/dof by much (from 4.9 to 3.7). Points near 1000s shows a lot of scatter, this seems to be an unavoidable feature of this set of data.

070419A

The early optical was very flat, those were taken out to get a better fit, with a better χ^2/dof. This does not change the evaluation of this GRB.

070518

The first (very early) and last optical points were taken out to get a better fit, with a better χ^2/dof. The early X-ray data had flaring activity and those points were not used for fitting.

070529

The late UVOT data was not used for fitting, as it was very flat. The first 2 X-ray points were not used for fitting, as they were very high, and possibly due to flaring activity.

080613A

This GRB did not have enough X-ray data to fit to a power law. The optical data was sparse, and not a smoothly decaying lightcurve, and was also not able to be fit to a power law.

071003

The optical data was not fit to a simple power law. Perley et al. (2008) fit the data by several power laws with 2 bumps, the form they used was:

GRB	Optical			X-ray		
	α	$t_{break}(s)$	χ^2/dof	α	$t_{break}(s)$	χ^2/dof
060110	-0.81 ± 0.06		2.3/3	-1.18 ± 0.66		0.4/4
060116	-1.17 ± 0.10		5.9/8	-1.04 ± 0.03		34/23
060708	-0.61 ± 0.02		9.6/10	-4.20 ± 0.12	197.5 ± 8.5	112/115
				-0.58 ± 0.04	8268 ± 1294	
				-1.21 ± 0.04		
070208	-0.48 ± 0.02		79.0/16	1.83 ± 0.62	369 ± 53	25/25
				-0.50 ± 0.06	9571 ± 1733	
				-1.53 ± 0.14		
070419A	3.83 ± 1.34	465 ± 38	24.5/22	-1.89 ± 0.12	220 ± 10	133.4/100
	-0.76 ± 0.17	1662 ± 582		-3.68 ± 0.12	1904 ± 0	
	-1.31 ± 0.09			-0.69 ± 0.09		
070518	-0.79 ± 0.04	72148 ± 22576	2.7/4	-2.10 ± 0.37	992 ± 234	17.9/12
	-0.23 ± 0.09			-0.74 ± 0.04		
070529	-2.07 ± 0.06	508.5 ± 9.2	89.1/54	-0.72 ± 0.09	2381 ± 752	29.8/33
	-1.07 ± 0.05			-1.31 ± 0.05		
071003	see text			-1.60 ± 0.04		71.2/56
071011	-0.70 ± 0.07		20.9/12	-0.89 ± 0.03	587279 ± 86686	26.5/19
				-2.92 ± 0.69		
080613A	see text			see text		

Table 5.2 ABC GRBs and the optical and X-ray decay rates

$$(5.13) \quad F_\nu = F_{0,\nu}(t - dt_0)^{-\alpha} + F_{1,\nu}[\frac{1}{2}(\frac{t - dt_1}{t_{p1}})^{-s_1\alpha_{1,b}} + \frac{1}{2}(\frac{t - dt_1}{t_{p1}})^{-s_1\alpha_{1,a}}]^{-1/s_1}$$

$$+ F_{2,\nu}[\frac{1}{2}(\frac{t - dt_2}{t_{p2}})^{-s_2\alpha_{2,b}} + \frac{1}{2}(\frac{t - dt_2}{t_{p2}})^{-s_2\alpha_{2,a}}]^{-1/s_2}$$

with a best fit of $\alpha_0 = 1.466 \pm 0.006$, $\alpha_{1,b} = -1.710 \pm 0.258$, $\alpha_{1,a} = 5.174 \pm 0.247$, $\alpha_{2,b} = -1.124 \pm 0.164$, $\alpha_{2,a} = 1.724 \pm 0.068$, $dt_0 = -0.01 \pm 3.01s$, $dt_1 = 60 \pm 20s$, $dt_2 = 1245 \pm 311s$, and $\chi^2/dof = 111.1/77$. Their fit included ABC data, as well as data from P60, Keck, KAIT, and Gemini.

071011

This burst has a lot of scatter in the points, and unlike the other bursts, has many points of data from different telescopes taken from the GCN.

GRB	Γ
060110	$1.79^{+0.84}_{-0.58}$
060116	$1.89^{+0.17}_{-0.22}$
060708	$2.24^{+0.07}_{-0.10}$
070208	$2.16^{+0.14}_{-0.18}$
070419A	$2.13^{+0.19}_{-0.16}$
070518	$2.22^{+0.26}_{-0.22}$
070529	$1.89^{+0.09}_{-0.10}$
071003	$2.04^{+0.13}_{-0.15}$
071011	$2.36^{+0.45}_{-0.41}$
080613A	$1.26^{+0.34}_{-0.24}$

Table 5.3 The photon index, Γ, taken from the $Swift$ XRT Repository. All of these values are taken from the website (http://www.swift.ac.uk/xrt_curves/), on Oct 23, 2008, and all are from XRT PC mode data.

Spectral Index β

The second piece needed to compare the data to the fireball model is to know what the spectral index β is. These can be obtained from the $Swift$ XRT Repository (http://www.swift.ac.uk/xrt_curves/), which provides lightcurves, spectra , Γ, and other characteristics of all of the bursts detected or observed by $Swift$. The equation to convert between the two is $\beta = \Gamma - 1$. The β that is calculated here is only valid for the X-ray segment of the data. In some instances, β_o can be calculated, but only when there is optical data in other wavelengths at similars times.

5.4.3   GRBs that fit the model

Roughly half of the ABC GRBs with optical detections fit the fireball model. This section describes those GRBs that fit this model, and why they do, using the closure relations of (Zhang et al., 2006).

GRB060116

The X-ray data can be fit with a single power law, with $\alpha_x = -1.04 \pm 0.03$, and the optical data can be fit with a single power law, with $\alpha_o = -1.17 \pm 0.10$. Using the ISM slow cooling ($\nu > \nu_c$) case ($\alpha_x = (3\beta_x - 1)/2$) gives $\beta_x = .69$, which is

within the errors of Γ, $(\beta = \Gamma - 1)$ listed in Table 5.3. The optical decay, due to the large errors, could be similiar the X-ray decay, and therefore could be in the same regime $(\nu > \nu_c)$. It is also possible that the optical decay is in a different regime $(\nu_m < \nu < \nu_c)$, but it is not possible to determine which of these cases is the best fit for the optical data, as there are no other optical observations to calculate β_o.

GRB060708

During the part of the lightcurve with optical data, the X-ray decays like $\alpha_x = -0.58 \pm 0.04$ and the optical decays like $\alpha_o = -0.61 \pm 0.02$. These are essentially the same decay rate. None of the no-injection fireball models work, but the ISM/slow cooling model with energy injection for $\nu_m < \nu < \nu_c$ works, and using values of $\alpha = 0.60$ and $\beta = 1.24$ gives a reasonable value of $q = 0.23$. This assumes that both the X-ray and optical are in the $\nu_m < \nu < \nu_c$ regime.

GRB070518

GRB070518 has X-ray flares during the early afterglow, but the later data still fits the fireball model. Not counting the early flares, the X-ray lightcurve first decays like $\alpha_{x1} = -2.10 \pm 0.37$, and after $t_{break} = 992s$, has $\alpha_{x2} = -0.74 \pm 0.04$. The optical afterglow, excluding the early points, which were not R band or did not have estimates for the errors, starts at around 1000s and fades as $\alpha_o = -0.79 \pm 0.03$. These 2 decays are essentially the same. Like 060116, the only case that fits is the ISM/slow cooling $(\nu > \nu_c)$ model, which has $\alpha_x = (3\beta_x - 1)/2$, and gives $\beta_x = 0.81$, which is just outside the errors of Γ listed in Table 5.3. In this table, it lists $\Gamma = 2.22^{+0.26}_{-0.22}$, so the lowest β within errors is 1.00. This is not far from 0.81, and it fits the fireball model reasonably well. The optical data has a similar decay as in the X-ray, so it is reasonable to assume that the optical data is in the $(\nu > \nu_c)$ regime.

GRB071011

The optical lightcurve for 071011 can be fit with $\alpha_o = -0.70 \pm 0.07$, and the X-ray (near the optical data) can be fit by $\alpha_x = -0.89 \pm 0.03$. These are similar, and the ISM/slow cooling model for $\nu > \nu_c$ fits the closure relations the best. Using $\alpha_x = (3\beta_x - 1)/2$, and solving for β, gives $\beta_x = 0.89$. From Table 5.3, $\beta = 1.36^{+0.45}_{-0.41}$, so the lowest β within errors is 0.95, which is not far from 0.89, and it fits the fireball model reasonably well. Using observations from the GCN (Kuroda et al., 2007), $\beta_o = 0.44 \pm 0.02$, using pairs of R and I data at different times. The closure relation $(\alpha_o = 3\beta_o/2)$ for the $\nu_m < \nu < \nu_c$ regime fits the optical data the best. Using $\alpha_o = 3\beta/2$ gives $\beta_o = 0.47$, which is similar to 0.44.

5.4.4 GRBs that do not fit the model

About half of ABC GRBs with detections do not fit the fireball model, and this section contains those GRBs. Some of the GRBs have sections of data that do fit the fireball model, but other sections of the lightcurve can not be explained either with the fireball model or with modifications to the model.

GRB 070419A

The X-ray data is fit by 3 power laws, $\alpha_{x0} = -1.89 \pm 0.62$, $\alpha_{x2} = -3.68 \pm 0.12$, and $\alpha_{x0} = -0.69 \pm 0.09$, with break times of $t_1 = 220 \pm 10$ and $t_2 = 1904 \pm 0$. The X-ray is very steep at early times, and there are no closure relations that will fit the fireball model, without energy injection. Assuming α_{x2} is the segment that gets energy injection, $q < 0$, which is unphysical, and thus, the fireball model is not a valid model for this burst. Melandri et al. (2008) also analyzes this burst, and finds that it does not fit the fireball model, unless there is significant energy injection, more than the central engine could provide.

GRB 070208

The optical data is fit by a single power law with $\alpha_o = -0.48 \pm 0.02$, and the X-ray has 3 segments, with $\alpha_{x1} = 1.83 \pm 0.62$, $\alpha_{x2} = -0.50 \pm 0.06$, $\alpha_{x3} = -1.53 \pm 0.14$, with $t_1 = 369 \pm 53$, $t_2 = 9571 \pm 1733$. The optical data overlaps with the X-ray during the latter 2 power-law segments. $\alpha_o \simeq \alpha_{x2} = -0.50$ is reasonable for a fireball model. The last segment, with $\alpha_o = -0.48$ and $\alpha_{x3} = -1.53$ implies $\delta\alpha = 1.03$, which is very large, and impossible to reconcile in the fireball model. Melandri et al. (2008) also analyzes this burst, and concludes that it does not fit the fireball model, since the optical decay is much shallower than the X-ray decay. They hypothesize that the X-ray flares (late time internal shocks) coupled with energy injection would make the X-ray steeper than the optical decay.

GRB 070529

This GRB is unique because it has evidence of a reverse shock, which has only been seen a handful of times since GRB 990123. It was expected that many GRBs, especially in the $Swift$ era, with prompt afterglow observations, would have reverse shock emission. There have only been a few GRBs with evidence for reverse shocks, despite many afterglow observations starting seconds of when the GRB was detected. This GRB does not feature an unusually early or bright afterglow.

The X-ray afterglow is fit by 2 power law segments, the first with $\alpha_{x1} = -0.72 \pm 0.09$, the second with $\alpha_{x2} = -1.31 \pm 0.05$, with a $t_{break} = 2381 \pm 752$. The late X-ray afterglow is fit by the ISM slow cooling model, $\nu_m < \nu < \nu_c$ regime. With the closure relation $\alpha = 3\beta/2$, $\alpha = 1.34$, which is close to the value of α_{x2}. None of the other closure relations are reasonable for α_{x2} and Γ. The early part of the X-ray lightcurve can be explained by energy injection, except that using the formulas for

energy injection gives an unphysical number of -0.42 for q. Therefore, this GRB does not fit the fireball model.

If the optical afterglow is fit by taking the sum of the X-ray fit and an additional power law decay, then the additional power law decay can be attributed to a reverse shock component. The X-ray fit is the forward shock component, and at late times, the forward shock dominates, but at early times, the reverse shock dominates, which is why the earlier optical decay is steeper.

GRB 071003

The optical data fit is described in 5.4.2. The X-ray data is not coincident with the optical data, however, the optical data has features which can not be explained by the fireball model. There are 2 bumps present in the data: one at 120 seconds, and one that peaks at 12000 seconds.

The first bump is nearly simultaneous with a bump in the BAT light curve. Perley et al. (2008) suggests that it arises from internal-shock emission, therefore this is not part of the afterglow.

The second rebrightening show several features: the afterglow rebrightens by 1 magnitude, the decay is steeper by $\Delta\alpha = 0.25 \pm 0.14$, and the spectral index is steeper by $\Delta\beta = 0.80 \pm 0.30$ (Perley et al., 2008). This is the problematic part of the afterglow that does not fit the fireball model.

5.4.5   GRBs with insufficient data

This section contains GRBs detected by the ABC without sufficient information to determine whether the fireball model is a good fit or not. These have sparse optical and sparse X-ray data, and no overlap between the optical and X-ray data.

GRB 060110

GRB060110 has optical data spanning from 7s to roughly 6500 seconds, although this is somewhat sparse, and X-ray data from 250ks to 450ks. The optical decay rate is somewhat flatter than in the X-ray, but it is not reasonable to compare the afterglow at early times (0.03 days) to what happens at late times (3.5 days). The optical and X-ray αs seem reasonable for a fireball model, but the model is neither ruled out or confirmed.

GRB 080613A

GRB 080613A has ABC data spanning from roughly 1000s to 2700s, and X-ray data from 25ks to 60ks. There is one additional GCN point at 4s, which implies that the lightcurve was relatively flat between 4s and 1000s. For completeness, the data is included in the thesis, but it is impossible to determine if the fireball model works for this burst or not.

5.5 Conclusion

GRBs 060116, 060708, 070518, 071011 fit the fireball model. All four of these GRBs had good coverage in X-ray and optical, and had optical data from other observatories. GRB 060116 was unusually faint at early times, and this is discussed in the next chapter, and was the inspiration for (Akerlof & Swan, 2007), but otherwise behaved exactly according to the fireball model. GRB 060708 was the only GRB to be detected with the grating in place, and it was observed when nothing interesting happened (no break in the light curve). The other two GRBs were fairly unremarkable, and were fit without much trouble.

GRBs 071003, 070529, 070208, 070419A do not fit the fireball model. Only GRB 071003 was lacking good X-ray data, however, the optical lightcurve was so

remarkable that it was possible to determine that it did not fit the fireball model from the optical lightcurve alone. There was no way to explain the late, bright re-brightening with the fireball model. GRBs 070208 and 070419A are both similar in that an unphysical amount of energy injection is necessary to explain the data with the fireball model. GRB 070529 is unique in that it is one of the few cases that the optical looks like a reverse shock. However, the X-ray lightcurve defies explanation using the fireball model.

For the ABC GRBs that fit the fireball model, the best fits occurred in an ISM, and none were in a wind-like medium. This is similar to what others have found, most GRBs that fit the fireball model are in an ISM, and only a small fraction are in a wind-like environment. The ABC GRBs that do not fit the fireball model usually have more optical and X-ray data than the bursts that do fit the fireball model, at least for the bursts presented in this chapter. It seems that for other bursts, not just for bursts detected by the ABC, but by other telescopes as well, when more data is collected, segments will fit the fireball model, but the entire burst will not. When there is less data, it is easier to fit to the models. For the bursts with sufficient data, roughly half seem to fit the fireball model. This seems to be the case with ROTSE bursts as well: GRBs 041006 and 050502A fit the fireball model, GRBs 051109A and 050801 fit it after a certain time (early times do not fit), GRBs 050319 and 050525A experience rebrightenings that can not be explained by the fireball model, and GRB 030418A can't be explained by the fireball model at all.

Figure 5.2 Flux Density plot of GRB 051117B. The X-ray data is represented by the black points and ABC data by red points.
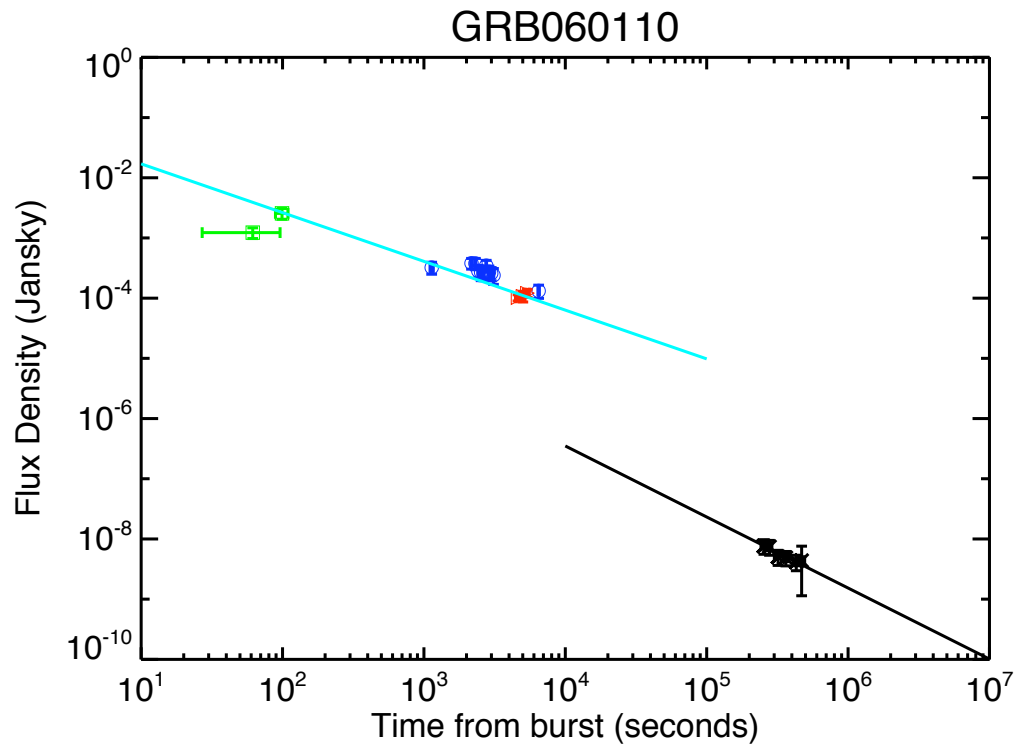
Figure 5.3 Flux Density plot of GRB 060110. The X-ray data is represented by the black points, ABC data by red points, and ROTSE data by green points. The cyan line is the best optical fit, and the black line is the best X-ray fit.
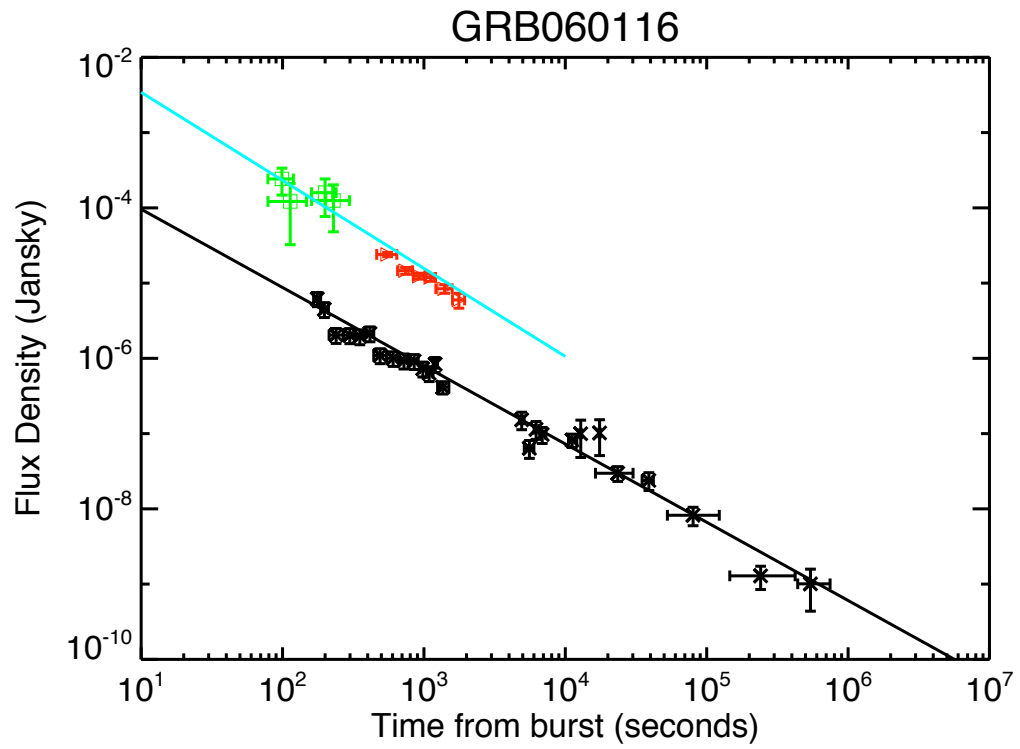
Figure 5.4 Flux Density plot of GRB 060116. The X-ray data is represented by the black points, ABC data by red points, and ROTSE data by green points.The cyan line is the best optical fit, and the black line is the best X-ray fit.
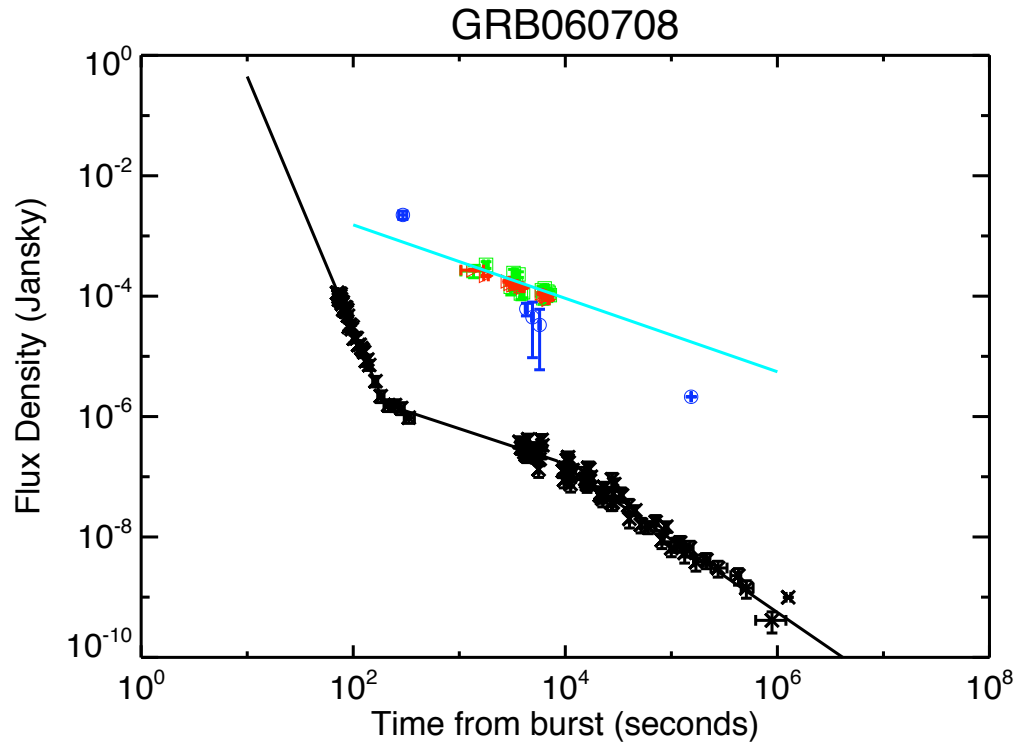
Figure 5.5 Flux Density plot of GRB 060708. The X-ray data is represented by the black points, ABC data (0th order) by red points, ABC data (first order) by green points, and GCN data by blue points. The cyan line is the best optical fit, and the black line is the best X-ray fit. The GCN data is not included in the optical fit, because it is V band data.
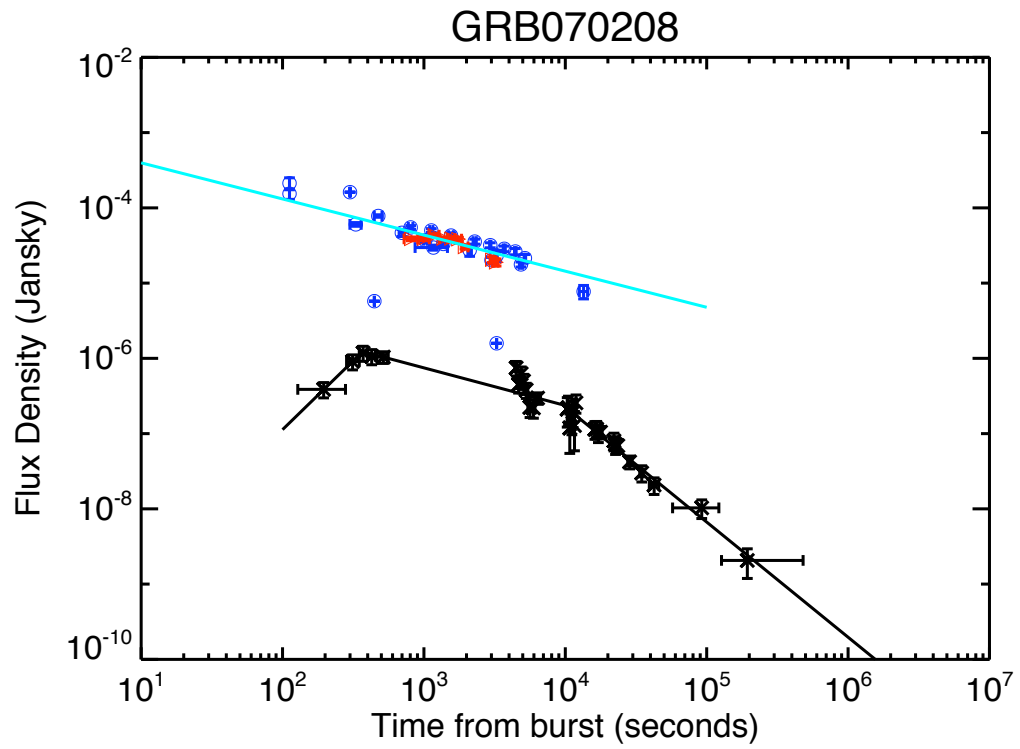
Figure 5.6 Flux Density plot of GRB 070208. The X-ray data is represented by the black points, ABC data by red points, and GCN and literature data by blue points. The cyan line is the best optical fit, and the black line is the best X-ray fit.
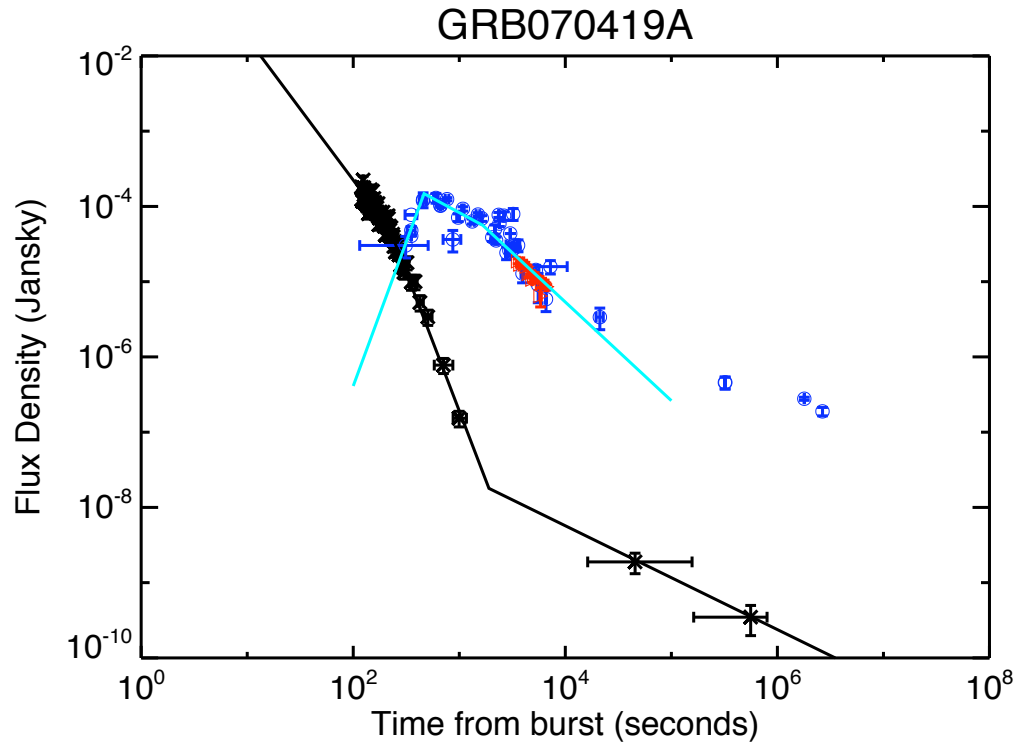
Figure 5.7 Flux Density plot of GRB 070419A. The X-ray data is represented by the black points, ABC data by red points, and GCN and literature data by blue points. The cyan line is the best optical fit, and the black line is the best X-ray fit. The late optical GCN points are not included in the fit.
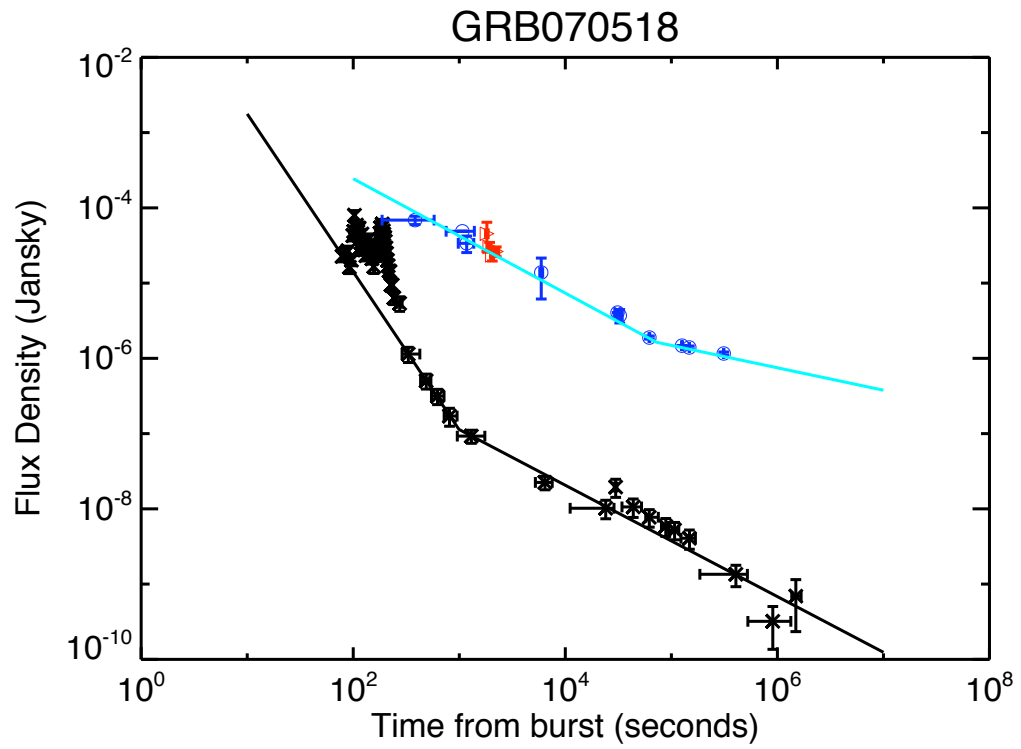
Figure 5.8 Flux Density plot of GRB 070518. The X-ray data is represented by the black points, ABC data by red points, and GCN and literature data by blue points. The cyan line is the best optical fit, and the black line is the best X-ray fit. The X-ray flare is not included in the fit.
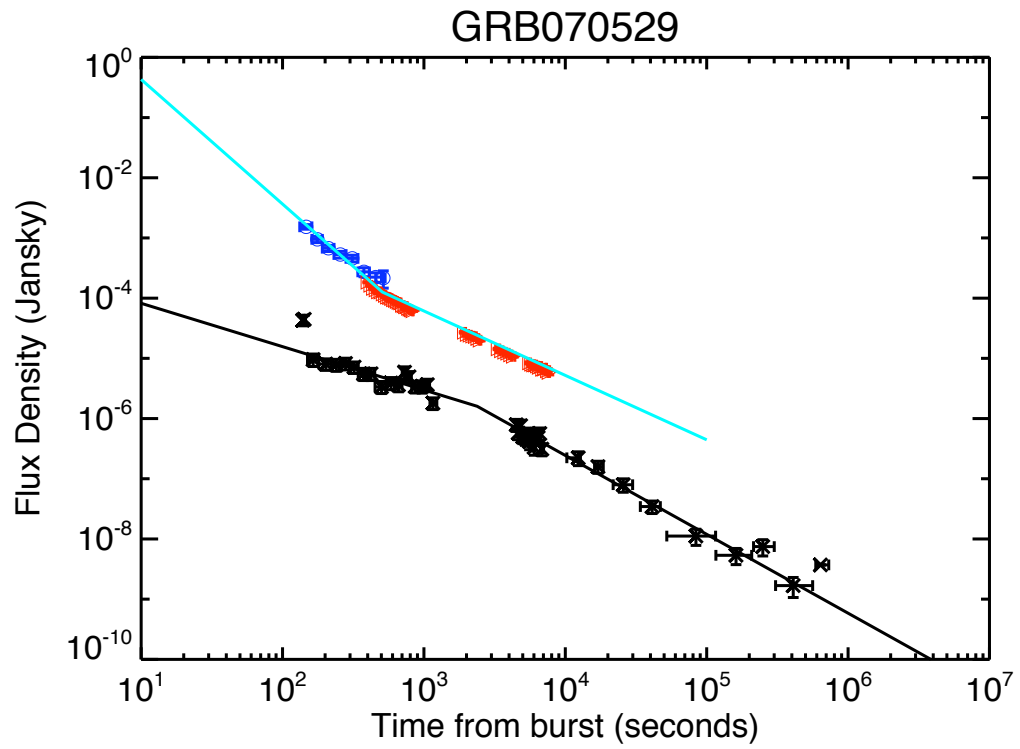
Figure 5.9 Flux Density plot of GRB 070529. The X-ray data is represented by the black points, ABC data by red points, and UVOT data by blue points. The cyan line is the best optical fit, and the black line is the best X-ray fit. The first few X-ray points are not included in the fit.
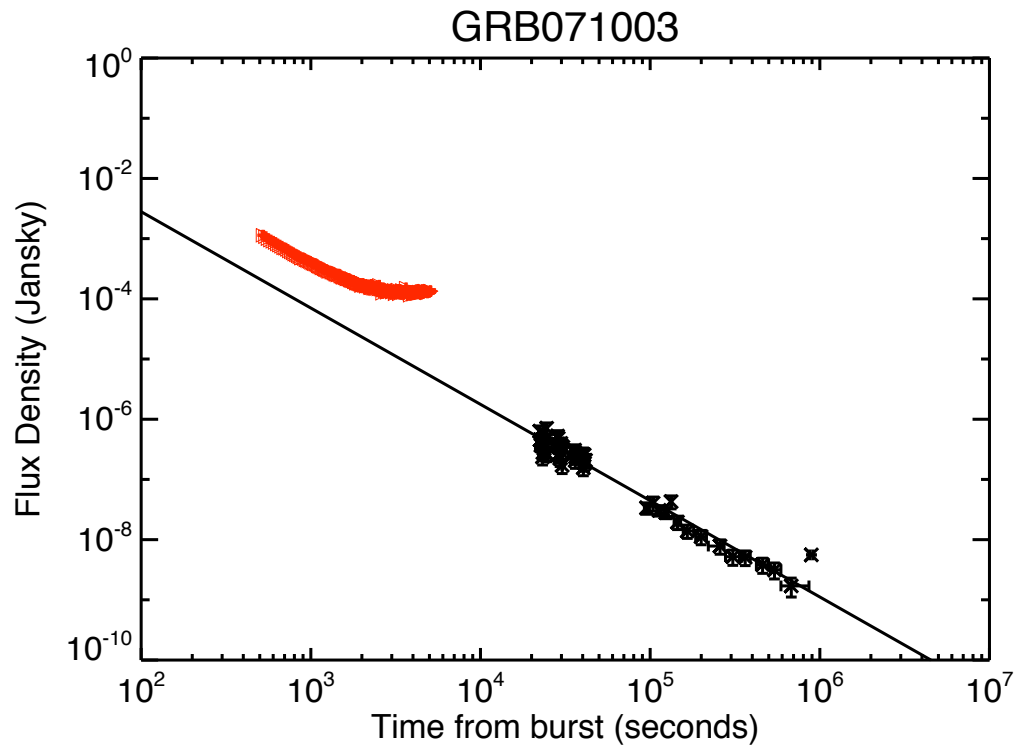
Figure 5.10 Flux Density plot of GRB 071003. The X-ray data is represented by the black points and ABC data by red points. The black line is the best X-ray fit.
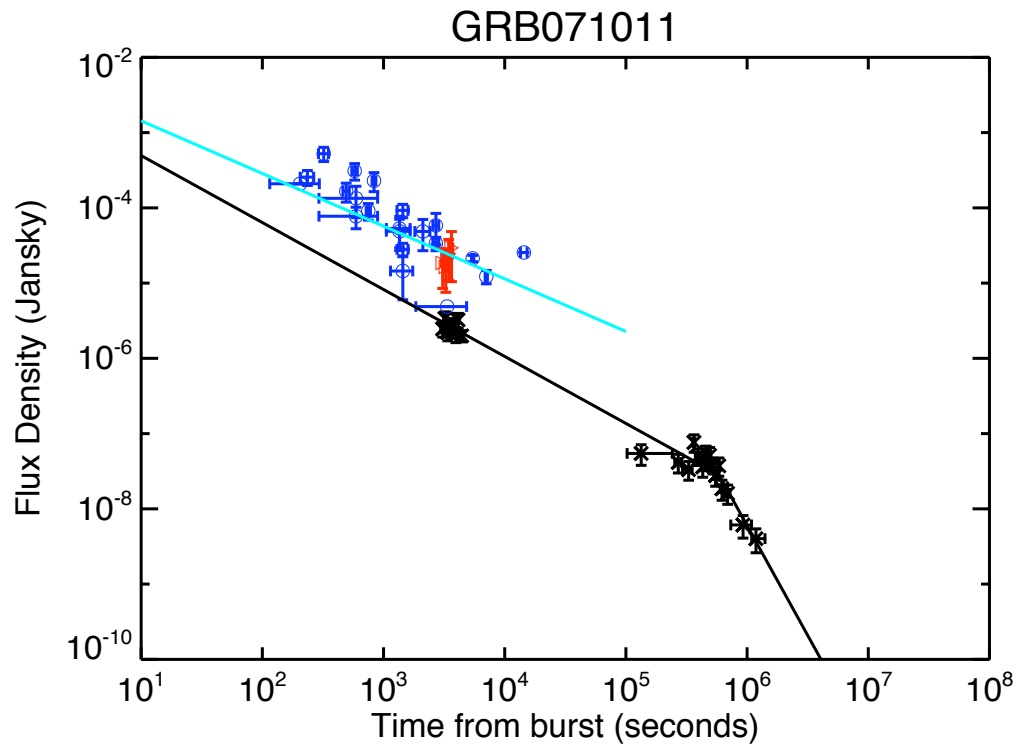
Figure 5.11 Flux Density plot of GRB 071011. The X-ray data is represented by the black points, ABC data by red points, and GCN and literature data by blue points. The cyan line is the best optical fit, and the black line is the best X-ray fit.
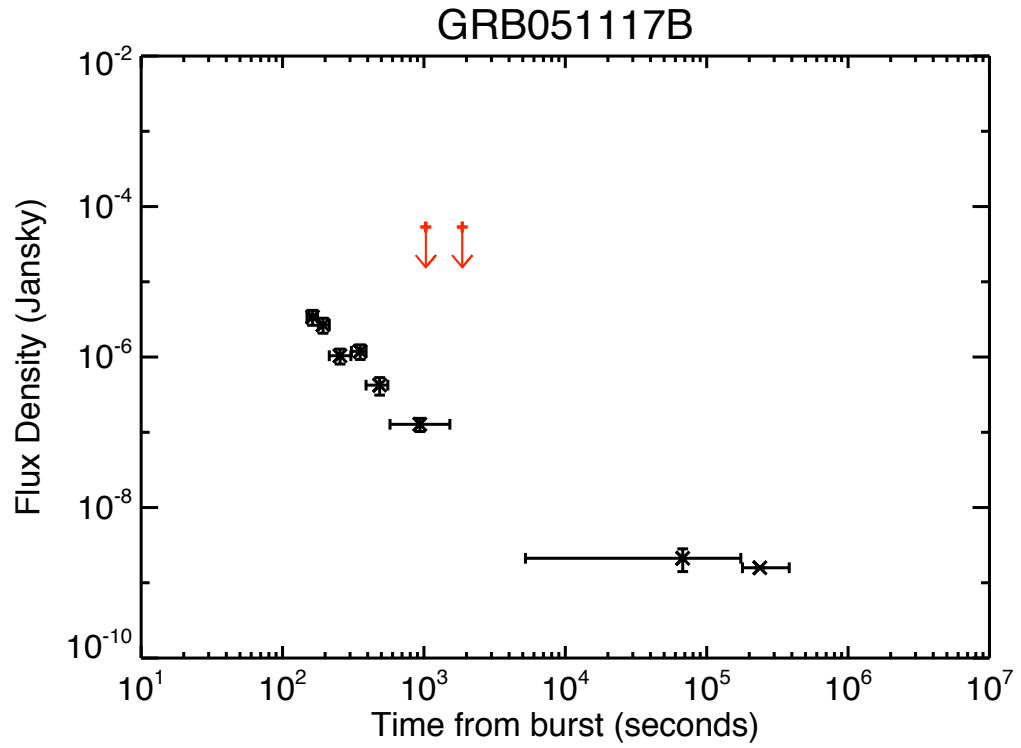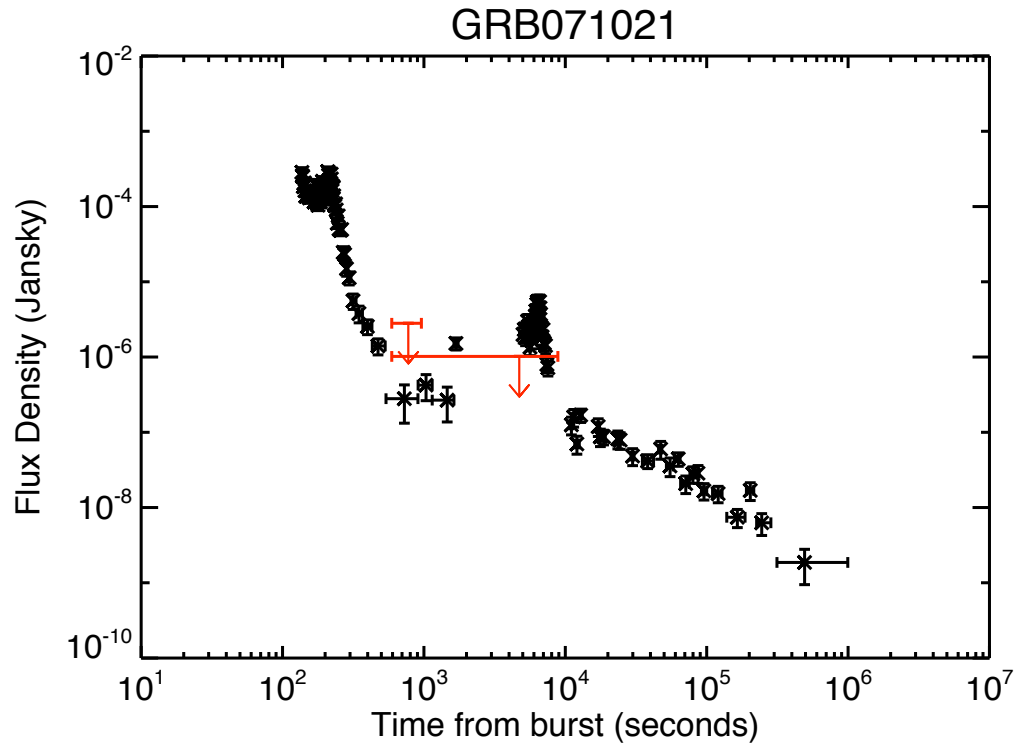
Figure 5.12 Flux Density plot of GRB 071021. The X-ray data is represented by the black points and ABC data by red points.
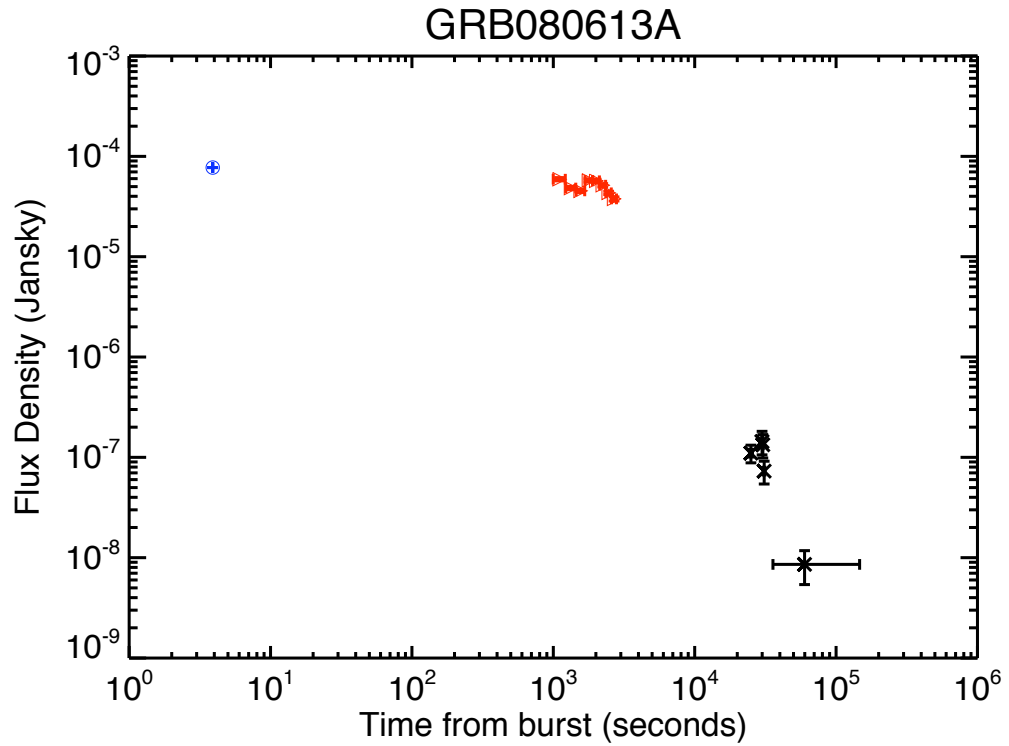
Figure 5.13 Flux Density plot of GRB 080613A. The X-ray data is represented by the black points and ABC data by red points.

CHAPTER VI

Dark GRBs

6.1   Introduction

In this chapter, many aspects of dark bursts are explored. Dark bursts are an interesting puzzle, because despite small error circles and fast localizations from $Swift$, and despite rapid followups by ROTSE, ABC and many other telescopes, 50% of the GRBs are not detected in the optical. There are at least 3 reasons why this might be the case: the GRB could be at a high redshift ($z > 6$), and therefore the light is redshifted out of the optical, the GRB could be obscured by dust, and thus the afterglow would be opaque in the optical, the GRB could be intrinsically dimmer than average, or perhaps some combinations of these.

This chapter is laid out in three parts. First, terminology is explained, because different papers use the same terms to mean different things, and the terminology is unclear. Next, a method of classifying dark bursts is explained, by calculating the optical-to-x-ray spectral index (β_{ox}), with calculations of β_{ox} for all ABC GRB data that is possible, as well as discussions of the results. Then, another aspect of dark bursts (the deepest and earliest limits) are discussed, which allows us to estimate the GRB afterglow apparent optical brightness distribution function using the statistics of many GRBs. Finally, results are compared from both of these different methods

of categorizing dark bursts.

6.2   Dark and Dim Bursts

This section discusses the nomenclature used in this chapter, specifically the term "dark burst". The literature is inconsistent, and often uses "dark GRB" or "dark burst" to mean a burst that has no optical afterglow. However, there are also papers that refer to dark GRBs as those which have a faint optical afterglow, or which are faint by some other criteria. To avoid confusion, the following convention is used throughout this chapter:

- Dark – A GRB that has $\beta_{ox} < 0.5$. It could have an afterglow or not.

- Dim – There is an optical afterglow, and by some criteria this burst is fainter than most.

- Undetected – There is no detected afterglow for this burst.

This will be used in place of other writer's conventions. Jakobsson et al. (2004) defines all bursts with $\beta_{ox} < 0.5$ to be classified as dark, usually even if an afterglow is detected. That convention is adopted here.

6.3 β_{ox}

The values of β_{ox} were calculated for all but 3 of the ABC GRBs with afterglows, and for 2 of the limits. The remaining GRBs were excluded because the X-ray data was at a much later time or there was no X-ray counterpart. It does not make sense to extrapolate and calculate what the X-ray flux density would be during the optical observations if the X-ray data occurs at a very late time, as the X-ray lightcurve is not a single power law. These calculations are different than those in Jakobsson et al. (2004) because they are calculated for any time with an optical observation

by the ABC, which usually takes observations between 15 minutes and 2 hours after the burst. Jakobsson et al. (2004) calculates β_{ox} at 11 hours after the burst.

The procedures for calculating β_{ox} are as follows: First, the optical magnitudes are corrected for local galactic extinction, using the NED Galactic Extinction Calculator (http://nedwww.ipac.caltech.edu/forms/calculator.html). GRB 060116 and GRB 071011 have really high values for the extinction, but the others were much smaller. GRB 060116 was in a patchy part of the sky, with highly variable extinction, so values from Tanvir et al. (2006) were used instead. The extinction for GRB 071011 was really high, but no better values for that extinction are known. Then, the X-ray data was extrapolated to the time of the optical observation. Finally, the formula $\beta_{ox} = -ln(F_o/F_x)/ln(\nu_o/\nu_x)$ is used to calculate β_{ox}, where F_o, F_x are the flux densities of the optical and x-ray at a given time, and ν_o, ν_x are the frequencies of the optical and X-ray light.

The calculated values of β_{ox} for ABC GRBs are given in Tables 6.1, 6.2, and 6.3. GRB 070208, GRB 070529 and GRB 071021 are dark GRBs, because β_{ox} is < 0.5. GRB 060116 should be considered marginally dark, because although β_{ox} evolves with time, it is < 0.5 for the early points, and the others that are > 0.5 have larger errors, and are not much higher than 0.5. GRB 060708, GRB 070419A, GRB 070518, GRB 071011 are not dark, because $\beta_{ox} > 0.5$. GRB 051117B has a limit for $\beta_{ox} < 0.87$, therefore it is not possible to determine if this GRB is dark.

Since β_{ox} is calculated for many points of data for each GRB, it is possible to see if β_{ox} evolves with time. If the X-ray and optical light curve fluxes decay like $F \propto t^{-\alpha}$, and α is similar for both the X-ray and optical, then β_{ox} will not evolve with time. Only GRB 070529 shows a variable β_{ox}, which makes sense for several reasons. First, GRB 070529 has very unique optical and X-ray lightcurves, fit with multiple power

laws which causes β_{ox} to change with time. The other GRBs, at least when using only ABC data, are fit with just a simple power law, so it is not expected that they would have much variability in β_{ox}. If other data are included, β_{ox} would change in time for GRB 070419A and GRB 070208, but not for any of the other GRBs.

Jakobsson et al. (2004), published before the $Swift$ launch, found that 10% of bursts had $\beta_{ox} < 0.5$. Of the 9 ABC bursts for which β_{ox} was calculated, 4 were dark, 4 were bright, and 1 was unable to be determined because it was a limit. Throwing out that 1 burst, means that half of the ABC bursts with β_{ox} calculations are dark. This may seem high, however, both Cenko et al. (2008) (with 29 bursts) and Melandri et al. (2008) (with 63 bursts) find that roughly 50% of their bursts have $\beta_{ox} < 0.50$. Cenko et al. (2008) features bursts detected with the robotic Palomar 60 inch telescope, with a typical response time of 3 minutes and a limiting magnitude of $R < 20.5$. They provide a sample of 29 long GRBs detected by $Swift$, with P60 observations starting at most one hour after the burst trigger time. Melandri et al. (2008) features 63 bursts observed by Liverpool, and Faulkes North and South. Of those 63, optical counterparts were detected in 24 of the bursts, with observations starting on average 2.5 minutes after the burst, and with detections ranging between $R = 10$ and 22. The 39 non-detections have limits of $R < 22$ mag. The ABC sample, although much smaller, is very similar to Cenko et al. (2008) and Melandri et al. (2008), and finds a similar percentage of dark bursts.

6.4 Statistics of GRB optical afterglows

In Akerlof & Swan (2007), the first ~ 100 $Swift$ detected GRBs were used, along with public observational data, to make an estimate of the GRB apparent optical brightness distribution function. The idea for this paper came about after

GRB	A_R	β_{OX}	time
060116	2.2	0.39 ± 0.14	99.05
		0.32 ± 0.14	113.27
		0.43 ± 0.09	199.82
		0.42 ± 0.21	229.17
		0.58 ± 0.18	553.13
		0.56 ± 0.14	741.13
		0.57 ± 0.14	929.08
		0.59 ± 0.14	1117.03
		0.57 ± 0.16	1399.63
		0.56 ± 0.13	1766.68
060708	0.029	0.91 ± 0.08	1362.00
		0.98 ± 0.08	1788.00
		0.95 ± 0.08	3055.00
		1.03 ± 0.08	3243.00
		0.97 ± 0.08	3431.00
		1.03 ± 0.08	3619.00
		0.95 ± 0.08	3807.00
		0.96 ± 0.08	3995.00
		1.03 ± 0.09	6015.00
		0.99 ± 0.09	6203.00
		1.05 ± 0.09	6391.00
		1.01 ± 0.09	6579.00
		1.04 ± 0.09	6767.00
		1.04 ± 0.09	6955.00
		1.03 ± 0.09	7143.00
		0.92 ± 0.08	1362.00
		0.93 ± 0.08	1788.00
		0.97 ± 0.07	2867.00
		0.97 ± 0.07	3055.00
		0.97 ± 0.07	3243.00
		0.98 ± 0.08	3431.00
		0.99 ± 0.07	3807.00
		0.99 ± 0.08	3995.00
		1.02 ± 0.09	6015.00
		1.02 ± 0.09	6391.00
		1.02 ± 0.09	6579.00
		1.02 ± 0.09	6767.00
		1.01 ± 0.09	6955.00
070208	0.039	0.43 ± 0.00	814.00
		0.44 ± 0.01	1002.00
		0.46 ± 0.02	1190.00
		0.46 ± 0.03	1378.00
		0.46 ± 0.03	1566.00
		0.47 ± 0.03	1754.00
		0.45 ± 0.04	1951.00
		0.42 ± 0.03	3042.00
		0.42 ± 0.03	3239.00

Table 6.1 β_{ox} calculated from ABC data and with XRT data extrapolated to be at the same time as the ABC observations. All times are in seconds since the burst time.

GRB	A_R	β_{OX}	time
070419A	0.074	0.78 ± 0.06	3585.00
		0.77 ± 0.06	3773.00
		0.79 ± 0.06	3961.00
		0.78 ± 0.07	4150.00
		0.78 ± 0.07	4338.00
		0.75 ± 0.07	4526.00
		0.76 ± 0.07	4715.00
		0.74 ± 0.07	4903.00
		0.76 ± 0.07	5091.00
		0.76 ± 0.07	5280.00
		0.76 ± 0.07	5468.00
		0.76 ± 0.07	5656.00
		0.70 ± 0.08	5845.00
		0.75 ± 0.07	6033.00
		0.76 ± 0.08	6316.00
		0.75 ± 0.08	6692.00
070518	0.046	0.83 ± 0.05	1820.00
		0.78 ± 0.02	1933.00
		0.75 ± 0.02	2046.00
		0.78 ± 0.02	2231.00
070529	0.807	0.53 ± 0.07	400.90
		0.52 ± 0.07	419.70
		0.51 ± 0.07	438.60
		0.51 ± 0.07	457.50
		0.50 ± 0.11	476.30
		0.50 ± 0.11	495.10
		0.50 ± 0.11	513.90
		0.50 ± 0.10	532.80
		0.49 ± 0.08	551.70
		0.49 ± 0.08	570.50
		0.49 ± 0.08	589.30
		0.49 ± 0.08	608.10
		0.49 ± 0.08	626.80
		0.48 ± 0.08	645.60
		0.48 ± 0.08	664.40
		0.48 ± 0.08	683.20
		0.47 ± 0.07	702.00
		0.47 ± 0.07	720.80
		0.47 ± 0.07	739.60
		0.47 ± 0.07	758.40
		0.47 ± 0.07	777.30
		0.46 ± 0.07	796.10
		0.46 ± 0.07	814.90
		0.46 ± 0.07	833.80
		0.43 ± 0.07	1926.50
		0.43 ± 0.07	2020.70
		0.43 ± 0.07	2114.80

Table 6.2 β_{ox} calculated from ABC data and with XRT data extrapolated to be at the same time as the ABC observations. All times are in seconds since the burst time.

GRB	A_R	β_{OX}	time
		0.43 ± 0.07	2209.00
		0.44 ± 0.07	2303.20
		0.44 ± 0.06	2397.60
		0.43 ± 0.06	2491.80
		0.44 ± 0.08	3341.50
		0.44 ± 0.08	3529.90
		0.44 ± 0.07	3718.10
		0.45 ± 0.07	3906.50
		0.44 ± 0.07	4095.00
		0.45 ± 0.07	4283.30
		0.46 ± 0.08	5577.70
		0.46 ± 0.07	5765.80
		0.46 ± 0.10	5953.80
		0.46 ± 0.06	6141.70
		0.46 ± 0.06	6329.70
		0.46 ± 0.06	6517.70
		0.47 ± 0.07	6705.70
		0.46 ± 0.08	6893.70
		0.47 ± 0.08	7081.70
		0.48 ± 0.08	7269.70
		0.47 ± 0.07	7457.70
		0.46 ± 0.07	7645.70
071011	5.336	0.88 ± 0.13	3075.00
		0.87 ± 0.13	3263.00
		0.93 ± 0.13	3451.00
		0.96 ± 0.13	3639.00
071021	0.149	$< 0.32 \pm 0.06$	775.75
		$< 0.42 \pm 0.10$	4723.17
051117B	0.175	$< 0.80 \pm 0.02$	1031.00
		$< 0.87 \pm 0.04$	1866.00

Table 6.3 β_{ox} calculated from ABC data and with XRT data extrapolated to be at the same time as the ABC observations. All times are in seconds since the burst time.

GRB 060116, which was extraordinarily faint at early times, was detected by the ABC. This is a purely statistical method, which does not address the reasons why a particular burst may or may not have an optical afterglow. In this method, public data is used to find the best limiting magnitudes and the detected magnitudes near 1000s. This is a convolution of the distribution of afterglow magnitudes (at 1000s) that Nature gives us, and of the available instruments that can observe the afterglow. From the public data of a wide range of observatories, it is possible to infer what the apparent afterglow optical brightness distribution function is. This part of the thesis, Section 6.4, follows Akerlof & Swan (2007), which explains how the data was selected, how the optical brightness function was calculated, discusses results, and finally, adds the ABC observations, which were not part of that paper.

6.4.1 Data Selection and Correction

Data selection incorporated 118 $Swift$ GRBs between February 15, 2005 and May 7, 2006. The following selection criteria were used. First, the optical observations were required to lie between 100 and 10,000s after the burst was detected, and were restricted to V, R or unfiltered bands. These restrictions omitted 10 GRBs, 9 because of the time cut and 1 because of the wavelength cut. After selection, the data was compensated for galactic absorption using the NED extragalactic calculator (http://nedwwwipac. caltech.edu/forms/calculator.html). The V band data was adjusted by -0.41 mags, which is the average color difference between V and R for time periods between 0.2 and 1 days for 5 GRBs with many measurements of V and R at many different times. The 5 GRBs used for this average color difference are: GRB 990510 (Stanek et al., 1999), 020813 (Covino et al., 2003), 021004 (Bersier et al., 2003), 030329(Burenin et al., 2003), (Rumyantsev et al., 2003), (Zharikov et al., 2003), and 05052A (Guidorzi et al., 2005b). These GRBs showed no evidence

of chromatic variability.

For the GRBs with detections, the logarithmically closest measurement to $1000s$ was chosen. It was possible to extract a powerlaw α for 37 of the 43 GRBs, in order to extrapolate the measurements at t to $t_c = 1000s$. A similar calculation was done assuming $\alpha = -0.70$. The GRBs with detections, the magnitudes closest to 1000s (m_{det}), α, and other details are listed in Table 6.4. Both probability distributions are plotted in Figure 6.1. They look similar, and according to the Smirnov-Cramér-von Mises test, they are effectively identical. This gives confidence in extrapolating the magnitude limits to t_c using $\alpha = -0.70$ for the bursts with no detected afterglows.
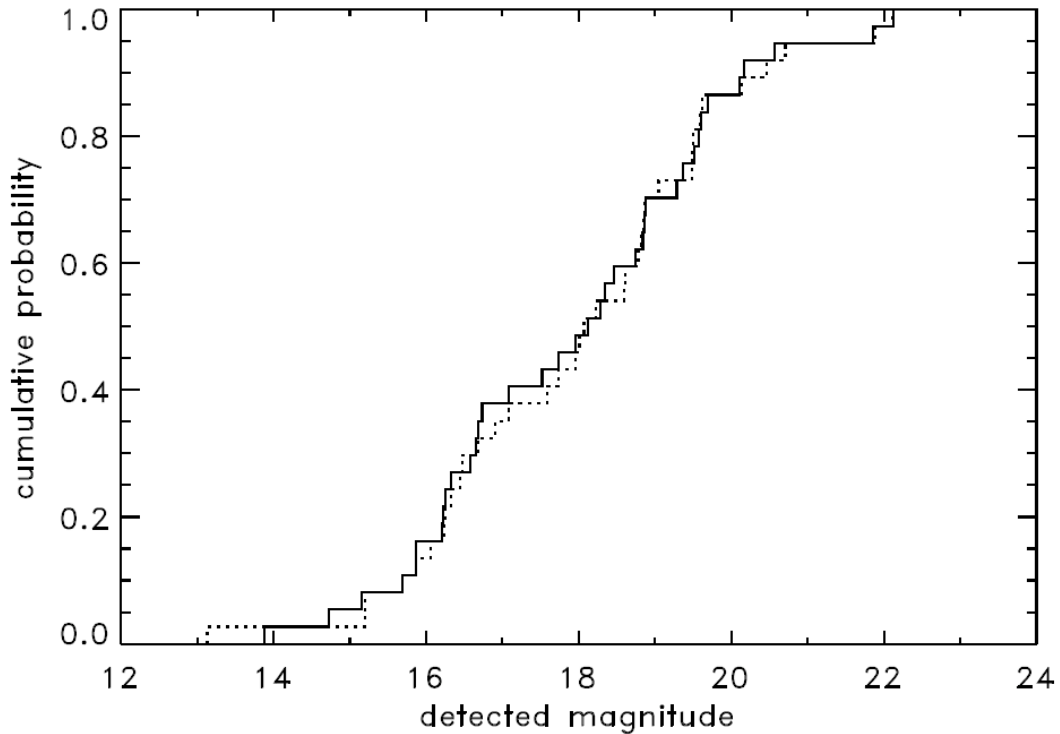
Figure 6.1 Cumulative distribution for the 37 GRBs with detected afterglows. The solid line shows each magnitude extrapolated to $t_c = 1000$ using an individually calculated α, and the dotted line shows each magnitude extrapolated to $t_c = 1000$ using $\alpha = -0.70$.

The next part was to find m_{lim} for all of the bursts. For the burst without detections, the limiting magnitude reports were transformed as if they were detections

to t_c, only requiring an observation time between 100 and 10,000s. The maximum magnitude of each set is taken as m_{lim} for that burst, and these are listed in Table 6.5.

For bursts with detections, the next step was the estimation of m_{lim}, which should lie somewhere between $m_{det} + \sigma_{det}$ (σ_{det} is the magnitude error) and the best limiting magnitude ever reported. The simplest thing is to take the median of the m_{lim} in that range, and add it in to the entire set of m_{lim}. This was done recursively for the detected GRBs ordered by decreasing m_{det} to determine the missing values of m_{lim}.

Table 6.4. GRB Afterglow Detections

GRB	RA	DEC	Filter	A_V	A_R	α	m_{det}[a]	$t_{burst}(s)$	m_{det} @ t_c[b]	Reference
050318	03:18:51.15	-46:23:43.70	V	0.054	0.043	-0.87	17.80	3230.00	16.445	1
050319	10:16:50.76	+43:32:59.90	none	0.036	0.029	-0.88	18.00	1015.00	17.960	2
050401	16:31:28.82	+02:11:14.83	none	0.216	0.174	-0.76	18.58	241.35	19.486	3
050406	02:17:52.30	-50:11:15.00	V	0.073	0.059	-0.75	19.44	138.00	20.462	4
050416	12:33:54.60	+21:03:24.00	V	0.098	0.079	*	19.38	115.00	20.516	5
050505	09:27:03.20	+30:16:21.50	none	0.071	0.057	*	18.40	1009.00	18.336	6
050525	18:32:32.57	+26:20:22.50	none	0.315	0.254	-1.23	16.12	1002.30	15.864	7
050607A	20:00:42.79	+09:08:31.50	R	0.516	0.416	-1.00	22.50	960.00	22.115	8
050712A	05:10:47.90	+64:54:51.50	V	0.753	0.607	-0.73	17.38	959.00	16.249	9
050713A	21:22:09.53	+77:04:29.50	R	1.371	1.106	-0.67	21.41	2963.00	19.478	10
050721	16:53:44.53	-28:22:51.80	R	0.894	0.721	-1.29	17.93	1484.00	16.909	11
050726	13:20:12.30	-32:03:50.80	V	0.206	0.166	0	17.35	173.00	18.067	12
050730	14:08:17.13	-03:46:16.70	R	0.168	0.135	-0.54	17.07	1848.00	16.468	13
050801	13:36:35.00	-21:55:41.00	none	0.319	0.257	-1.31	16.93	996.00	16.676	14
050802	14:37:05.69	+27:47:12.20	V	0.070	0.057	-0.85	18.35	1463.00	17.581	15
050815	19:34:23.15	+09:08:47.47	V	1.457	1.175	*	20.00	117.00	19.764	16
050820A	22:29:38.11	+19:33:37.10	Rc	0.146	0.118	-0.97	15.42	1146.00	15.198	17
050824	00:48:56.05	+22:36:28.50	none	0.116	0.093	-0.55	18.60	1440.00	18.230	18
050908	01:21:50.75	-12:57:17.20	Rc	0.083	0.067	-0.93	18.80	900.00	18.813	19
050922C	21:09:33.30	-08:45:27.50	none	0.342	0.276	-1.00	16.00	640.00	16.063	20
051109A	22:01:15.31	+40:49:23.31	none	0.630	0.508	-0.65	17.59	1004.00	17.079	21
051111	23:12:33.36	+18:22:29.53	none	0.537	0.433	-0.74	16.13	1007.00	15.692	21
051117A	15:13:34.09	+30:52:12.70	V	0.080	0.065	-0.35	20.01	210.00	20.706	22
051221A	21:54:48.63	+16:53:27.16	R	0.227	0.183	-0.93	20.20	4680.00	18.844	23
060108	09:48:01.98	+31:55:08.60	R	0.059	0.047	-0.43	21.84	879.00	21.891	24
060110	04:50:57.85	+28:25:55.70	none	2.107	1.699	-0.70	17.90	847.00	16.327	25
060111A	18:24:49.00	+37:36:16.10	none	0.094	0.076	*	18.30	173.50	19.555	26
060111B	19:05:42.47	+70:22:33.10	none	0.368	0.297	-1.08	18.90	792.00	18.780	27
060115	03:36:08.40	+17:20:43.00	Rc	0.441	0.356	0.00	19.10	1190.00	18.612	28
060116	05:38:46.28	-05:26:13.14	none	0.873	0.704	-1.09	20.78	926.08	20.134	29
060117	21:51:36.13	+59:58:39.10	R	4.292	0.010	-1.70	12.62	502.90	13.132	30
060124	05:08:25.50	+69:44:26.00	V	0.449	0.362	0.15	16.79	663.00	16.243	31
060203	06:54:03.85	+71:48:38.40	Rc	0.514	0.414	-0.90	19.90	3240.00	18.593	32
060204B	14:07:14.80	+27:40:34.00	R	0.059	0.048	-0.80	20.40	3096.00	19.493	33
060206	13:31:43.42	+35:03:03.60	r'	0.041	0.033	-1.00	17.80	1036.00	17.740	34
060210	03:50:57.37	+27:01:34.40	none	0.309	0.249	-1.30	18.12	835.00	18.008	35
060218	03:21:39.68	+16:52:01.82	none	0.471	0.380	*	18.09	858.95	17.826	36
060223	03:40:49.56	-17:07:48.36	V	0.385	0.311	-0.75	19.60	935.00	18.856	37
060313	04:26:28.40	-10:50:40.10	R	0.230	0.186	-0.13	19.90	1134.00	19.618	38
060323	11:37:45.40	+49:59:05.50	none	0.050	0.040	*	18.20	540.00	18.628	39
060418	15:45:42.40	-03:38:22.80	Rc	0.743	0.599	-1.20	16.47	2412.00	15.202	40
060428B	15:41:25.63	+62:01:30.30	none	0.049	0.040	0.05	19.64	1013.00	19.590	41
060502A	16:03:42.48	+66:36:02.50	R	0.109	0.088	-0.45	19.80	2400.00	19.047	42

[a]m_{det} is the measured magnitude at t_{burst} seconds after the GRB trigger.

[b]m_{det} @ t_c is the inferred value for m_{det} at $t_c = 1000$ s after correcting for galactic absorption and average GRB color differences.

References. — (1)(Still et al., 2005) (2)(Quimby et al., 2006b) (3)(Rykoff et al., 2005a) (4)(Schady et al., 2006) (5)(Schady et al., 2005c) (6)(Klotz et al., 2005a) (7)(Klotz et al., 2005d) (8)(Pagani et al., 2006) (9)(De Pasquale et al., 2006) (10)(Guetta et al., 2007) (11)(Antonelli et al., 2006) (12)(Poole et al., 2005c) (13)(Pandey et al., 2006) (14)(Rykoff et al., 2006a) (15)(Mc-Gowan et al., 2005a) (16)(Schady et al., 2005a) (17)(Cenko et al., 2006a) (18)(Lipunov et al., 2005) (19)(Torii, 2005a) (20)(Rykoff et al., 2005b) (21)(Yost et al., 2007) (21)(Yost et al., 2007) (22)(Holland et al., 2005a) (23)(Wren et al., 2005) (24)(Oates et al., 2006) (25)(Li, 2006) (26)(Klotz et al., 2006a) (27)(Klotz et al., 2006b) (28)(Yanagisawa et al., 2006) (29)(Swan et al., 2009) (30)(Jelínek et al., 2006) (31)(Romano et al., 2006) (32)(Bikmaev et al., 2006) (33)(Guidorzi et al., 2006b) (34)(Monfardini et al., 2006a) (35)(Stanek et al., 2007) (36)(Quimby et al., 2006a) (37)(Marshall et al., 2006) (38)(Cobb, 2006) (39)(Zheng et al., 2006) (40)(Koppelman, 2006) (41)(Li et al., 2006) (42)(Cenko et al., 2006b)

Table 6.5.   GRB Afterglow Non-Detections

GRB	RA	DEC	Filter	A_V	A_R	m_{lim}[a]	$t_{burst}(s)$	m_{lim} @ t_c[b]	Reference
050215A	23:13:31.68	+49:19:19.20	none	0.715	0.577	17.40	1080.00	16.765	1
050215B	11:37:48.03	+40:47:43.40	V	0.063	0.050	19.50	1797.00	18.582	2
050219A	11:05:39.24	-40:40:58.00	V	0.536	0.432	20.70	971.00	19.776	3
050219B	05:25:16.31	-57:45:27.31	V	0.109	0.088	19.41	3186.00	18.010	4
050223	18:05:32.49	-62:28:21.07	none	0.295	0.238	18.00	2580.00	17.042	5
050306	18:49:14.00	-09:09:10.40	none	2.255	1.818	17.50	3600.29	14.708	6
050315	20:25:54.10	-42:36:02.20	V	0.159	0.128	18.50	140.19	19.424	7
050326	00:27:49.10	-71:22:16.30	V	0.123	0.099	18.91	3313.33	17.467	8
050410	05:59:12.90	+79:36:09.20	V	0.369	0.297	19.90	2865.50	18.321	9
050412	12:04:25.06	-01:12:03.60	Rc	0.066	0.053	24.90	8336.74	23.235	10
050416B	08:55:35.20	+11:10:32.00	r	0.102	0.082	20.00	5160.00	18.671	11
050421	20:29:00.94	+73:39:11.40	none	2.693	2.172	18.40	144.29	17.699	12
050422	21:37:54.50	+55:46:46.60	V	4.609	3.716	17.90	374.10	13.628	13
050502B	09:30:10.10	+16:59:44.30	V	0.098	0.079	21.80	1219.97	21.141	14
050509A	20:42:19.70	+54:04:16.20	V	1.981	1.597	18.23	1853.00	15.370	15
050509B	12:36:13.67	+28:58:57.00	R	0.064	0.051	21.80	1402.27	21.492	16
050528A	23:34:03.60	+45:56:16.80	R	0.533	0.430	20.00	1799.71	19.123	17
050713B	20:31:15.50	+60:56:38.40	R	1.548	1.248	21.60	1782.43	19.913	18
050714B	11:18:48.00	-15:32:49.90	R	0.181	0.146	20.00	3387.74	18.927	19
050716	22:34:20.40	+38:40:56.70	R	0.358	0.289	19.80	228.10	20.634	20
050717	14:17:24.90	-50:32:13.20	V	0.786	0.634	18.71	128.00	19.076	21
050724	16:24:44.37	-27:32:27.50	V	2.032	1.639	18.84	1663.00	16.011	22
050803	23:22:38.00	+05:47:02.30	V	0.246	0.198	18.80	235.01	19.245	23
050813	16:07:57.00	+11:14:52.00	V	0.185	0.149	18.15	152.00	18.987	24
050814	17:36:45.39	+46:20:21.60	V	0.093	0.075	18.00	217.00	18.658	25
050819	23:55:01.20	+24:51:36.50	R	0.406	0.327	21.60	7864.99	19.706	26
050820B	09:02:25.03	-72:38:44.00	R	0.417	0.336	15.30	4716.00	13.785	27
050822	03:24:26.70	-46:02:01.70	V	0.049	0.040	19.50	138.24	20.545	28
050826	05:51:01.58	-02:38:35.80	V	1.944	1.568	19.00	155.00	18.063	29
050904	00:54:50.79	+14:05:09.42	V	0.200	0.161	18.90	214.00	19.462	30
050906	03:31:11.75	-14:37:18.10	R	0.220	0.177	19.70	470.02	20.097	31
050911	00:54:37.70	-38:50:57.70	R	0.034	0.028	21.00	2160.00	20.387	32
050915A	05:26:44.80	-28:00:59.27	R	0.086	0.070	21.00	1098.14	20.859	33
050915B	14:36:26.50	-67:24:36.50	V	1.292	1.041	21.40	9360.00	17.998	34
050922B	00:23:13.20	-05:36:16.40	V	0.122	0.098	20.10	3169.50	18.691	35
050925	20:13:54.24	+34:19:55.20	R	7.510	6.056	19.00	197.86	14.175	36
051001	23:23:48.80	-31:31:17.00	R	0.051	0.041	21.50	1175.90	21.336	37
051006	07:23:13.52	+09:30:24.48	V	0.218	0.176	18.80	207.00	19.369	38
051008	13:31:29.30	+42:05:59.00	R	0.039	0.031	22.60	3822.34	21.550	39
051016	08:11:16.30	-18:17:49.20	V	0.293	0.236	19.10	114.91	20.041	40
051016B	08:48:27.60	+13:39:25.50	Rc	0.123	0.099	15.70	105.41	17.311	41
051021B	08:24:11.80	-45:32:30.80	V	3.852	3.106	19.00	178.00	16.050	42
051105	17:41:03.28	+34:59:03.60	V	0.112	0.090	20.00	9566.50	17.762	43
051109B	23:01:50.21	+38:40:46.00	R	0.557	0.449	21.00	5436.29	19.264	44
051117B	05:40:43.00	-19:16:26.50	R	0.185	0.149	20.80	2885.76	19.846	45
051221B	20:49:35.10	+53:02:12.20	R	4.543	3.663	18.20	281.66	15.500	46
051227	08:20:58.11	+31:55:31.89	Rc	0.140	0.113	17.70	3944.16	16.544	47
060105	19:50:00.60	+46:20:58.00	V	0.568	0.458	18.00	191.00	18.280	48
060109	18:50:43.50	+31:59:29.70	V	0.478	0.386	19.00	204.00	19.320	49
060202	02:23:22.88	+38:23:04.30	R	0.157	0.126	21.50	252.29	22.421	50
060211A	03:53:32.80	+21:29:21.00	V	0.637	0.514	19.00	283.00	18.912	51
060211B	05:00:17.20	+14:56:58.90	R	1.349	1.088	22.10	2257.63	20.393	52
060219	16:07:21.10	+32:18:56.30	V	0.108	0.087	18.60	120.10	19.693	53
060223B	16:56:58.80	-30:48:46.00	R	1.301	1.049	13.70	326.59	13.501	54
060306	02:44:23.00	-02:08:52.80	V	0.118	0.096	18.40	193.00	19.122	55
060312	03:03:06.12	+12:50:03.50	none	0.585	0.472	18.30	1270.94	17.646	56
060319	11:45:33.80	+60:00:39.00	R	0.073	0.059	21.00	5238.43	19.682	57

Table 6.5 (cont'd)

GRB	RA	DEC	Filter	A_V	A_R	m_{lim}[a]	$t_{burst}(s)$	m_{lim} @ t_c[b]	Reference
060403	18:49:21.80	+08:19:45.30	V	4.251	3.428	19.25	5066.50	13.356	58
060413	19:25:07.70	+13:45:27.30	V	6.472	5.219	19.20	1160.00	12.205	59
060421	22:54:32.63	+62:43:50.07	V	4.236	3.416	17.70	285.00	14.008	60
060427	08:17:04.40	+62:40:18.30	V	0.165	0.133	18.50	333.00	18.761	61
060428A	08:14:10.98	-37:10:10.30	V	4.128	3.328	19.10	271.00	15.554	62
060501	21:53:29.90	+43:59:53.40	none	0.951	0.767	17.40	426.82	17.280	63
060502B	18:35:45.89	+52:37:56.20	none	0.145	0.117	20.00	719.71	20.133	64
060507	05:59:51.70	+75:14:56.60	R	0.514	0.414	19.20	3828.38	17.766	65

[a]m_{lim} is the magnitude upper limit at t_{burst} seconds after the GRB trigger.

[b]m_{lim} @ t_c is the inferred value for m_{lim} at $t_c = 1000$ s after correcting for galactic absorption and average GRB color differences.

References. — (1)(Smith et al., 2005) (2)(Roming et al., 2005) (3)(Schady et al., 2005b) (4)(Poole et al., 2005a) (5)(Smith, 2005) (6)(Klotz et al., 2005c) (7)(Rosen et al., 2005) (8)(Holland et al., 2005b) (9)(Boyd et al., 2005b) (10)(Kosugi et al., 2005) (11)(Berger et al., 2005) (12)(Rykoff et al., 2005c) (13)(McGowan et al., 2005b) (14)(Cenko et al., 2005) (15)(Poole et al., 2005b) (16)(Wozniak et al., 2005) (17)(Monfardini et al., 2005) (18)(lin et al., 2005) (19)(Malesani et al., 2005) (20)(Guidorzi et al., 2005a) (21)(Hurkett et al., 2005) (22)(Chester et al., 2005) (23)(Brown et al., 2005a) (24)(Retter et al., 2005a) (25)(Retter et al., 2005b) (26)(Bikmaev et al., 2005) (27)(Jelinek et al., 2005) (28)(Page et al., 2005) (29)(Mangano et al., 2005) (30)(Cucchiara et al., 2005) (31)(Fox et al., 2005a) (32)(Tristram et al., 2005a) (33)(Cenko & Fox, 2005) (34)(Cobb & Bailyn, 2005) (35)(Pasquale et al., 2005) (36)(Guidorzi et al., 2005c) (37)(Tristram et al., 2005b) (38)(Norris et al., 2005) (39)(Rumyantsev et al., 2005) (40)(Boyd et al., 2005a) (41)(Torii, 2005b) (42)(Retter et al., 2005c) (43)(Brown et al., 2005b) (44)(Huang et al., 2005) (45)(Chen et al., 2005) (46)(Klotz et al., 2005b) (47)(Yanagisawa et al., 2005) (48)(Ziaeepour et al., 2006) (49)(Pasquale et al., 2006) (50)(Monfardini et al., 2006b) (51)(Hurkett et al., 2006) (52)(Sharapov et al., 2006) (53)(Breeveld & Moretti, 2006) (54)(Torii, 2006) (55)(Angelini et al., 2006) (56)(Schaefer et al., 2006) (57)(Guziy et al., 2006) (58)(Poole & Boyd, 2006) (59)(Boyd et al., 2006) (60)(Goad et al., 2006) (61)(Mangano et al., 2006b) (62)(Mangano et al., 2006a) (63)(Rykoff et al., 2006b) (64)(Zhai et al., 2006) (65)(Halpern & Mirabal, 2006)

6.4.2   Finding the Optical Brightness Distribution Function

The optical brightness distribution function $F(m)$ was originally going to be represented by a set of cubic B-splines, uniformly spaced over a range of observed magnitudes. $F(m)$ needs to be either 0 or 1 at the endpoints, so to avoid those problems, $m(F)$ is described by cubic splines.

To predict the observed distribution of actual detections, the estimated limiting magnitude distribution is convolved with the function describing the true GRB afterglow distribution. This starts with the integral distribution of upper limits m_{lim}, which is a staircase function with uniform vertical steps between irregular intervals ($\Delta m = m_{i+1} - m_i$), where the probability $p(m_i \rightarrow m_{i+1})$, is uniform. In each interval of magnitude, the expected number of detected GRB events increases by

$\Delta F_i^{calc} = \Delta F_i p_i$ where $\Delta F_i = F(m_i) - F(m_{i-1})$ is the change in the brightness distribution function over Δm. $F(m_i)$ is then calculated by inverting the cubic spline representation of $m(F)$.

The cumulative probability distribution for the expected number of detected events is $f_i^{calc} = \Sigma^i \Delta f_j^{calc}$. The experimentally observed cumulative distribution for these events, f_i^{obs} is a sequence of rational fractions, $(1, 2, 3, ..., n_{det})/n_{total}$, where n_{det} is the number of detected GRBs, and n_{total} is the number of events, both detected and undetected. To find $F(m)$, take $\delta_i = (f_i^{calc} - f_i^{obs})$, and minimize the sum of squares $\Sigma^{n_{det}} \delta_i^2$.

These calculations were carried out with 4,5,6 and 7 degrees of freedom using cubic B-splines (see Figure 6.2). For all 4 spline curves, the fits were very similar and quite good.
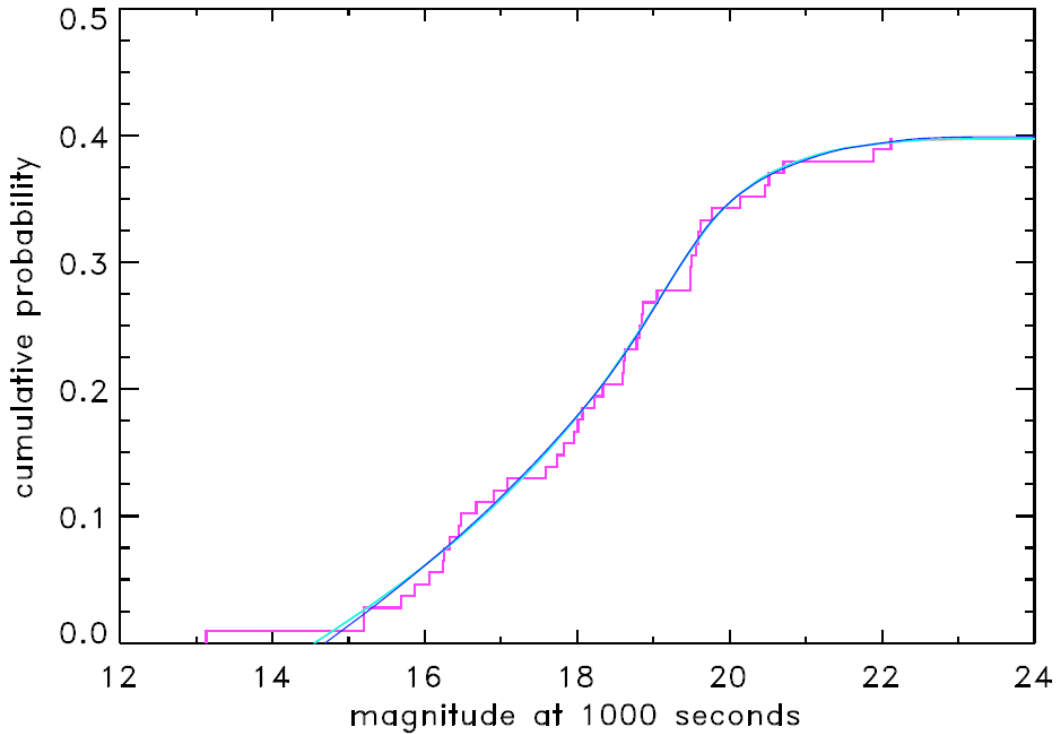

Figure 6.2 Cumulative distribution of detected GRB optical afterglows. The experimentally observed distribution is the violet line. The red, green, cyan and blue lines correspond to the least squares estimates of the B-spline curves with 4,5,6 and 7 degrees of freedom.

6.4.3 Results

The optical brightness distribution function can be seen in Figure 6.3. All of the fits are very similar, but the last useful point occurs when $m_{det} = 22.1$, and the distribution reaches 71%. We found that 29% are lost because they are dimmer than $m_{det} \simeq 22$ and the rest are missed because of observational limits.
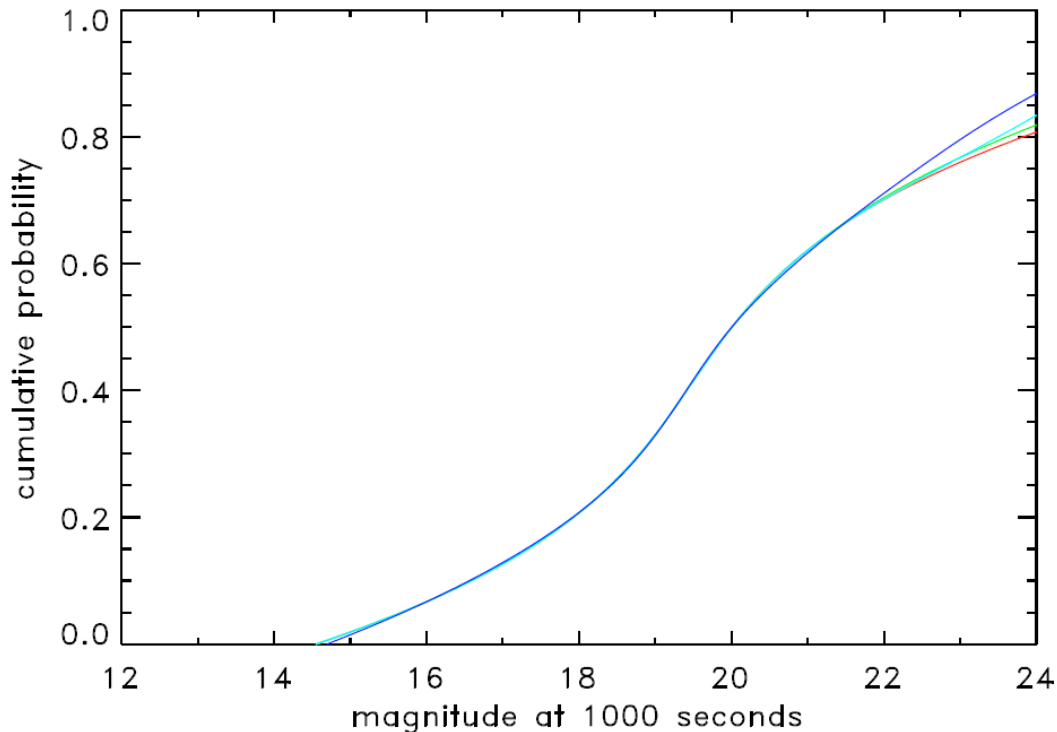
Figure 6.3 Intrinsic cumulative GRB apparent optical afterglow distribution. Red, green, cyan, and blue correspond to B-spline curves with 4,5,6, and 7 degrees of freedom. 71% of all GRB afterglows have $m_R < 22$ at $t = 1000$ seconds.

6.4.4 ABC

The ABC observed 21 GRBs between September 2005 and June 2008. Of those 21, 17 had optical afterglows, but 3 of them were in the IR. Of those 17, the ABC observed 10 of them. The other 7 were not seen by the ABC, because the afterglow had faded too much to be seen by the ABC or the seeing conditions were not optimal to view the GRB. For 9 of the 21 bursts, the diffraction grating was used, which

further reduced the limiting magnitude of the images, and reduced the ability of the ABC to detect afterglows.

The limiting magnitudes for ABC GRB observations ranges from 17.3 to 23.7. The percent of all ABC bursts with detections is 10/21 or 48%. Including observations from other telescopes, this number is 14/21, or 67%. There are 9 bursts taken with the grating, and 5 have an afterglow, but only 1 was seen by the ABC. There are a couple of reasons for this. First, the grating disperses the light, causing a poorer limiting magnitude, so that fainter afterglows will not be seen with the grating. Second, in grating images, stars and other objects do not look like dots, making it difficult for the operators to focus the images, which also hurts the limiting magnitude. Excluding the bursts which use the grating from these statistics, there are no GRBs that are detected by other observatories, but not detected by the ABC. The percent of ABC bursts (no filter) with detections is 9/12, or 75%. This is similar to the number of bursts predicted to be brighter than 22nd magnitude at 1000s (71%).

6.5   Summary

There are two things discussed in this chapter, a way to categorize "dark" bursts, and the statistics of undetected bursts, which led to a calculation of the optical brightness distribution function. Neither of these seeks to understand the physics behind why a particular burst might be fainter than normal.

Dark bursts are defined by calculating β_{ox}, and those with values less than 0.5 are labeled as "dark". Prior to $Swift$, about 10% were dark, but in the $Swift$ era, 50% are. This is likely due to better and faster positions from $Swift$, which allows for faster responses from telescopes. It's more likely to detect a faint fading afterglow if

GRB	Filter	ABC Limit	Detection?	ABC Detection?
050906	Grating	19.0	N	N
050925	Grating	19.3	N	N
051117B	Grating	19.4	N	N
060108	Grating	19.7	Y	N
060110	None	21.8	Y	Y
060116	None	22.5	Y	Y
060202	Grating	19.0	IR	N
060428B	Grating	18.6	Y	N
060510B	Grating	19.9	Y	N
060708	Grating	19.5	Y	Y
060912	Grating	17.3	Y	N
060923	None	23.0	IR	N
060930	None	21.0	N	N
070208	None	21.5	Y	Y
070419A	None	23.6	Y	Y
070518	None	21.6	Y	Y
070529	None	24.4	Y	Y
071003	None	21.2	Y	Y
071011	None	21.1	Y	Y
071021	None	23.7	IR	N
080613A	None	19.6	Y	Y

Table 6.6 Best ABC magnitude limits for all GRB with observations. Limits are between 100 and 10,000 seconds after the burst.

it is observed early.

Calculating the optical brightness distribution function reveals that 71% of all bursts are brighter than 22nd magnitude. The ABC data agrees with this, 75% of the unfiltered bursts are detected, and the ABC is mounted on a large, 3.67m telescope, which obtains data within minutes of when the GRB is detected. Half of all GRBs are undetected, 25% are lost because they are fainter than 22nd magnitude, and therefore difficult to be observed by most telescopes, the rest are missed because the available telescopes are inadequate.

CHAPTER VII

Conclusions

Between July, 2005, and August, 2008, there were 50 GRBs that were faxed or called in to the AEOS control room. Of those 50 GRBs, 29 were not observed for various reasons: bad weather prevented 19, equipment failure prevented 3, 5 were not observed because the AEOS is closed on the weekends, and 2 were not observed because the experimenter did not call the operators to confirm the fax.

The ABC observed 21 GRBs, and of those, 10 had optical afterglows (060110, 060116, 060708, 070208, 070419A, 070518, 070529, 071003, 071011, and 080613A). All of those were unfiltered observations, except for 060708, which was observed with the diffraction grating. The remaining 11 GRBs observed with the ABC had upper limits, but only 4 had interesting limits (050925, 071021, 060930, and 051117B). The other 7 were not interesting, either because there were earlier or deeper upper limits, or because there were detections of an afterglow by other observatories. All but one of the 7 observations used the diffraction grating, which decreased the sensitivity of the ABC. The median time when the first image was taken (after the burst) for the 21 observed GRBs is 11 minutes.

GRBs 060110, 060116, 060708, 070208, 070419A, 070518, 070529, 071003, and 071011 were fit with various power law decays in both the optical and the X-ray

(see Table 5.2), in order to see if they fit the fireball model. GRBs 060110 and 080613A had sparse data, therefore it was not possible to determine if they fit the fireball model. GRBs 060116, 060708, 070518 and 071011 fit the fireball model. All four of these GRBs had good coverage in X-ray and optical, and all had optical data from other observatories. GRBs 071003, 070529, 070208 and 070419A do not fit the fireball model, because the power law decays were different than expected for the fireball model. GRBs 070419A and 070529 require unphysical amounts of energy injection to fit the fireball model, GRB 070208 has a very steep break in the light curve that is not predicted by the fireball model, and GRB071003 has a bright rebrightening that can't be fit. This is similar to what others have found, that about half of the GRBs fit the fireball model, and half do not.

Jakobsson et al. (2004) defines bursts with an optical-to-x-ray spectral index (β_{ox}) of less than 0.5 to be dark. These are GRBs which are optically subluminous with respect to the fireball model. Within the ABC set of data, 4 GRBs (GRB 060116, GRB 070208, GRB 070529, GRB 071021) had values of $\beta_{ox} < 0.5$. Cenko et al. (2008) and Melandri et al. (2008), which both have larger samples of GRBs, and both observe GRB with large telescopes, find that $\sim 50\%$ of the GRBs have $\beta_{ox} <$ 0.5, which is similar to what the ABC found. Prior to $Swift$, roughly 10% of the GRBs were dark, this is possibly because dark GRBs need faster and more accurate positions than $Swift$ provides in order to be observed.

GRB 060116, observed by the ABC, had one of the faintest optical afterglows detected. This is not a unique burst; there are a handful of other bursts that are also extremely faint at early times. Without large telescopes and prompt observations, which would not be possible without fast localizations from $Swift$, these afterglows would have been missed. Except for the faintness, GRB 060116 behaves like a typical

GRB. This prompted further investigations (Akerlof & Swan, 2007), which used GCN and literature data for 118 $Swift$ bursts to estimate the GRB afterglow apparent optical luminosity distribution function. The main result is that about 71% of GRBs are brighter than 22.1 at 1000 seconds after the burst.

7.1 The Future

About half of all GRBs observed do not fit the fireball model. This is the most successful model so far, but there are problems with it. What sort of observations are needed in order to learn more about GRBs? A few types of observations come to mind: many observations spanning long periods of time, and observations with more color information.

The ABC observed GRBs with many data points spanning long periods of time. This occurred for GRBs 070529 and 071003. Neither of these two bursts fit the fireball model, however, with less data, it is conceivable that they would have. The ABC GRBs that fit the fireball model generally had less data, and no breaks in the light curve. Longer periods of observations, with more data, would probably find more GRBs that do not fit the fireball model.

The ABC attempted to observe GRBs with a low resolution diffraction grating, in order to get color information, and successfully observed GRB 060708. Unfortunately, this is the only burst that was observed with a grating, and nothing interesting was seen (no color change was observed, and the observation did not occur during a break in the light curve). More GRBs need to be observed in this way, because the models predict color changes. The problem is that early GRB optical afterglows tend to be fainter than expected, and using a diffraction grating, similar to the ABC, hurts the sensitivity, making such observations very difficult.

Currently, half of all GRBs have no detected afterglows. Many reasons have been proposed for this, but Chapter VI and Akerlof & Swan (2007) found that 70% are brighter than 22nd magnitude at 1000s, and suggest that the reason so many are not seen is because the telescopes that observe GRB optical afterglows are inadequate. Large, possibly robotic telescopes (2m or larger) would reduce the number of missed afterglows. The ABC, which is mounted on a 3.67m telescope, is not robotic, but does not consistently follow GRB afterglows for extended periods of time due to other observing constraints. However, the ABC does see 75% of all afterglows that it observes. P60, which is a robotic 1.5m telescope, detected 76% of the GRBs that they observed, similar to the ABC numbers, and similar to the 70% of Akerlof & Swan (2007).

Swift detects GRBs quickly, with accurate coordinates, allowing the AEOS, a large telescope, to observe GRBs about 10 minutes after they were detected. Smaller, robotic telescopes, like Faulkes Telescope North, a 2m telescope also located on Haleakala, detected most of the GRBs that the ABC did, despite only being 2m, because it was faster. The ABC found an optical afterglow for GRB 060116, while others were unable to, because of the large size and fast speed of the AEOS. Roughly 1/10 of the bursts detected by the ABC required both the large aperture and speed of the AEOS, the rest of the bursts were found with faster, but smaller, robotic telescopes, or with the UVOT. Both speed and size are important for GRB afterglow detection, and the AEOS had both. For GRB studies, most projects must choose between a combination of telescope speed and aperture size, and speed is more important for the detection of the afterglow and explanation of the early afterglow.

Bibliography

Akerlof, C., et al. Apr, 1999, Nature, 398, 400

Akerlof, C. W., et al. Jan. 2003, PASP, 115, 132

Akerlof, C. W. & Swan, H. F. Dec. 2007, ApJ, 671, 1868

Angelini, L., et al. 2006, GCN Circ. No. 4848

Antonelli, L. A., et al. 2006, A&A, 456, 509

Baliyan, K. S., Ganesh, S., & Priyanksha, . 2007. GRB 070529: Optical aterglow
from MIRO. GCN Circular 6471

Band, D., et al. 2005. GRB 051117B: Swift detection of a burst. GCN Circular 4281

Barat, C., et al. Nov. 1984, ApJL, 286, L5

Barbier, L., et al. 2007. GRB 071021, Swift-BAT refined analysis. GCN Circular
6966

Barthelmy, S., et al. 2006. GRB 060116: Refined analysis of the Swift-BAT burst.
GCN Circular 4531

Beardmore, A., Page, K., Goad, M., & Kennea, J. 2005. GRB 051117B: Swift XRT
position. GCN Circular 4282

Berger, E., Fox, D. B., & Cucchiara, A. 2007. GRB 070529: Gemini Redshift. GCN
Circular 6470

Berger, E., Mulchaey, J., Morrell, N., & Krzeminski, W. 2005, GCN Circ. No. 3283

Bersier, D., et al. 2003, ApJL, 584, L43

Bikmaev, I., et al. 2005, GCN Circ. No. 3831

Bikmaev, I., et al. 2006, GCN Circ. No. 4652

Bloom, J. S. 2006. GRB 060110: IR Candidate Afterglow. GCN Circular 4471

Bloom, J. S. 2007. GRB 070208: Early IR detection and afterglow astrometry. GCN Circular 6079

Boyd, P., et al. 2005, GCN Circ. No. 4096

Boyd, P., et al. 2005, GCN Circ. No. 3230

Boyd, P., Weigand, R. E., Holland, S. T., & Blustin, A. 2006, GCN Circ. No. 4958

Breeveld, A. & Moretti, A. 2006, GCN Circ. No. 4798

Brown, P. J., Band, D. L., Boyd, P., Norris, J., Hurley, K., & Gehrels, N. 2005, GCN Circ. No. 3759

Brown, P. J., Mineo, T., Chester, M., Angelini, L., Meszaros, P., & Gehrels, N. 2005, GCN Circ. No. 4200

Burenin, R., et al. 2003, GCN Circ. No. 2001

Cameron, P. B. & Frail, D. A. 2005. GRB 050906: Radio Observations. GCN Circular 3933

Campana, S., Barthelmy, S., Gehrels, N., Gronwall, C., Kennea, J., Markwardt, C., Page, K., Palmer, D., & Perri, M. 2006a. GRB 060116: Swift-BAT detection of a burst. GCN Circular 4519

Campana, S., Perri, M., Romano, P., & Burrows, D. N. 2006b. GRB 060116: XRT position. GCN Circular 4522

Campana, S., Perri, M., Romano, P., Burrows, D. N., Norris, J., & Hurley, K. 2006c. GRB 060116: XRT refined analysis. GCN Circular 4529

Castro-Tirado, A. J., et al. 2007a. GRB 071021: correction to GCN 6968. GCN Circular 6971

Castro-Tirado, A. J., et al. 2007b. GRB 071021: optical and NIR observations. GCN Circular 6968

Castro-Tirado, A. J., et al. 2007c. GRB 071021: optical and NIR observations. GCN Circular 6968

Cenko, S. B. 2007. GRB 071011: P60 Optical Afterglow Candidate. GCN Circular 6895

Cenko, S. B. & Fox, D. B. 2005, GCN Circ. No. 3981

Cenko, S. B. & Fox, D. B. 2007. GRB 070419: P60 Confirmation of Optical Afterglow. GCN Circular 6306

Cenko, S. B., Fox, D. B., Rich, J., Schmidt, B., Christiansen, J., & Berger, E. 2005, GCN Circ. No. 3357

Cenko, S. B., Gezari, S., Small, T., Fox, D. B., & Berger, E. 2007. GRB 070419: Keck/LRIS Absorption Redshift. GCN Circular 6322

Cenko, S. B., et al. 2006, ApJ, 652, 490

Cenko, S. B., et al. Aug. 2008, ArXiv e-prints

Cenko, S. B., Ofek, E. O., & Fox, D. B. 2006, GCN Circ. No. 5048

Chen, Y. T., Huang, K. Y., Ip, W. H., Urata, Y., Qiu, Y., & Lou, Y. Q. 2005. GRB 051117B: Lulin R and I band observation. GCN Circular 4285

Chester, M., Covino, S., Schady, P., & Roming, P. 2005, GCN Circ. No. 3670

Chevalier, R. A. & Li, Z.-Y. June 2000, ApJ, 536, 195

Chornock, R., Li, W., & Filippenko, A. V. 2007. GRB 070419 optical afterglow candidate. GCN Circular 6304

Clemens, C., Updike, A., Kruehler, T., Greiner, J., Yoldas, A. K., Yoldas, A., Szokoly, G., & Garching), M. 2008. GRB 080613A: GROND Confirmation of the Afterglow Candidate. GCN Circular 7880

Cline, T. L., et al. Nov. 1984, ApJL, 286, L15

Cobb, B. E. 2006, GCN Circ. No. 4872

Cobb, B. E. & Bailyn, C. D. 2005, GCN Circ. No. 3994

Cool, R. J., Eisenstein, D. J., Hogg, D. W., Blanton, M. R., Schlegel, D. J., Brinkmann, J., Lamb, D. Q., Schneider, D. P., & Berk, D. E. V. 2007. GRB 070208 - SDSS Pre-Burst Observations. GCN Circular 6080

Covino, S., et al. 2003, AAP, 404, L5

Covino, S., Tagliaferri, G., Chincarini, G., Antonelli, L. A., Israel, G. L., Andreuzzi, G., & Escudero, A. G. d. G. 2007. GRB 070518: TNG observations. GCN Circular 6426

Cucchiara, A., Cummings, J., Holland, S., Gronwall, C., Blustin, A., Marshall, F., Smale, A., Cominsky, L., & Gehrels, N. 2005, GCN Circ. No. 3923

Cucchiara, A., Fox, D. B., Cenko, S. B., & Price, P. A. 2007a. GRB 070208: Absorption and emission redshift from Gemini. GCN Circular 6083

Cucchiara, A., Marshall, F. E., & Guidorzi, C. 2007b. GRB 070518: UVOT refined analysis. GCN Circular 6419

De Pasquale, M., et al. 2006, MNRAS, 370, 1859

Eichler, D., Livio, M., Piran, T., & Schramm, D. N. July 1989, Nature, 340, 126

Fenimore, E., et al. 2006. GRB 060708: Refined analysis of the Swift-BAT burst. GCN Circular 5295

Fox, D. 2005. GRB 051117B: Optical observations. GCN Circular 4284

Fox, D. B., Cenko, S. B., & Schmidt, B. P. 2005a. GRB 050906: P60 Observations. GCN Circular 3931

Fox, D. B., Ofek, E., & Cenko, S. B. 2007. GRB 070208: Afterglow confirmation from P60. GCN Circular 6078

Fox, D. B., Pagani, C., Angelini, L., Burrows, D. N., Osborne, J. P., & Parola, V. L. 2005b. GRB 050906: Possible X-ray Counterpart. GCN Circular 3956

Garnavich, P., et al. 2007. GRB 070518, deep LBT photometry. GCN Circular 6462

Goad, M. R., et al. 2006, GCN Circ. No. 4985

Gotz, D., Mereghetti, S., Paizis, A., Lazos, M., Mowlavi, N., Beck, M., & Borkowski, J. 2006. GRB 060930: A long X-ray rich GRB detected by INTEGRAL. GCN Circular 5665

Gotz, D., Paizis, A., Mereghetti, S., Beckmann, V., Beck, M., Galis, R., & Borkowski, J. 2008. GRB 080613 : a long GRB detected with INTEGRAL. GCN Circular 7871

Grazian, A., et al. 2006. GRB 060116: photometric redshift - the farthest GRB? GCN Circular 4545

Guetta, D., et al. 2007, A&A, 461, 95

Guidorzi, C., et al. 2007a. GRB 070518: Swift detection of a burst with optical afterglow. GCN Circular 6415

Guidorzi, C., et al. 2006a. GRB 060930: Faulkes Telescope South observation. GCN Circular 5670

Guidorzi, C., et al. 2005, GCN Circ. No. 3625

Guidorzi, C. & Markwardt, C. B. 2008. GRB 080613A: Swift-XRT detection of the afterglow. GCN Circular 7882

Guidorzi, C., et al. 2005, ApJL, 630, L121

Guidorzi, C., et al. 2005, GCN Circ. No. 4035

Guidorzi, C., et al. 2007b. GRB 070208: Faulkes Telescope North Afterglow Identification. GCN Circular 6077

Guidorzi, C., et al. 2006, GCN Circ. No. 4661

Guziy, S., Velarde, G. G., & Castro-Tirado, A. J. 2006, GCN Circ. No. 4896

Halpern, J. P. & Mirabal, N. 2006, GCN Circ. No. 5086

Holland, S. T., Band, D., Mason, K., Marshall, F., & Gehrels, N. 2005, GCN Circ. No. 4300

Holland, S. T., et al. 2007. GRB 070529: Swift detection of a burst with an optical aterglow. GCN Circular 6466

Holland, S. T., et al. 2005, GCN Circ. No. 3150

Hoversten, E. A. & Holland, S. T. 2008. GRB 080613A: Swift/UVOT Upper Limits. GCN Circular 7881

Huang, F. Y., Huang, K. Y., Ip, W. H., Urata, Y., Qiu, Y., & Lou, Y. Q. 2005, GCN Circ. No. 4231

Hurkett, C., Beardmore, A., Godet, O., Kennea, J. A., Krimm, H., Marshall, F., Osborne, J., Palmer, D., & Parsons, A. 2006, GCN Circ. No. 4736

Hurkett, C., Page, K., Kennea, J., Burrows, D., Blustin, A., Barbier, L., Markwardt, C., Parsons, A., & Gehrels, N. 2005, GCN Circ. No. 3633

Iizuka, R. & Maeno, S. 2007. GRB 071011: NAYUTA Optical Observation, correction to GCN 6886. GCN Circular 6900

Jakobsson, P., et al. 2005. GRB 050906: Optical observations at the Very Large Telescope. GCN Circular 3940

Jakobsson, P., Hjorth, J., Fynbo, J. P. U., Watson, D., Pedersen, K., Björnsson, G., & Gorosabel, J. Dec. 2004, ApJL, 617, L21

Jakobsson, P., et al. Mar. 2006, AAP, 447, 897

Jakobsson, P., et al. 2006b. GRB 060708: VLT spectroscopy. GCN Circular 5319

Jelinek, M., Castro-Tirado, A. J., Casanova, V., Gorosabel, J., Postigo, A. d. U., Vitek, S., Cunniffe, R., & Kubanek, P. 2007. GRB 070518: OSN observation. GCN Circular 6418

Jelínek, M., et al. 2006, A&A, 454, L119

Jelinek, M., Prouza, M., Kubanek, P., Nekola, M., & Hudec, R. 2005, GCN Circ. No. 3854

Klebesadel, R. W., Strong, I. B., & Olson, R. A. June 1973, ApJL, 182, L85+

Klotz, A., Boer, M., & Atteia, J. L. 2005, GCN Circ. No. 3403

Klotz, A., Boer, M., & Atteia, J. L. 2005, GCN Circ. No. 4386

Klotz, A., Boer, M., & Atteia, J. L. 2006, GCN Circ. No. 4483

Klotz, A., Boer, M., Atteia, J. L., & Stratta, G. 2005, GCN Circ. No. 3084

Klotz, A., Boër, M., Atteia, J. L., Stratta, G., Behrend, R., Malacrino, F., & Damerdji, Y. 2005, A&A, 439, L35

Klotz, A., Gendre, B., Stratta, G., Atteia, J. L., Boër, M., Malacrino, F., Damerdji, Y., & Behrend, R. 2006, A&A, 451, L39

Kocevski, D., Bloom, J. S., & McGrath, E. J. 2006. GRB 060116: IR Candidate Afterglow. GCN Circular 4528

Koppelman, M. 2006, GCN Circ. No. 4977

Kosugi, G., Kawai, N., Aoki, K., Hattori, T., Ohta, K., & Yamada, T. 2005, GCN Circ. No. 3263

Krimm, H., et al. 2007. GRB 070518, Swift-BAT refined analysis. GCN Circular 6417

Krimm, H., et al. 2005. GRB 050906: Swift/BAT Detection of a possible burst. GCN Circular 3926

Kuroda, D., Yanagisawa, K., Yoshida, M., Ishimura, T., & Kawai, N. 2007. GRB 071011: MITSuME Optical Observations. GCN Circular 6922

Landsman, W. & Stamatikos, M. 2007. GRB 070419a: Swift UVOT observations. GCN Circular 6340

Lazzati, D. & Begelman, M. C. Apr, 2006, ApJ, 641, 972

Li, W. 2006, GCN Circ. No. 4499

Li, W., California, U. o., & Berkeley, . 2007. GRB 071003: KAIT optical afterglow observations. GCN Circular 6838

Li, W., Chornock, R., Butler, N., Bloom, J., & Filippenko, A. V. 2006, GCN Circ. No. 5027

lin, Z. Y., Huang, K. Y., Ip, W. H., Urata, Y., Qiu, Y., & Lou, Y. Q. 2005, GCN Circ. No. 3593

Lipunov, V., et al. 2005, GCN Circ. No. 3883

MacFadyen, A. I. & Woosley, S. E. Oct. 1999, ApJ, 524, 262

Malesani, D., D'Avanzo, P., Israel, G. L., Piranomonte, S., Chincarini, G., Stella, L., Tagliaferri, G., & Depagne, E. 2005, GCN Circ. No. 3614

Malesani, D., Piranomonte, S., Tagliaferri, G., Chincarini, G., Covino, S., Fiore, F., & Stella, L. 2007. GRB 071021: Z-band detection. GCN Circular 6972

Mangano, V., et al. 2005, GCN Circ. No. 3884

Mangano, V., et al. 2006, GCN Circ. No. 5014

Mangano, V., et al. 2006, GCN Circ. No. 5006

Markwardt, C., et al. 2007. GRB 070208, Swift-BAT refined analysis. GCN Circular 6081

Marshall, F., Chester, M., & Cummings, J. 2006, GCN Circ. No. 4814

Marshall, F. E., et al. 2007. GRB 071011: Swift detection of a burst. GCN Circular 6882

McGowan, K., Band, D., Brown, P., Gronwall, C., Huckle, H., & Hancock, B. 2005, GCN Circ. No. 3739

McGowan, K., et al. 2005, GCN Circ. No. 3317

Melandri, A., et al. Oct. 2008, ApJ, 686, 1209

Meszaros, P. & Rees, M. J. June 1997, ApJL, 482, L29+

Monfardini, A., Gomboc, A., Guidorzi, C., Mundell, C. G., Steele, I. A., Mottram, C. J., Carter, D., Smith, R. J., & Bode, M. F. 2005, GCN Circ. No. 3503

Monfardini, A., et al. 2006, ApJ, 648, 1125

Monfardini, A., et al. 2006, GCN Circ. No. 4630

Moretti, A., et al. 2006. GRB 060708: Swift detection of a burst with an UVOT countpart. GCN Circular 5292

Narayan, R., Piran, T., & Shemi, A. Sept. 1991, ApJL, 379, L17

Norris, J., et al. 2005, GCN Circ. No. 4061

Oates, S. R., et al. 2006, MNRAS, 372, 327

Paciesas, W. S., et al. June 1999, APJS, 122, 465

Pagani, C., et al. 2006, ApJ, 645, 1315

Pagani, C., Parola, V. L., & Burrows, D. N. 2005. GRB 050906: Swift XRT upper limit. GCN Circular 3934

Page, K. L., Gehrels, N., & Sakamoto, T. 2007. GRB 071021: Swift-XRT Team refined analysis. GCN Circular 6963

Page, K. L., Goad, M. R., Beardmore, A. P., Burrows, D. N., Smale, A., & Cominsky, L. 2006. GRB 060110: XRT position and analysis. GCN Circular 4525

Page, M. J., Ziaeepour, H., Blustin, A. J., Chester, M., Fink, R., & Gehrels, N. 2005, GCN Circ. No. 3859

Pandey, S. B., et al. 2006, A&A, 460, 415

Pandey, S. B., Misra, K., & Roy, R. 2007. GRB 071011, Optical afterglow. GCN Circular 6899

Parris, S., Smith, A., Nysewander, M., Reichart, D., Ivarsen, K., Foster, A., La-Cluyze, A., & Crain, J. A. 2006. GRB 060708: PROMPT Optical Limits. GCN Circular 5299

Parsons, A., et al. 2005a. GRB 051117B: Refined analysis of the Swift-BAT burst. GCN Circular 4288

Parsons, A., et al. 2007. GRB 070529, Swift-BAT refined analysis. GCN Circular 6468

Parsons, A., et al. 2005b. GRB 050906: Swift-BAT refined analysis. GCN Circular 3935

Pasquale, M. D., et al. 2006, GCN Circ. No. 4455

Pasquale, M. D., Norris, J., Kennedy, T., Mason, K., & Gehrels, N. 2005, GCN Circ. No. 4028

Perley, D. A., Kocevski, D., Poznanski, D., Bloom, J. S., & Modjaz, M. 2007. GRB 071011: Confirmation of P60 optical afterglow. GCN Circular 6898

Perley, D. A., et al. May 2008, ArXiv e-prints

Piran, T. June 1999, Physics Reports, 314, 575

Piran, T. 2000, Physics Reports, 333, 529

Piran, T. Jan. 2005, Reviews of Modern Physics, 76, 1143

Piranomonte, S., et al. 2006. GRB 060116: Further analysis of VLT photometry and optical spectroscopy. GCN Circular 4583

Poole, T., et al. 2005, GCN Circ. No. 3050

Poole, T., Hurkett, C., Hunsberger, S., Breeveld, A., Boyd, P., Gehrels, N., Mason, K., & Nousek, J. 2005, GCN Circ. No. 3394

Poole, T., Moretti, A., Holland, S. T., Chester, M., Angelini, L., & Gehrels, N. 2005, GCN Circ. No. 3698

Poole, T. S. & Boyd, P. T. 2006, GCN Circ. No. 4951

Price, P. A. & Minezaki, T. 2007. GRB 070518: Optical/NIR observation. GCN Circular 6443

Quimby, R., Schaefer, B. E., & Swan, H. 2006, GCN Circ. No. 4782

Quimby, R. M., et al. 2006, ApJ, 640, 402

Rees, M. J. & Meszaros, P. Mar. 1998, ApJL, 496, L1+

Retter, A., et al. 2005, GCN Circ. No. 3788

Retter, A., et al. 2005, GCN Circ. No. 3799

Retter, A., Barthelmy, S., Burrows, D., Chester, M., Gehrels, N., Kennea, J., Marshall, F., Palmer, D., & Racusin, J. 2005, GCN Circ. No. 4126

Rol, E., Tanvir, N., & Kerr, T. 2007. Infrared detection of GRB 070419A with UKIRT. GCN Circular 6309

Romano, P., et al. 2006, A&A, 456, 917

Roming, P., et al. 2005, GCN Circ. No. 3026

Rosen, S., et al. 2005, GCN Circ. No. 3095

Ruderman, M. Oct. 1975, New York Academy Sciences Annals, 262, 164

Rujopakarn, W., McKay, T. A., Yuan, F., Swan, H., Smith, D. A., & Yost, S. A. 2006. GRB 060110: ROTSE-III Confirmation of Optical Counterpart. GCN Circular 4472

Rujopakarn, W., Swan, H., Schaefer, B., Yuan, F., & Guver, T. 2005. GRB 051117B: ROTSE-III Optical Limits. GCN Circular 4283

Rumyantsev, V., Biryukov, V., Pozanenko, A., & Ibrahimov, M. 2005, GCN Circ. No. 4087

Rumyantsev, V., Pavlenko, E., Efimov, Y., Antoniuk, K., Antoniuk, O., Primak, N., & Pozanenko, A. 2003, GCN Circ. No. 2005

Rykoff, E. 2005. Prompt Observations of Gamma-Ray Burst Afterglows with ROTSE-III. Thesis

Rykoff, E. S., et al. 2006, ApJL, 638, L5

Rykoff, E. S., Schaefer, B. E., Yost, S. A., & Quimby, R. 2006, GCN Circ. No. 5041

Rykoff, E. S., et al. Oct. 2005, ApjL, 631, L121

Rykoff, E. S., Yost, S. A., Rujopakarn, W., Quimby, R., Smith, D. A., & Yuan, F. 2005, GCN Circ. No. 4012

Rykoff, E. S., Yost, S. A., & Swan, H. 2005, GCN Circ. No. 3304

Rykoff, E. S., Yost, S. A., & Swan, H. 2006c. GRB 060116: ROTSE-III Optical Limits. GCN Circular 4523

Sakamoto, T., et al. 2007a. GRB 071021: Swift detection of a burst. GCN Circular 6958

Sakamoto, T., et al. 2007b. GRB 071011, Swift-BAT refined analysis. GCN Circular 6889

Sakamoto, T., Gehrels, N., & Page, K. 2007c. GRB 071021: possible high-z burst. GCN Circular 6967

Sari, R. & Mészáros, P. May 2000, ApJL, 535, L33

Sari, R. & Piran, T. Aug. 1999, ApJ, 520, 641

Sari, R., Piran, T., & Narayan, R. Apr, 1998, ApJL, 497, L17+

Sato, G., et al. 2007. GRB 070208: Swift detection of a burst. GCN Circular 6074

Sbarufatti, B., Mangano, V., Parola, V. L., Troja, E., Evans, P., Beardmore, A., Burrows, D. N., & Marshall, F. E. 2007a. GRB 071011: Swift-XRT refined analysis. GCN Circular 6902

Sbarufatti, B., Parola, V. L., Troja, E., Mangano, V., Kennea, J., & Marshall, F. E. 2007b. GRB 071011: XRT afterglow detection. GCN Circular 6891

Schady, P., et al. 2007. GRB 071003: Swift detection of a bright burst. GCN Circular 6837

Schady, P., Fox, D., Roming, P., Cucchiara, A., Still, M., Holland, S. T., Blustin, A., & Gehrels, N. 2005, GCN Circ. No. 3817

Schady, P., et al. 2005, GCN Circ. No. 3039

Schady, P., et al. 2006, ApJ, 643, 276

Schady, P. & Moretti, A. 2006. GCN 060708: Swift-UVOT Observations. GCN Circular 5296

Schady, P., Sakamoto, T., McGowan, K., Boyd, P., Roming, P., Nousek, J., & Gehrels, N. 2005, GCN Circ. No. 3276

Schaefer, B. E., Yuan, F., & Yost, S. A. 2007. GRB 070419A: ROTSE-III Optical Limits. GCN Circular 6303

Schaefer, B. E., Yuan, F., Yost, S. A., & Quimby, R. 2006, GCN Circ. No. 4860

Sharapov, D., Ibrahimov, M., & Pozanenko, A. 2006, GCN Circ. No. 4925

Smith, D. A. 2005, GCN Circ. No. 3056

Smith, D. A., Rykoff, E. S., & Yost, S. A. 2005, GCN Circ. No. 3021

Stamatikos, M., et al. 2007a. GRB 070419A Swift-BAT Refined Analysis. GCN Circular 6326

Stamatikos, M., et al. 2007b. GRB 070419: Swift detection of a burst. GCN Circular 6302

Stanek, K. Z., et al. 2007, ApJL, 654, L21

Stanek, K. Z., Garnavich, P. M., Kaluzny, J., Pych, W., & Thompson, I. 1999, ApJL, 522, L39

Starling, R. & Schady, P. 2007. GRB 071003: Swift XRT position. GCN Circular 6845

Still, M., et al. 2005, ApJ, 635, 1187

Strong, I. B., Klebesadel, R. W., & Olson, R. A. Feb. 1974, ApJL, 188, L1+

Swan, H., Akerlof, C., Rykoff, E., Yost, S., & Smith, I. 2006a. GRB 060116: MARGE optical observations. GCN Circular 4568

Swan, H., Akerlof, C., & Skinner, M. 2006b. GRB 060930: MARGE Optical Limits. GCN Circular 5736

Swan, H., Rujopakarn, W., & Smith, I. 2005. GRB 051117B: MARGE Optical Limits. GCN Circular 4293

Swan, H., Rujopakarn, W., Yost, S. A., Rykoff, E. S., & Schaefer, B. E. 2006c. GRB 060930: ROTSE-III Optical Limits. GCN Circular 5666

Swan, H., Rykoff, E., Yost, S., McKay, T., Akerlof, C., & Smith, I. 2006d. GRB 060708: MARGE low resolution spectrum observations. GCN Circular 5318

Swan, H., Smith, I., Akerlof, C., Rykoff, E., & Skinner, M. 2007a. GRB 070419A: MARGE Observations. GCN Circular 6339

Swan, H., Smith, I., Akerlof, C., Rykoff, E., & Skinner, M. 2007b. GRB 071021: MARGE Optical Limits. GCN Circular 7007

Swan, H., Smith, I., Akerlof, C., & Skinner, M. 2007c. GRB 070529: MARGE Observations. GCN Circular 6472

Swan, H., Smith, I., Akerlof, C., Yost, S., & Skinner, M. 2006e. GRB 060110: MARGE observations. GCN Circular 4491

Swan, H., Smith, I., Rujopakarn, W., Yuan, F., Yost, S., Akerlof, C., Skinner, M., & Russell, R. 2007d. GRB 071003: MARGE Observations. GCN Circular 6841

Swan, H., Smith, I., Skinner, M., & Russell, R. 2007e. GRB 070208: MARGE Optical Observations. GCN Circular 6090

Swan, H. F., et al. 2009, manuscript in preparation

Swan, H. F. & Smith, I. 2005. GRB 050906: MARGE Optical Limits. GCN Circular 3936

Tanvir, N. R., Levan, A. J., Priddey, R. S., Fruchter, A. S., & Hjorth, J. 2006. GRB 060116 HST observations. GCN Circular 4602

Thompson, C. Oct. 1994, MNRAS, 270, 480

Torii, K. 2005, GCN Circ. No. 3943

Torii, K. 2005, GCN Circ. No. 4112

Torii, K. 2006, GCN Circ. No. 4826

Tristram, P., Castro-Tirado, A. J., Guziy, S., Postigo, A. d. U., Jelinek, M., Gorosabel, J., & Yock, P. 2005, GCN Circ. No. 3965

Tristram, P., Jelinek, M., Castro-Tirado, A. J., Postigo, A. d. U., Guziy, S., Gorosabel, J., & Yock, P. 2005, GCN Circ. No. 4055

Ukwatta, T., et al. 2007. GRB 071003, Swift-BAT refined analysis. GCN Circular 6842

Urata, Y., Huang, K. Y., Ip, W. H., & Albert, L. 2007. GRB 071021 : CFHT Ks-band observation. GCN Circular 6993

Vestrand, W. T., et al. May 2005, Nature, 435, 178

Wozniak, P., Vestrand, W. T., Wren, J., Evans, S., & White, R. 2005, GCN Circ. No. 3414

Wren, J., Vestrand, W. T., White, R., Wozniak, P., & Evans, S. 2005, GCN Circ. No. 4380

Xin, L. P., Zhai, M., Qiu, Y. L., Wei, J. Y., Hu, J. Y., Deng, J. S., Urata, Y., & Zheng, W. K. 2007a. GRB 070518: OT confirmed form Xinglong TNT observation. GCN Circular 6416

Xin, L. P., Zhai, M., Qiu, Y. L., Wei, J. Y., Hu, J. Y., Deng, J. S., Urata, Y., & Zheng, W. K. 2007b. GRB 071011: Xinglong TNT Optical afterglow observations. GCN Circular 6904

Yanagisawa, K., Sakamoto, T., & Kawai, N. 2005, GCN Circ. No. 4418

Yanagisawa, K., Toda, H., & Kawai, N. 2006, GCN Circ. No. 4517

Yost, S. A., et al. 2007, ApJ, 657, 925

Yuan, F., Rujopakarn, W., Swan, H., & Rykoff, E. S. 2007. GRB 070208: ROTSE-III Optical Limits. GCN Circular 6076

Zane, S., Barthelmy, S., Blustin, A. J., Gehrels, N., Markwardt, C., Norris, J., Page, K., & Palmer, D. 2006. GRB 060110: Swift-BAT detection of a burst. GCN Circular 4463

Zhai, M., Qiu, Y. L., Wei, J. Y., Hu, J. Y., Deng, J. S., Wang, X. F., Huang, K. Y., & Urata, Y. 2006, GCN Circ. No. 5057

Zhang, B., Fan, Y. Z., Dyks, J., Kobayashi, S., Mészáros, P., Burrows, D. N., Nousek, J. A., & Gehrels, N. May 2006, ApJ, 642, 354

Zhang, B. & Mészáros, P. May 2001, ApJL, 552, L35

Zhang, B. & Mészáros, P. 2004, International Journal of Modern Physics A, 19, 2385

Zharikov, S., Benitez, E., Torrealba, J., & Stepanian, J. 2003, GCN Circ. No. 2022

Zheng, W. K., Zhai, M., Qiu, Y. L., Wei, J. Y., Hu, J. Y., & Deng, J. S. 2006, GCN Circ. No. 4930

Ziaeepour, H., et al. 2006, GCN Circ. No. 4429